Louisiana State University
LSU Scholarly Repository

LSU Master's Theses | Graduate School

2014

Mechanical behavior of FRP-confined self-healing concrete

Yueqiang Sui
Louisiana State University and Agricultural and Mechanical College

Follow this and additional works at: https://repository.lsu.edu/gradschool_theses

 Part of the Civil and Environmental Engineering Commons

Recommended Citation

Sui, Yueqiang, "Mechanical behavior of FRP-confined self-healing concrete" (2014). *LSU Master's Theses*. 402.
https://repository.lsu.edu/gradschool_theses/402

This Thesis is brought to you for free and open access by the Graduate School at LSU Scholarly Repository. It has been accepted for inclusion in LSU Master's Theses by an authorized graduate school editor of LSU Scholarly Repository. For more information, please contact gradetd@lsu.edu.

MECHANICAL BEHAVIOR OF FRP-CONFINED SELF-HEALING CONCRETE

A Thesis

Submitted to the Graduate Faculty of the
Louisiana State University and
Agricultural and Mechanical College
in partial fulfillment of the
requirements for the degree of
Master of Science

in

The Department of Civil and Environmental Engineering

by
Yueqiang Sui
B.S., Xiamen University, 2011
May 2014

This work is sincerely dedicated to my parents.

ACKNOWLEDGEMENTS

First and foremost, I would like to express my gratitude towards my parents, Fengchun and Xiangyu Sui, for the encouragement and support they have given me throughout my entire life. Without their support, the success I have achieved would not have been possible. I would like to thank Dr. Barbato for not only providing me with the opportunity to pursue my graduate studies at LSU, but also for the outstanding guidance, extremely long hours, and dedication to my focus. I would also like to sincerely thank the other members of my advisory committee, Dr. Ayman Okeil, Dr. Steve Cai and Dr. Marwa Hassan, for providing me with useful advice and assistance as needed throughout my course of study and research, and also for serving on my examination committee. I would like to thank the Gulf Coast Center for Evacuation and Transportation Resiliency (CETR) at Louisiana State University for funding the research project. Also, the author gratefully acknowledges the Louisiana Transportation Research Center (LTRC) for granting access to their laboratory. Additional support from the Department of Construction Management and the Department of Civil and Environmental Engineering is also greatly acknowledged. Lastly, I would like to give a sincere thank you to the rest of my friends and family who were always present with open ears to listen when I simply needed to talk to someone.

TABLE OF CONTENTS

ACKNOWLEDGEMENTS iii

LIST OF TABLES vi

LIST OF FIGURES vii

ABSTRACT x

1 INTRODUCTION 1
1.1 Motivation 1
1.2 Objectives and Scope 3
1.3 Thesis Outline 5

2 LITERATURE REVIEW 6
2.1 Introduction 6
2.2 A Brief Review of Self-Healing Methods in Cementitious Materials 6
2.2.1 Autogenous Healing of Concrete 6
2.2.2 Embedment/Encapsulation of Healing Agents 8
2.2.3 Bacteria-Based Self-Healing Concrete 14
2.2.4 SMA Systems 18
2.3 Microencapsulation-Based Self-Healing Cementitious Materials 22
2.3.1 Introduction of Concept 22
2.3.2 Microcapsule Properties and Shell Materials 24
2.3.3 Healing Agents 28
2.3.4 Review of Applications 35
2.4 FRP-Confined Concrete 38
2.4.1 Confinement Effect 38
2.4.2 Anticorrosive Effect 41
2.4.3 Behavior of FRP-Confined Concrete 44
2.5 Previous Work by Other Researchers at LSU on Microencapsulation-Based Self-Healing Concrete 46
2.6 Application of SEM Technology in Concrete Research 48

3 EXPERIMENTAL EVALUATION OF SELF-HEALING MECHANISM 52
3.1 Introduction 52
3.2 Experimental Equipment 52
3.2.1 Concrete Compression Strength Testing Machine 52
3.2.2 Concrete Stiffness Test Machine 53
3.2.3 Vertical Displacement Measurement System 54
3.2.4 Data Acquisition System (DAQ) 55
3.3 Methodology 56
3.3.1 Test Materials and Specimen Preparation 56
3.3.2 Experimental Matrix 58

3.3.3 Experimental Investigation Protocol 59
3.4 Experimental Results and Discussion 60
3.4.1 Results of the Preliminary Tests 60
3.4.2 Results of the Self-Healing Stiffness Tests 64
3.4.3 Results of the Strength Test 70
3.5 Conclusions Regarding the Tested Hypothesis Based on Self-Healing Stiffness and Strength Tests 76

4 FURTHER INVESTIGATION OF THE RESULTS 78
4.1 Proposed Hypotheses 78
4.2 Investigation of Hypothesis #3 80
4.3 Investigation of Hypotheses #4 to #6 82
4.3.1 Experimental Matrix of SEM Test 83
4.3.2 Sample Preparation of SEM Tests 83
4.3.3 Experimental Methodology 85
4.3.4 Results of the SEM Test #1 (Large Scale EDX Analysis) 86
4.3.5 Results of the SEM Test #2 (Small Scale EDX Analysis Focused on Potential Microcapsules) 92
4.3.6 Results of the SEM Test #3 (SEM Imaging Tests Using Focused Ion Beam Cuts) 100

5 CONCLUSIONS AND RECOMMENDATIONS 103

6 REFERENCES 106

7 APPENDIX: SODIUM SILICATE MICROENCAPSULATION PROCEDURE 118

8 VITA 120

LIST OF TABLES

Table 3-1: Required chemicals for interfacial polymerization synthesis.....57

Table 3-2: Cured FRP laminate properties with Sikadur Hex 300 (SikaWrap Hex-100G).....57

Table 3-3: Experimental test matrix 59

Table 3-4: Results of the preliminary tests 61

Table 3-5: Residual and maximum strains at each load cycle of tested concrete specimens 66

Table 3-6: Stiffness variation of the self-healing stiffness tests 68

Table 3-7: Concrete strength test results.....75

Table 4-1: Stiffness variation of SH50PL cylinders 81

Table 4-2: Experimental matrix for the SEM tests 83

Table 4-3: Results of the large scale EDX analysis.....91

Table 4-4: EDX analysis results of particles with sodium.....99

LIST OF FIGURES

Figure 1-1: Hypothesis of Improved Self-Healing Mechanism due to FRP Confinement: (a) Self-Healing in Unconfined Concrete, and (b) Self-Healing in FRP-Confined Concrete 4

Figure 2-1: Healing Mechanism for Hollow Fiber Systems 9

Figure 2-2: Internal Healing Agent Supply System (adapted from Thao et al. 2009) 10

Figure 2-3: External Healing Agent Supply System (adapted from Mihashi et al. 2000) 12

Figure 2-4: Schematic Diagram of the Self-Healing Structure Composed of a Microvascular Substrate and a Brittle Epoxy Coating (adapted from Toohey et al. 2007) 13

Figure 2-5: Mechanism of the Bacteria-Based Self-Healing Concrete(adapted from Jonkers et al. 2008) 15

Figure 2-6: Viability Study Results of Bacterial Spores (B. cohnii) in Aged Cement Stone Specimens (adapted from Jonkers et al. 2010) 17

Figure 2-7: Stress-strain Curves for SMAs: (a) Shape Memory Effect; (b) Superelasticity Effect (adapted from Dong et al. 2011) 18

Figure 2-8: Intelligent RC Structure Using SMAs (adapted from Song and Mo 2003) 19

Figure 2-9: Mechanism of Microencapsulation-Based Self-Healing Materials (adapted from White et al. 2001) 23

Figure 2-10: Microcapsules-Based Healing Reaction Mechanisms with Agents Encapsulated by Spherical/Cylindrical Microcapsules: (a)-(b) Reaction upon Contact with Moisture or Air or due to Heating; (c) (d) Reaction with the Cementitious Matrix; (e) (f) Reaction with a Second Component Mixed in the Matrix; or (g) (h) Reaction with a Second Component Provided by Additional Microcapsules (adapted from Tittelboom and Belie 2013) 29

Figure 2-11: Stress-Strain Response for FRP Confined Concrete (Pantazopoulou and Mills 1995, Spoelstra and Monti 1999) 40

Figure 2-12: Multi-Surface Plasticity Model for Concrete Subjected to Biaxial Loading (adapted from Murray et al. 1979) 40

Figure 2-13: Average Reinforcement Mass Loss for Unconfined and FRP-Confined Specimens (adapted from Masoud and Soudki 2006) 43

Figure 2-14: Effect of Preparation pH of Microcapsules on Concrete Modulus of Elasticity before and after Healing (adapted from Gilford et al. 2013) 47

Figure 2-15: Effect of Amount of Microcapsules (% of Cement Weight) on Concrete Modulus of Elasticity before and after Healing (adapted from Gilford et al. 2013) 47

Figure 2-16: Working Mechanism of SEMs (adapted from Voutou et al. 2008) 49

Figure 3-1: Concrete Compression Strength: (a) Test Machine, and (b) Test Setup.....53

Figure 3-2: MTS Machine and Stiffness Test Setup: (a) MTS Machine, (b) MTS Controller, and (c) Stiffness Test Setup 54

Figure 3-3: Vertical Displacement Measurement System 55

Figure 3-4: Data Acquisition System.....56

Figure 3-5: Failure Modes of the Specimens in the Preliminary Tests: (a) PR00PL#1, (b) PR00PL#2, (c) PR00PL#3, (d) PR00FRP#1, (e) PR00FRP#2, and (f) PR00FRP#3 62

Figure 3-6: Stress-Strain Response for Unconfined Ordinary Concrete Specimens (Experimental Curve Corresponding to Specimen SH00PL #3).....63

Figure 3-7: Stress-Strain Response for FRP Confined Ordinary Concrete Specimens (Experimental Curve Corresponding to Specimen SH00FRP #2) 63

Figure 3-8: Concrete Stiffness Before and After Healing 69

Figure 3-9: Stress-Strain Response for Ordinary Concrete Specimens: (a) Unconfined, and (b) FRP-Confined 71

Figure 3-10: Stress-Strain Response for Concrete Specimens with 1.0% SS: (a) Unconfined, and (b) FRP-Confined.....72

Figure 3-11: Stress-Strain Response for Concrete Specimens with 2.5% SS: (a) Unconfined, and (b) FRP-Confined.....73

Figure 3-12: Stress-Strain Response for Concrete Specimens with 5.0% SS: (a) Unconfined, and (b) FRP-Confined.....74

Figure 3-13: Concrete Strength Test Results.....75

Figure 4-1: Results of the Third Set of Stiffness Test for SH50PL Cylinders 81

Figure 4-2: Sample Preparation Method for SEM Tests 84

Figure 4-3: Concrete Samples for SEM Tests: (a) Sample Sections and Locations of Samples for SEM Tests; and (b) Final Samples.....85

Figure 4-4: EDX Response of SH00PL-H Sample.....87

Figure 4-5: EDX Response of SH00PL-NH Sample 87

Figure 4-6: EDX Response of SH00FRP-NH Sample 88

Figure 4-7: EDX Response of SH50PL-H Sample 88

Figure 4-8: EDX Response of SH50PL-NH Sample 89

Figure 4-9: EDX Response of SH50FRP-NH Sample 89

Figure 4-10: SEM Imaging of Particles from SH00FRP-NH Samples 93

Figure 4-11: SEM Imaging of Particles from SH50PL-H Samples 93

Figure 4-12: SEM Imaging of Particles from SH50PL-NH Samples 94

Figure 4-13: SEM Imaging of Particles from SH50FRP-NH Samples 94

Figure 4-14: EDX Response of a Particle Selected from SH00FRP-NH 95

Figure 4-15: EDX Response of a Particle Selected from SH50PL-H 96

Figure 4-16: EDX Response of a Particle Selected from SH50PL-NH 96

Figure 4-17: EDX Response of a Particle Selected from SH50FRP-NH 97

Figure 4-18: SEM Imaging and EDX Response of the Particle with Sodium from SH00FRP-NH Sample #1 98

Figure 4-19: SEM Imaging and EDX Response of the Particle with Sodium from SH00FRP-NH Sample #4 98

Figure 4-20: SEM Imaging and EDX Response of the Particle with Sodium from SH50PL-NH Sample #8 99

Figure 4-21: SEM Imaging Results Using Ion Beam Cuts for SH50PL-H Particle #1: (a) Top View, (b) Cut Section View, and (c) Top View of Ion Beam 100

Figure 4-22: SEM Imaging Results Using Ion Beam Cuts for SH50PL-H Particle #2: (a) Top View, (b) Cut Section View, and (c) Top View of Ion Beam 101

Figure 4-23: SEM Imaging Results Using Ion Beam Cuts for SH50PL-H Particle #3: (a) Top View, (b) Cut Section View, and (c) Top View of Ion Beam 101

ABSTRACT

This research study is motivated by the need to reduce the costs of maintenance and repair of the aging transportation infrastructure in the US. The proposed approach is to use self-healing concrete. The objective of this study is to test the hypothesis that composite action due to fiber reinforced polymer (FRP) confinement of cylindrical concrete specimens may improve the self-repairing properties of self-healing concrete materials. Sodium silicate (Na_2SiO_3) is utilized as healing agent in this research. Concrete cylinders with 0.0%, 1.0%, 2.5%, and 5.0% of sodium silicate (SS) by weight of cement were cast and tested to evaluate the effectiveness of different content of SS on the self-healing capacities of concrete. Unconfined and FRP wrapped concrete cylinders were prepared for each different SS content level in order to investigate the effect of the FRP confinement on the self-repairing properties of concrete in terms of stiffness recovery and strength variation. The experimental results obtained from the stiffness tests were inconclusive. Several hypotheses were proposed and tested to explain the possible reasons why the self-healing mechanism was not activated. A second set of stiffness tests and a series of scanned electron microscopy (SEM) tests were designed and performed to investigate the different hypotheses proposed. The conclusions of this additional series of tests are: (1) Insufficient healing and poor SS microcapsule quality are not the reasons why the self-healing mechanism was not activated. (2) The results of the SEM tests suggest that the microcapsule shell may have had durability problems within the concrete environment and that the microcapsules may have been already broken and their content may have already solidified before the stiffness test was performed.

1 INTRODUCTION

1.1 Motivation

The aging civil infrastructure in the United States is faced with a serious challenge for maintenance and repair using only limited available social and economic resources. For example, the average age of a bridge in the US is 43 years, with a design lifetime usually assumed equal to 50 years at the time of their design. The American Association of State Highway and Transportation Officials (AASHTO) estimated that the cost to repair every deficient bridge in the country would be approximately $140 billion (AASHTO 2008). This repair cost does not include the cost associated with mandated annual bridge inspections, or the cost associated with traffic restrictions on structurally deficient or functionally obsolete bridges. Immediate improvement of this situation is difficult due to the economic crisis that the US has suffered in recent years. A long-term solution of this problem can only be accomplished with novel and transformative approaches that can significantly reduce the costs related to monitoring, inspection, maintenance, and repair of the infrastructure system.

This research explores one possible solution for this problem based on the new paradigm known as “self-healing concrete”. Self-healing concrete can be defined as concrete with the ability to automatically heal cracks that may generate throughout its structure. By introducing self-healing properties into the concrete material, it is expected that the long term reliability of concrete structures will improve, with the goal of positively impacting the transportation and concrete constructions in general. In addition, this research investigates the capabilities of improving self-healing concrete properties through composite action produced through confinement of the concrete using fiber reinforced polymers (FRP).

Self-healing concrete has received increasing attention as a smart material with interesting potential application in civil infrastructure (Sharp and Clemena 2004). Four mechanisms have been widely investigated for self-healing concrete application in recent years, i.e., hollow glass fiber systems (Thao et al. 2009), microencapsulation of self-healing agents (Min et al. 2012), bacteria-based self-healing concrete (Jonkers et al. 2010), and shape memory alloy (SMA) system (Sakai and Fukuta 2003). This research focuses on the use of microencapsulation of self-healing agents.

Since introduced at the end of the 1950's, microencapsulation has been modified and adapted for numerous purposes and applications. It has been tested and used in several industries, e.g., photography, printing, food, textile, biotechnology, electronics, agriculture, waste treatment, and medical. Considerable work has been done to evaluate its practical potential in construction materials including concrete, mortar, lime, cement, marble, sealant, and paints (Boh and Sumiga 2008). However, the results in field applications of self-healing concrete based on microencapsulation have not yet been satisfactory, since it is very difficult to limit the size of the cracks in the concrete to less than 150 μm (size beyond which the self-healing mechanism cannot be activated, see Yang et al. 2009).

FRP products have been used for more than two decades as confinement of reinforced concrete (RC) columns to improve their structural performance in terms of ultimate load bearing capacity and ductility (Nanni and Bradford 1995, Seible et al. 1997). The use of FRP confinement for RC cylindrical columns derives from the fact that, when concrete is subjected to an axial compression load, the concrete tends to expand laterally and to load the FRP confining jacket in axial tension along the radial direction. Thus, the concrete core of the column becomes subjected to a three-dimensional (3D) compressive stress condition, which can significantly

increase the compressive strength and the ductility of otherwise brittle concrete. It is noteworthy that, while extensive research is available to document the positive effects on strength and ductility due to FRP confinement of RC columns subjected to axial and bending actions, no information is available in the literature regarding the effects of FRP confinement on self-healing concrete.

Thus, the driving motivation of this research is the hypothesis that the use of the composite materials may significantly promote the efficiency of the self-healing materials by providing confinement and limiting the internal and/or external crack size to the healing capacity of the self-healing mechanism.

1.2 Objectives and Scope

The main objective of this research project was to test the hypothesis that composite action in RC structures can drastically improve the self-repairing properties of self-healing concrete materials (see Figure 1-1). Figure 1-1 (a) represents the behavior of a specimen of unconfined self-healing concrete. When an axial load is applied to the concrete cylinder, the concrete specimen starts cracking. As the applied axial load increases, cracks' count and size increases. When the load is removed, the self-healing mechanism is activated in the concrete and the cracks partially close. However, if the cracks are too large, the self-healing mechanism cannot activate and the cracks do not close. The self-healing mechanism hypothesized for FRP-confined concrete is represented in Figure 1-1 (b). The application of an axial load produces the opening of cracks in the concrete. The width of these cracks is smaller than in the case of unconfined concrete, providing a significant advantage for activation of the self-healing mechanism. In addition, when the applied axial load is removed, the confinement provided by the FRP contributes to the closing of the concrete cracks even more. It is expected that the width of

concrete cracks can be reduced significantly, thereby activating the self-healing mechanism and virtually healing all concrete cracks.

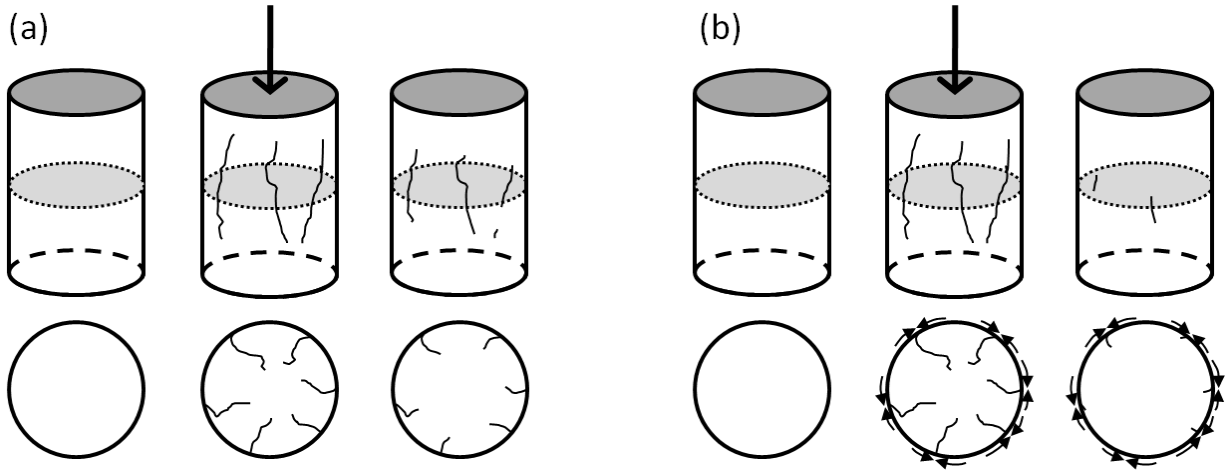


Figure 1-1: Hypothesis of Improved Self-Healing Mechanism due to FRP Confinement: (a) Self-Healing in Unconfined Concrete, and (b) Self-Healing in FRP-Confined Concrete

The goal of this research was to significantly advance the self-repairing capability of RC bridge components and systems. This capability is currently limited to the closure of small surface cracks produced in a controlled environment. This self-healing property mimics the self-healing of human skin after small cuts. It is hypothesized that the composite action due to confinement with FRPs can help close larger cracks in the concrete. In comparison with the human body, this self-healing capability would be equivalent to the cicatrization of deep cuts and the healing of bone fractures.

This research explored a completely innovative and untested idea, since it represents the first attempt of using composite action to enhance the performance of self-healing concrete materials. This research focused on self-healing concrete based on microencapsulation of self-healing agents and confinement with glass FRP of cylindrical concrete specimens.

1.3 Thesis Outline

Chapter 1 of this thesis gives an introduction and illustrates the motivation and the objective of this research.

Chapter 2 presents a literature review on application of microencapsulation in self-healing materials, use of FRP products in civil engineering as external confinement, and utilization of the scanning electron microscopy (SEM) technology for analysis of material compositions and behavior.

Chapter 3 presents the experimental equipment, testing protocol, and result analysis of the self-healing test. This chapter describes three phases of experimental tests: (1) a preliminary strength test, (2) the stiffness test, and (3) the strength test. The preliminary strength test is conducted to estimate the strength and the modulus of the concrete material, which is necessary to finalize the testing protocol for the stiffness test. Results regarding the self-healing stiffness and strength tests are presented and discussed. This chapter also reports ASTM specifications and safety procedures with respect to concrete stiffness and strength test, which were followed during the experimental testing.

Chapter 4 presents the hypotheses made to explain the non-activation of the self-healing mechanism, as well as the methodology and results of the additional experimental campaign performed to investigate the proposed hypotheses.

Chapter 5 presents the conclusions of this study, makes recommendations for implementation of the results presented, and provides suggestions for future research.

2 LITERATURE REVIEW

2.1 Introduction

This research investigated the interaction between two different technologies: (1) microencapsulation-based self-healing concrete, and (2) FRP-based confinement of concrete. In this chapter, a brief literature review of commonly used self-healing methods in concrete is provided. A more detailed literature review about these two technologies is presented, which focuses on the application studied in this research project and on previous research completed by other researchers at Louisiana State University (LSU).

In addition, a brief literature review on the SEM technology, which was adopted in this research to shed light on some of the obtained results, is also provided.

2.2 A Brief Review of Self-Healing Methods in Cementitious Materials

2.2.1 Autogenous Healing of Concrete

The first applications of autogenous healing concrete were developed in the field of structures subjected to water pressure load, e.g., basements, water retaining structures and reservoirs, for which water-tightness is an important consideration in addition to load carrying capacity and durability. Although the design of this type of structures tries to minimize cracks by using concrete as a compressive material only, cracks will generally occur throughout the service life of RC structures because of restrained shrinkage of concrete, or other external factors such as excessive loading and harsh environmental exposure (e.g., freeze-thaw cycles, wet-dry cycles). Due to the presence of the cracks, the permeability of the concrete increases to certain extent, and may further cause serviceability and durability problems of the structure. It was observed that fractured concrete, under favorable temperature and moisture conditions, can exhibit partial or complete recovery of its original integrity (Kurinnyi 1955, Lauer and Slate 1956). This

phenomenon is defined as autogenous healing of concrete. Thus, the key motivation of research on autogenous healing of concrete is the fact that the cracks in the concrete can be healed to certain extent over time, the permeability of the concrete can be reduced, and properties such as the freeze-thaw resistance can be increased.

The autogenous healing of concrete was first observed by the French Academy of Science in 1836 in water retaining structures, culverts, and pipes (Hearn and Morley 1997). This phenomenon was studied by Hyde and Smith at the end of the nineteenth century (Hyde and Smith 1889). A more systematic study of the autogenous healing was conducted by Glanville (1931), who made a distinction between concepts of self-healing and self-sealing. Self-healing was defined as recovery of concrete strength as well as closure of leaking cracks, whereas the self-sealing was defined as a procedure that would close leaking cracks without recovery of the concrete strength. Additional research was performed after Glanville's work to further prove the contribution of autogenous healing to the recovery of concrete strength and to study its effects in cementitious materials (Lauer and Slate 1956, Kurinnyi 1955). Numerous studies were completed to gain extensive knowledge regarding the influence of autogenous healing on permeability and freeze-thaw resistance of the concrete since the 1980's. It was found that the highest autogenous healing rate of the cracked concrete occurs during the first three to five days of water exposure, and the permeability of the concrete can be reduced by one to twenty percent of the initial value after a five to twenty weeks' testing period (Edvardsen 1999). It was also showed that autogenous healing can increase the frost resistance of concrete by about 3-4 times at -17 ºC and about 2-2.5 times at -50 ºC under discontinuous freezing and thawing (Sukhotskaya et al. 1983).

Autogenous healing was investigated under various conditions. The effects of various parameters on autogenous healing were discussed in previous works, e.g., crack width, water pressure, pH of healing water, temperature, water hardness, water chloride concentration, and concrete composition (Edvardsen, 1996, Aldea et al. 2000, Reinhardt and Jooss 2003). A few mechanisms have been proposed to explain the autogenous healing in concrete (Wu et al. 2012):

(1) crystallization of calcium carbonate or calcium hydroxide;

(2) further hydration of the unreacted cement or cementitious materials;

(3) closing of cracks by solid matter (impurities) in the water by losing concrete particles resulting from crack spalling; and

(4) expansion of the concrete in the crack flanks (swelling of calcium silicate hydrate (C-S-H)).

Among these possible explanations, most researchers agree that crystallization of calcium carbonate within the crack is the main mechanism for self-healing of mature concrete (Yang et al. 2009).

2.2.2 Embedment/Encapsulation of Healing Agents

Two main mechanisms for the embedment of healing agents in concrete have been thoroughly investigated in the last few decades: (1) hollow fiber systems, and (2) microencapsulation of healing agents (Wu et al. 2012). As indicated by the names of the methods, the hollow fiber systems introduce healing agents in the concrete through hollow fibers (sometimes referred to as hollow pipettes or tubes depending on the diameter), whereas the microencapsulation method consists in encapsulating the healing agents within microcapsules that are added to the concrete mixture. The main idea of the embedment of healing agent method is the encapsulation, embedment, release and hardening of healing agents inside the host material matrix. Self-healing happens when the mechanism is triggered by the crack-induced rupture of

the embedment container. The microencapsulation system is the self-healing method used in this research and will be discussed in the next part of this chapter.

The idea of the hollow fiber system is to seal healing agents using hollow fibers and then embed the agent-filled fibers into the tension functional part of the host matrix. Thus, when cracks generate in the component under external load or other forces, the fibers break and the sealed healing agents flow into the cracks under the effect of gravity and capillary action. The hardening of the healing agents inside the cracks completes the healing procedure, which contributes to the recovery of load carrying capacity and stiffness, or reduction of permeability of the component (see Figure 2-1). The hollow fiber system provides an active mode of repair for

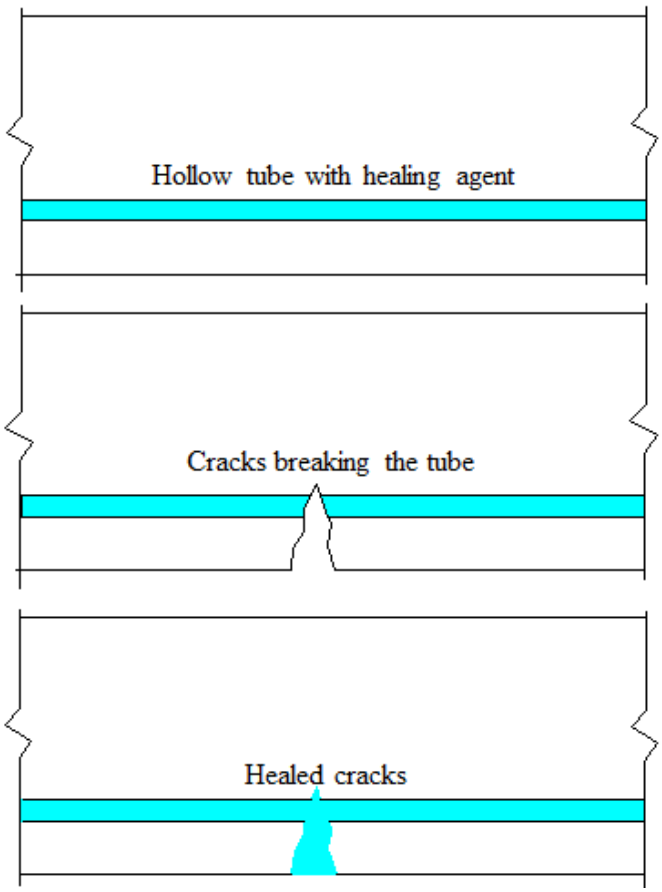


Figure 2-1: Healing Mechanism for Hollow Fiber Systems

the damaged structural components since the healing process is triggered by the damage and completed without external interference. Compared to passive mode of repairs, e.g., manual injection of the healing agent in the visible cracks, the hollow fiber system possesses great potential due to the fact that it may reduce the cost tremendously of health monitoring, damage detection, and maintenance of concrete structures.

The hollow fiber system requires an external or an internal healing agent supply system, on the method used to deliver the healing agent into the host matrix. Figure 2-2 shows a typical

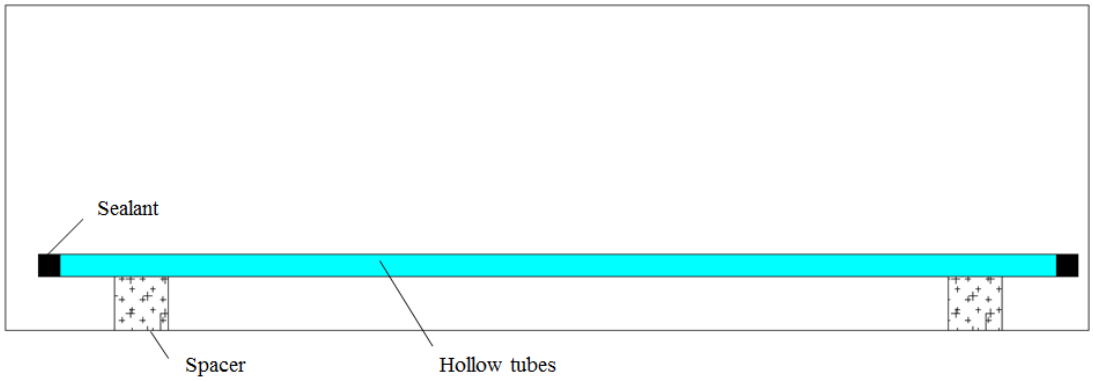


Figure 2-2: Internal Healing Agent Supply System (adapted from Thao et al. 2009)

layout of an internal healing agent supply system. The fiber containing healing agents is completely embedded into the component with both ends sealed. The hollow fiber was first proposed into self-healing concrete research and proven effective by Dry for self-healing of concrete beams (Dry 1990, Dry 1994). The delivery system was designed as an internal supply system with hollow porous polypropylene fibers containing methylmethacrylate (MMA) liquid as healing agent. Significant reduction of permeability was observed in the specimens with the self-healing system compared to the control group after the healing procedure. In a later work by Dry and McMillan (Dry and McMillan 1996), hollow channels were cast to encapsulate a three-part adhesive system (100 parts MMA, 4 parts cumine hydroperoxide and 2 parts cobalt

neodecanoate). A 20% increase of load carrying capacity was observed for self-healing beams after curing when compared to ordinary beams tested under the same three-point bending tests protocol. In addition, this system was demonstrated to possess the ability to restore flexural strength of components after impact damage (Pang and Bond 2005, Trask and Bond, 2006), and to regain elastic modulus under controlled laboratory conditions (Li et al. 1998).

However, only low self-healing efficiency was achieved using internal agent supply system, due to the fact that the healing agents cannot be injected into the cracks in sufficient quantity to achieve healing. The negative pressure forces produced by the sealed ends of the capillary tubes were believed to be responsible for the insufficient release of the healing agents into the cracks (Joseph et al. 2010). Under these conditions, the capillary attractive forces of the cracks and the gravitational force applied to the fluids were not sufficient to overcome the resistive forces of the tube and the negative pressure forces from the ends. Thus, in order to overcome these issues, an external agent supply system was proposed to increase the amount of healing agents entering the cracks.

Figure 2-3 shows a typical layout of an external healing agent supply system. The hollow fiber is sealed on one end and connected to the healing agent container on the other end, with both ends coming out from the structural component. Mihashi et al. (2000) and Joseph et al. (2007) conducted studies using similar external healing agent supply systems as the one shown in Figure 2-3. In Mihashi's research, glass pipes of outer diameter of 2 mm and inner diameter of 0.8 mm, respectively were filled with three different healing agents, i.e., a diluted (27%) alkali-silica solution, a non-diluted alkali-silica solution, and a two-component-blended-low-viscosity epoxy resin (Mihashi et al. 2000). The results showed that specimens with diluted and non-diluted alkali-silica solutions as healing agents obtained average strength recovery ratio of about

1.1 and 1.5, respectively, when compared to the ordinary specimens. However, specimens with the epoxy resin as healing agent showed little strength recovery. The researcher attributed this result to the insufficient mix of the two components. In Joseph's research, ethyl cyanoacrylate (CA) was encapsulated using curved plastic tubes with outer diameter of 4 mm and inner diameter of 3 mm (Joseph et al. 2007). Successful self-healing was observed in terms of recovery of the post-cracked stiffness, peak load, and ductility. In addition, significant penetration of the ethyl CA glue into the crack surfaces was observed under the capillary suction forces and gravity.

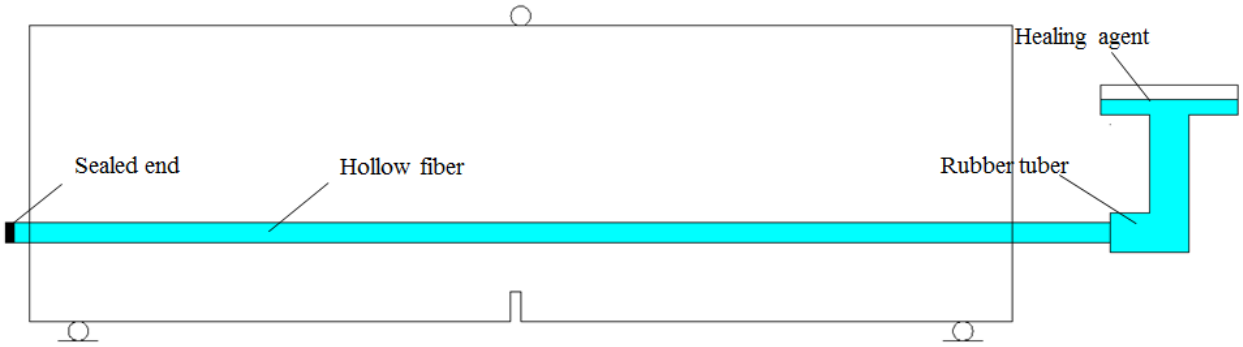


Figure 2-3: External Healing Agent Supply System (adapted from Mihashi et al. 2000)

Even for the external healing agent supply system, low healing efficiency has been one of the key factors that limited the development and application of the hollow fiber system in self-healing concrete. Sun et al. (2011) investigated the maximum healable crack width utilizing this mechanism and concluded that the best results were obtained when the crack width was limited to 0.3 mm. Considerable research efforts have been directed toward enhancing the healing agent delivery efficiency (the amount of healing agents that flow and becomes embedded into the cracks) and thereby the healing efficiency of this mechanism. A comparison study showed that glass fibers are more suitable to be used as carrier fiber due to the chemical inertness to epoxy resin and the brittleness which allows easier rupture when cracks are initiated (Thao et al. 2009).

Mihashi et al. (2000) introduced a low viscosity alkali silica solution as healing agent. Dry (1994) used a vacuum pump to inhale the healing agent from the tank into the glass tubes.

Traditional hollow fiber systems are usually designed to heal a single damage event in a given location. The self-repairing ability disappears once this location is depleted of healing agents. Toohey et al. (2007) proposed a coating-substrate delivery system (see Figure 2-4) in order to achieve automatic healing under repeated damages. Instead of using one or a few hollow fibers as the carrier of the healing agents, a 3D microvascular network was designed as the delivery system of dicyclopentadiene (DCPD) monomer. The vertical channels were used to deliver the monomer to the damaged position, whereas the horizontal channels enable the network to be refilled from the side. An acoustic emission sensor was used to detect the cracking of the substrate. Significant self-healing in terms of fracture toughness was observed after each of the seven repeated loading cycles that were applied to the.

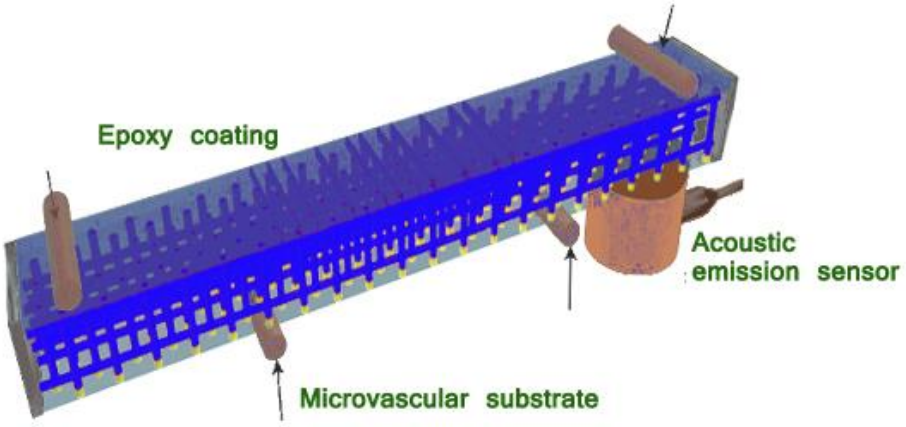


Figure 2-4: Schematic Diagram of the Self-Healing Structure Composed of a Microvascular Substrate and a Brittle Epoxy Coating (adapted from Toohey et al. 2007)

2.2.3 Bacteria-Based Self-Healing Concrete

Promising results toward the application of externally applied mineral-producing bacteria in healing pores and cracks of concrete are documented in the literature (Bang et al. 2001, Ramachandran et al. 2001, Ramakrishnan 2007). In most of the bacteria-based concrete studies, ureolytic bacteria of the genus Bacillus (B.) were used as agent for the biological production of calcium carbonate minerals (Wu et al. 2012). The metabolism of this type of bacteria involves the enzymatic hydrolysis of urea to ammonia and carbon dioxide. In addition, the reaction causes a pH increase from neutral to alkaline conditions, corresponding to the formation of bicarbonate and carbonate ions, which precipitate with the calcium ions in the concrete to form calcium carbonate minerals (Jonkers et al. 2010). The further crystallization of the calcium carbonate minerals heals the pores and cracks in the concrete.

Figure 2-5 shows the schematic diagram of bacteria-based self-healing concrete (Jonkers et al. 2008). The bacteria spores along with some nutrients are mixed into the concrete when it is poured. When a crack initiates in the concrete matrix, moisture and air enter the cracks and activate the bacteria spores, which starts to multiply. The carbon dioxide, which is released from the metabolic process of the bacteria, reacts with the calcium hydroxide, $Ca(OH)_2$, which is leached from the concrete matrix, to form calcium carbonate crystals, $CaCO_3$. The deposition of crystals on the crack surface heals the concrete. The bacterial production of $CaCO_3$ is determined by a number of factors, which include the concentration of dissolved inorganic carbon, the pH, the concentration of calcium ions, and the presence of nucleation sites (areas of extremely localized budding or reaction). The first three factors are provided by the metabolism of the bacteria while the cell walls of the bacteria act as nucleation sites (Tittelboom et al. 2010).

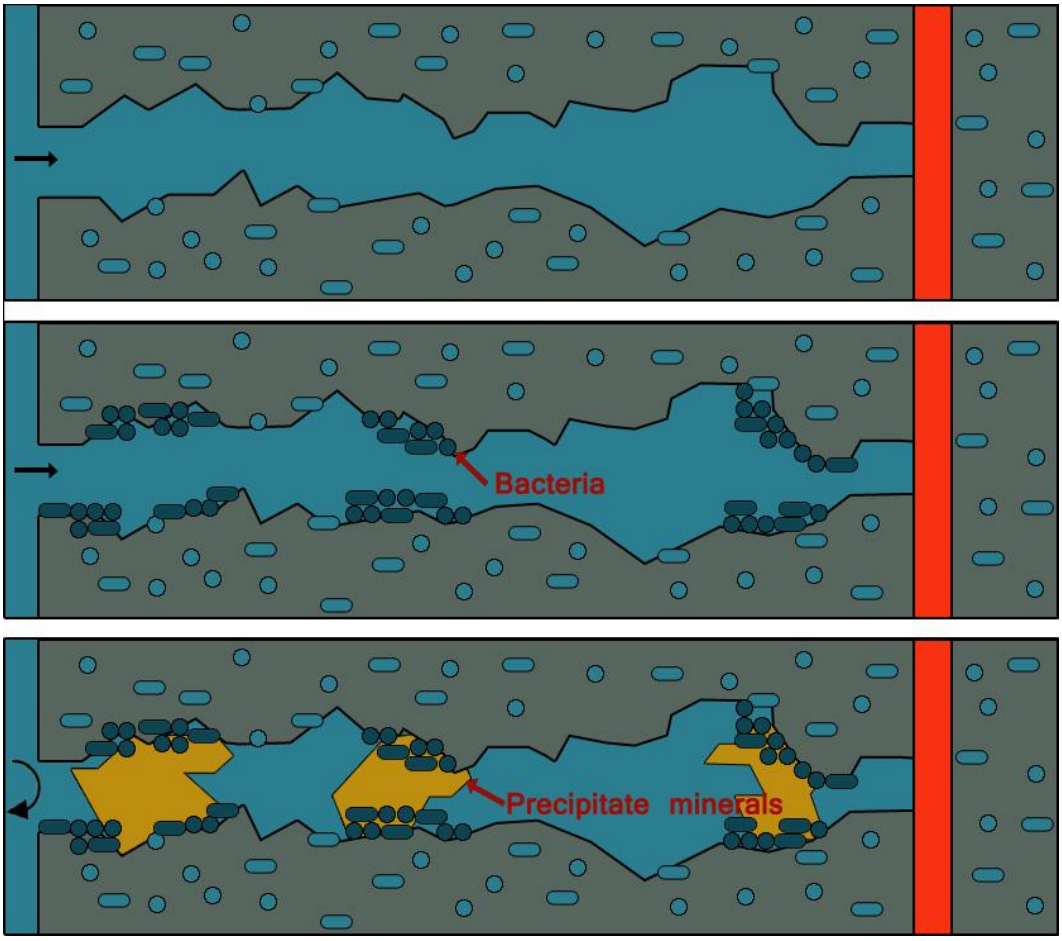


Figure 2-5: Mechanism of the Bacteria-Based Self-Healing Concrete
(adapted from Jonkers et al. 2008)

In Jonkers et al. (2010), two species from the genus Bacillus, the B. pseudofirmus DSM 8715 and the B. cohnii DSM 6307, were tested as healing agent in the self-healing concrete because of their excellent ability to resist high alkalinity and tolerance to oxygen. A comparative study was conducted between yeast extract, peptone, calcium acetate, and calcium lactate to test their applicability as nutrients. It was concluded that cement stone incorporated bacterial spores are able to convert incorporated calcium lactate to calcium carbonate-based minerals under the effect of water entering the cracks. Subsequent research (Wiktor and Jonkers 2011) was conducted to quantify the crack-healing potential of the bacteria-based self-healing concrete. A two-component bio-chemical agent was used in conjunction with B. alkalinitrilicus, an alkali-

resistant soil bacterium, as the healing agent and calcium lactate was used as the nutrient. The healing agent was impregnated into porous expanded clay particles, which acted as reservoir particles and replaced part of the regular concrete aggregates, and then mixed into the mortar specimens. Experimental results showed that cracks were healed in width up to 0.46 mm in bacterial concrete but only up to 0.18 mm in control specimens after 100 days submersion in water.

The viability of the bacteria spores inside the concrete environment has always been a major concern of the bacteria-based self-healing concrete study. Tests showed that the spores remained active only for a limited period of time, as the continuing cement hydration of the concrete crushes the cells when the matrix pore diameters become smaller than 1 μm, which is the size of the bacterial spores (Jonkers et al. 2010). In addition, bacterial activity decreases significantly in the highly alkaline environment inside the concrete (Tittelboom et al. 2010). In their viability tests over the B. sphaericus, Wang et al. (2012) found that the bacteria can remain viable and sustain high urease activity in a sealed sterile vial for about six months. Figure 2-6 shows the results of the viability study over B. cohnii bacterial spores inside of aged cement stone specimens (Jonkers et al. 2010). A substantial decrease of active spore concentration was found after 22 days of curing and almost all spores were found non-active after 135 days of curing.

Because of the viability issues, it is necessary to immobilize bacteria cells/spores before injecting them into or mixing them with the concrete to protect them in the concrete environment. Polyurethane (PU) has been widely used as an immobilization material for enzymes and whole cells because of its high mechanical strength and biochemical inertness. Bang et al. (2001) used cylindrical PU-foam to immobilize bacterial cells, which was used in an external crack repair technique. However, this immobilized healing agent is suitable for repairing of large cracks only

(cracks with a width of 3.18 mm). Tittelboom et al. (2010) incorporated B. sphaericus culture and a calcium source with silica gel. Protection of the bacteria cells using this gel matrix was proven effective as $CaCO_3$ precipitation and enhanced crack repairing were observed. Wang et al. (2012) conducted a comparison study between immobilization using silica gel and using PU, with emphasis on self-healing concrete applications. The experimental results showed that silica gel immobilized bacteria exhibited a higher activity than PU immobilized bacteria in $CaCO_3$ precipitation. However, cracked mortar specimens with PU immobilized bacteria had a higher strength recovery and lower water permeability when compared to specimens with silica gel immobilized bacteria, which indicated that PU immobilized bacteria possess a higher potential for self-healing concrete application than silica gel immobilized bacteria.

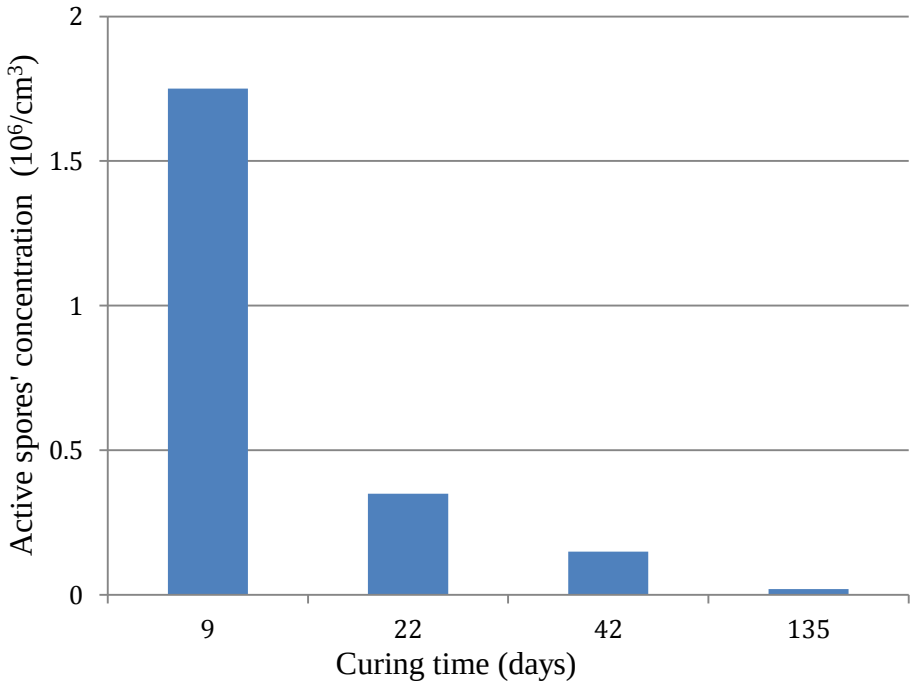


Figure 2-6: Viability Study Results of Bacterial Spores (B. cohnii) in Aged Cement Stone Specimens (adapted from Jonkers et al. 2010)

2.2.4 SMA Systems

The shape memory effect was noticed as early as in 1932, when the reversible transformation in gold-cadmium (Au-Cd) was first observed (Ölander 1932). In 1961, Buehler and Wiley (1961) developed a series of SMAs containing an equi-atomic composition of nickel and titanium (Ni-Ti), which was denoted as Nitinol and soon became the most commonly used type of SMA. Most SMAs exist in two stable and distinct phases: austenite, when $T > T_a$ (the austenite start temperature); and martensite, when $T < T_m$ (the martensite end temperature) (Dong et al. 2011). These two phases are reversible under proper temperature and stress conditions.

SMAs are characterized by two particular behaviors: (1) the shape memory effect, and (2) the superelasticity effect. The shape memory effect (Figure 2-7 (a)) refers to the ability of SMAs to

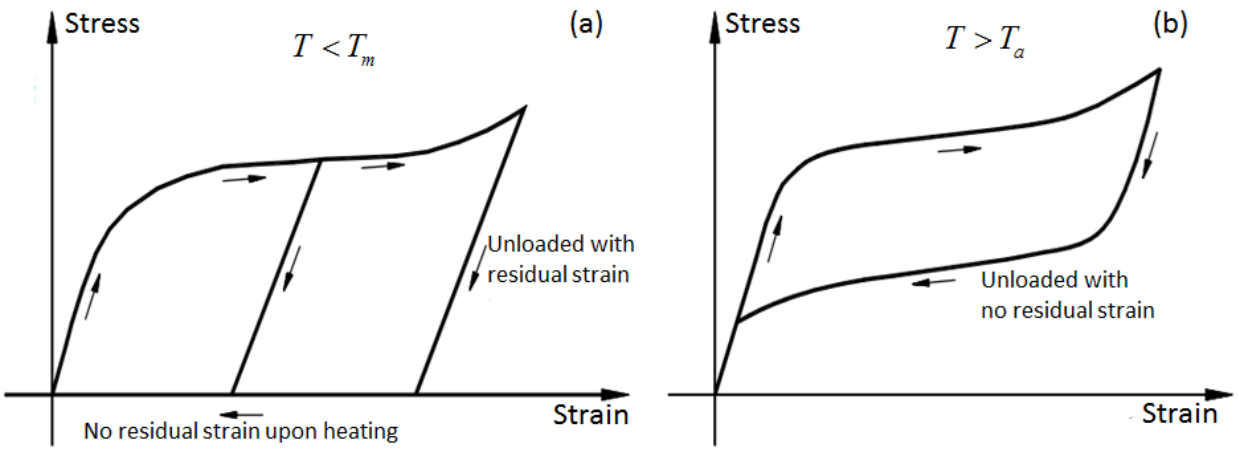


Figure 2-7: Stress-strain Curves for SMAs:
(a) Shape Memory Effect; (b) Superelasticity Effect (adapted from Dong et al. 2011)

undergo reversible transformations between these two phases. In the martensite phase, SMAs are capable to regain part of their residual strain after unloading. Once heated to enter into the austenite phase, all residual strain can be regained and the material transforms back to its original shape. The superelasticity effect (Figure 2-7 (b)) refers to the ability of the SMAs to deform

plastically after certain stress levels in the austenite phase and retrieve their original length and shape upon unloading with no residual strain. Besides these two effects, SMAs possess additional important characteristics, (e.g., hysteretic damping, highly reliable energy-dissipation ability, strain hardening at strains above 6%, and excellent corrosion resistance), which make them suitable for various application in civil engineering (Duerig et al. 1990).

The SMAs have been widely investigated for applications in structural engineering because of their excellent material characteristics, e.g., in isolation devices, energy dissipation devices, braces for frame structures, damping elements for bridges, connectors, and shape restoration (Song et al. 2006). In, addition, the shape memory effect and superelasticity effect of the SMAs endow them with great potential for applications in self-healing materials. Song and Mo (2003) proposed the concept of intelligent reinforced concrete structure with structural health monitoring and rehabilitation abilities using SMA. Figure 2-8 shows an intelligent RC beam reinforced with SMA by post-tensioning. In this beam, the change of electrical resistance of the SMA bars due to their elongation can be used to monitor the crack width in the concrete beam. The SMA cables can be electrically heated after the generation of cracks. The SMA cables can

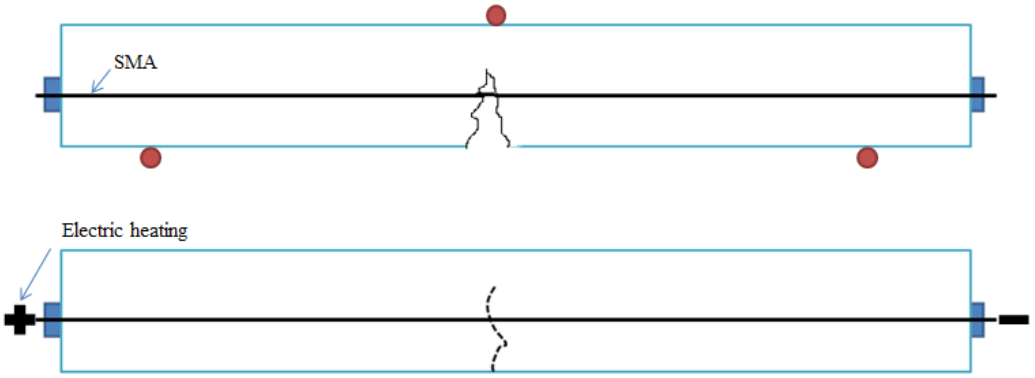


Figure 2-8: Intelligent RC Structure Using SMAs (adapted from Song and Mo 2003)

return to their original length under the shape memory effect, which can lead to the closure of the cracks.

In the experimental research presented in Song and Mo (2006), martensite Nitinol cables were utilized as bottom tension reinforcement for RC beams as shown in Figure 2-8. A crack with a width of up to 0.32 inches was generated through a three-point bending test (Song et al. 2006). Upon removal of the load and electrically heating the cables, this crack was completely closed. Kuang and Ou (2008) investigated self-repairing performance of concrete beams strengthened using superelastic SMA wires in combination with adhesives released from hollow fibers. Static loading tests were carried out in order to confirm the potential self-repairing capacity of smart concrete beams reinforced with SMA wires and brittle fibers containing adhesives. The experimental results showed that the superelastic SMA wires added self-restoration capacity to concrete beams, the deflection of the beams reversed and the crack healed almost completely after unloading. Sakai et al. (2003) performed another experimental research on self-restoration of a concrete beam using superelastic SMA wires, in which the mortar beam with SMA wires recovered almost completely after incurring an extremely large crack.

Most of the SMA-based self-healing concrete studies focused on the use of Nitinol SMA, which possesses superior thermomechanical and thermoelectrical properties compared to other SMAs. However, it is noteworthy that the cost of Nitinol is significantly higher than the cost of constructional steel. This higher cost has negatively impacted the diffusion of SMAs in civil engineering applications. In recent years, several low-cost iron-based and copper-based SMAs have been invented, developed, and commercialized for civil engineering applications. Sawaguchi et al. (2006) found a Fe-Mn-Si-based SMA Containing Nb-C. In their experimental test, four square SMA bars were used as prestressed reinforcement for small-size prismatic

mortar specimens (20mm × 20mm × 80mm, containing 80% of low heat Portland cement and 20% of silica fume) and heated above the start temperature of the reverse martensitic transformation. As a result, a shape recovery strain of 4% and a shape recovery stress of 300MPa were achieved. The chemical composition of the alloy used in their experimental investigation was Fe-28Mn-6Si-5Cr-0.53Nb-0.06C (wt%), which corresponded to the best shape memory properties among all investigated compositions. A feature of this Nb-C-containing Fe-Mn-Si-based SMAs is that the alloys exhibit good shape memory properties that are comparable to those of the training treated (a treatment procedure to enable the SMAs to memorize one or two configurations or shapes in martensite and/or austenite phases) Fe-Mn-Si-based SMAs, without being subjected to the training. Hayashi et al. (2000) studied Fe-Ni-Co-Ti SMA, a magnetically induced SMA with potentially high shape recovery power and low cost. The phase transformation from austenite to martensite was observed when the saturation magnetization was raised from 100 to 150emu/g. A possible composition was identified as Fe-28Ni-18Co-4Ti. The shape memory effect for this SMA showed near linear-elastic behavior up to strains of 0.5% with a Young's modulus of 70GPa.

In a research conducted by Sampath (2005), a Cu-Al-Ni low cost SMA with Al < 12% and Ni < 4% was produced. The strain recovery was reported to be effective up to a 7% strain level. In another experiment of Sampath (2006), a Cu-Zn-Al alloy with 30.36% by weight of Zn and 2.19% by weight of Al (Cu-Zn30.36%-Al2.19%) was produced. For this SMA, the strain-recovery due to shape memory effect was effective for strain levels as high as 8%. The alloy also showed higher hardness and ductility after grain refinement. Omori et al. (2007) developed a ductile Cu-Al-Mn alloys containing over 8% Mn and 17% Al. Using a combination of grain size and texture control, this Cu-Al-Mn alloys exhibited a superelastic strain of about 7%, which is

comparable to that of Ni-Ti alloys. It also showed related functional properties such as functionally graded capabilities, two-way shape memory effect, high damping characteristics, and the invar effect (i.e., exceptionally low thermal expansion effect) (Kainuma et al. 2002). The material cost of Cu-Al-Mn SMAs is as low as that of other Cu-based SMAs, which is about 15 to 30% of that of Ni-Ti SMAs (Araki et al. 2011). Furthermore, machining Cu-Al-Mn SMAs is as easy as machining normal steel. It is envisioned that the total cost (including machining) of Cu-Al-Mn SMAs could be reduced to less than 10% to that of Ni-Ti SMAs, which would make it economically competitive with ordinary steel.

2.3 Microencapsulation-Based Self-Healing Cementitious Materials

2.3.1 Introduction of Concept

The concept of microencapsulation self-healing materials is based on a healing agent being encapsulated and embedded in the host matrix (see Figure 2-9). For some healing agents, a catalyst is needed and mixed into the host matrix along with the microcapsules. When the crack propagates and reaches the microcapsule, the capsule breaks and the healing agent is released into the crack through capillary action (White et al. 2001). The healing agent polymerizes inside the cracks by interacting with the catalyst, and eventually heals the materials by filling its cracks. The healing of the cracks thereby accounts for the recovery of the material properties, e.g., fracture toughness of composites, compressive strength, water permeability, and modulus of elasticity.

Numerous studies have been performed to investigate different encapsulation procedures since the invention of microencapsulation. The major methods available for preparation of microcapsules are (Boh and Sumiga 2008):

(1) The mechanical method, in which the microcapsule wall is mechanically applied around the healing agent.

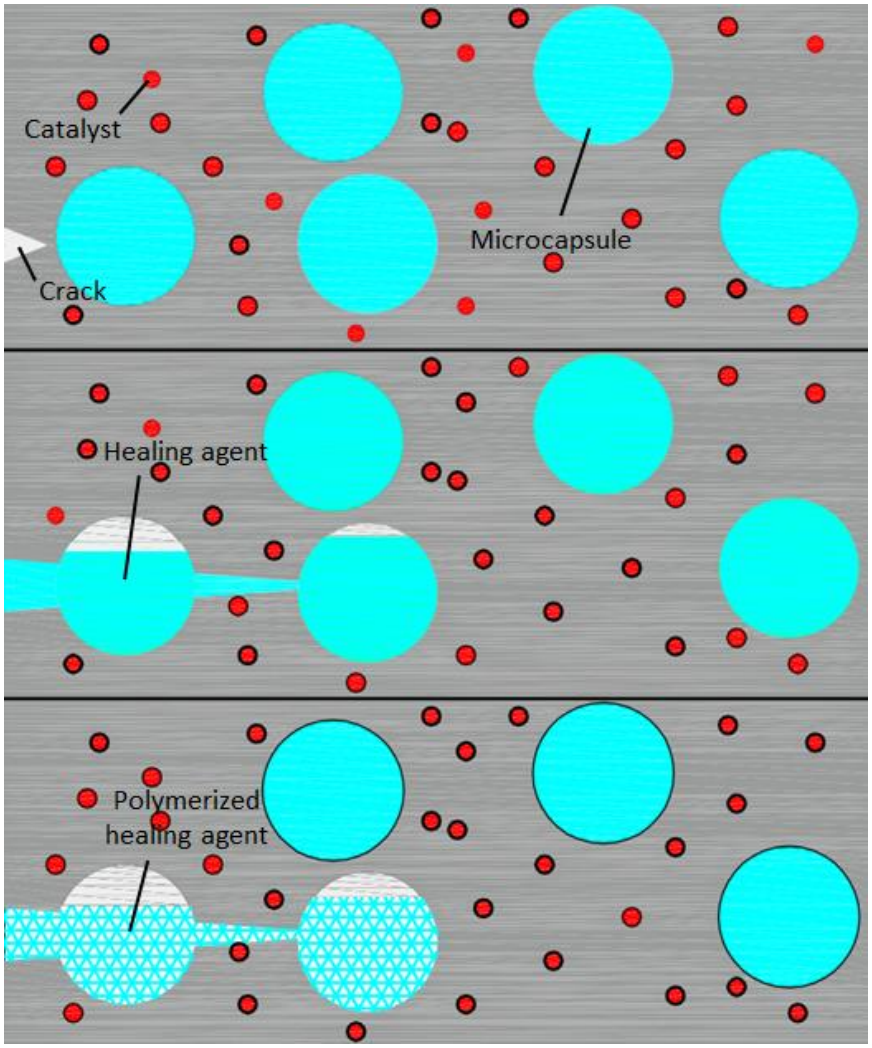


Figure 2-9: Mechanism of Microencapsulation-Based Self-Healing Materials
(adapted from White et al. 2001)

(2) The coacervation method, in which macro-molecular colloid-rich coacervate solidifies with cross-linking agents, and forms a viscous microcapsule wall around a microcapsule core made of the healing agent.

(3) The polymerization method, in which the healing agent is applied in an emulsion and the monomers solidify around the emulsion droplets to form the microcapsule wall. In the in-situ

polymerization, monomers or precondensates are added only to the aqueous phase of emulsion; whereas in the interfacial polymerization, one of the monomers is dissolved in the aqueous phase and the other in a lipophilic solvent.

Several mechanisms have been studied to release the encapsulated healing agents after embedment within the material to be healed, e.g., external pressure, inner pressure, enzymatic degradation, dissolution, abrasion, heat, and light (Boh and Sumiga 2008). The most common mechanism to trigger self-healing materials based on microencapsulation is through external pressure, which ruptures the microcapsule and releases the healing agent from its core. Thus, the microcapsules must be sufficiently strong to remain intact during processing, concrete mixing, pouring, and setting, but it must be sufficiently weak to break during damage of the material. In addition, the microcapsule shell provides a protective barrier between the catalyst and the healing agent to prevent polymerization during the preparation of the composite.

2.3.2 Microcapsule Properties and Shell Materials

The microcapsules' mechanical and geometric properties can affect the mechanical rupture of the microcapsules and thereby the self-healing capability. Such attributes include surface roughness, stiffness, wall thickness, and size of the microcapsules. A sufficiently rough surface ensures enough bonding strength between the matrix material and the microcapsule so that, when the cracks reach the microcapsule, the latter breaks and releases the healing agent instead of detaching from one side of the cracks. The relationship between the stiffness of the capsule and its surrounding host material determines the path of crack propagation. In particular, a lower stiffness of the microcapsules when compared to the surrounding material favors the rupture of the microcapsules (Keller and Sottos 2006). The wall thickness is the key parameter that ensures the survival of the microcapsules during the mixing procedure and the rupture upon triggering of

the crack propagation. Typical wall thickness ranges between 160 to 220 nm, as suggested by Brown et al. (2003). The size of the microcapsules has an essential impact on the fill content and resulting amount of healing agent available upon releasing. It is mainly determined by the agitation rate during the manufacturing process, for which the typical range is from 200 to 2000 rpm (Brown et al. 2003). In Rule et al. (2007) studied the effect of the size and weight fraction of microcapsules on the performance of self-healing polymers containing DCPD microcapsules and Grubbs' catalyst particles. Fracture tests performed on tapered double cantilever beam revealed that the best healing was achieved on specimens with 10 wt% of 386 μm microcapsules.

The selection of the shell materials is also a crucial component to ensure that the healing agent is released in the material when needed. An optimal shell material should be able to encapsulate agents in microcapsules with the proper capsule's geometric and mechanical parameters discussed above during a relatively easy and cost-effective manufacturing process. The production of shell made of urea formaldehyde (UF) is the most technically mature and technique for applications in microencapsulation-based self-healing materials (Kessler et al. 2001, 2002; Brown et al. 2002, 2003, 2005). Usually, this type of shell is manufactured using the in-situ polymerization technique, where urea and formaldehyde monomers are dissolved in a suitable stabilized core material aqueous emulsion. The reaction of the urea and formaldehyde creates a light molecular weight pre-polymer, which grows when the process continues and deposits at the interface between the healing agent and water. This urea-formaldehyde polymer becomes highly cross-linked and forms the microcapsule shell. Pre-polymer nanoparticles deposit on the surface of the microcapsules, which provides a rough surface that increases the adhesion of the microcapsules with the host material (Murphy and Wudl 2010). It is reported that the microcapsules made using this procedure average 10-1000 μm in diameter, with a smooth

inner membrane of a thickness about 160-220 nm and a fill content rate of 83-92% for liquid form healing agents (Brown et al. 2003). The UF shell has shown promising results in encapsulation of healing agents such as epoxy, DCPD, and SS, for applications in various self-healing materials, e.g., epoxy, fiber-reinforced polymer, structural composites, and cementitious materials (Mihashi et al. 2000; Kessler et al. 2001, 2002; Brown et al. 2002, 2003, 2005; Yin et al. 2007; Feng et al. 2008; Huang and Ye 2011). Thus, UF was selected as the shell material used to manufacture microcapsules in this research for its stability and excellent mechanical properties.

Melamine-formaldehyde (MF) is another well investigated shell material for manufacturing of microcapsules (Su et al. 2007). MF is a hard, thermosetting plastic material produced by polymerization of melamine and formaldehyde. It has been utilized in fire resistant materials. Since it is already a commercially available product in the industry, the material cost is relatively low. A similar in-situ polymerization fabrication procedure is followed for producing MF and UF microcapsules, by using different manufacturing parameters, which determine the properties of the microcapsules. Zhang et al. (2004) investigated the effects of the content of core material and emulsifier as well as of the stirring rate on the mean diameter, morphology, and thermal stabilities of the MF-shell microcapsules. Fan et al. (2010) reported that surface morphology of the microcapsules mainly depends on the pH value and stirring rate, while Su et al. (2006) identified the dropping speed of the shell materials as a key factor influencing the shell structure of the MF-shell microcapsules. The mean size of the microcapsules can range from 5 μm to 60 μm depending on the core material and processing method and parameters (Hu et al. 2009, Pan et al. 2012, and Su et al. 2013). Various core materials, e.g., styrene, n-octadecane, epoxy resins, DCPD, rejuvenator, have been successfully encapsulated with MF-shell microcapsules for applications of refining properties of materials or self-healing materials like asphalt concrete

(Wang et al. 2007, Su et al. 2007, Yuan et al. 2007, Hu et al. 2009, and Su et al. 2013). In addition, Su et al. (2013) evaluated a methanol modified MF pre-polymer as shell material for encapsulation of rejuvenator for self-healing asphalt concrete in order to gain better thermal stability and higher mechanical strength. The capsules were reported capable of standing $180\,^{\circ}C$.

Other shell materials that have been proven effective in microencapsulation of healing agents include PU, melamine-urea-formaldehyde (MUF), and silica/silica gel. Cho et al. (2006) proposed a poly(dimethylsiloxane)-catalyst system, for which hydroxyl end-functionalized poly(dimethylsiloxane) was used as healing agent and PU as the shell material. The catalyst was encapsulated using 50-450 μm PU-shell microcapsules to enhance the stability of the catalyst, whereas the healing agent, in the form of 1-20 μm phase-separated droplets, was added directly into the polymer matrix. This system exhibited advantages in self-healing under humid or wet conditions. MUF-shell microcapsules containing healing agents were produced by in-situ polymerization in an oil-in-water emulsion by Liu et al. (2009). Shell thickness ranged from 700-900 nm and mean capsule diameter was around 120 μm. The authors claimed that MUF-shell microcapsules exhibited superior properties compared to the UF-shell microcapsules in terms of thermal stability, permeability of the shell, and ease of fabrication. Silica/silica gel also showed promising results for encapsulation of healing agents including epoxy, MMA, and SS for self-healing material purposes (Huang and Ye 2011, Kaltzakorta and Erkizia 2011, Yang et al. 2011).

It is well known that only microcapsules with adequate shell's properties and a high durability can encapsulate and isolate the core healing agents from the host matrix until the self-healing process is triggered (Murphy and Wudl 2010). However, defining and producing the appropriate stability and durability of the microcapsules is a complex problem. The kinetics of the polymerization reactions is very sensitive to the parameters of the microencapsulation

process, which is one of the reasons responsible for difficulties of durable microcapsule preparation. Brown et al. (2003) noted that variations in shell and core material quantities, cleanness of glass-ware, and use of an unbalanced mixer can severely affect the thickness of the outer porous layer of the UF microcapsules. Liu et al. (2009) have subsequently reported that UF microcapsules can have thin and rubbery walls due to improper processing conditions, which results in low storage stability and synthesis difficulties. For MF microcapsules, polymerization of melamine pre-polymers starts and leads to formation of cured pre-polymers, which cannot be used for the capsule shell formation, if process duration, melamine to formaldehyde ratio and pH are not suitable (Yin et al. 2007). In addition, Nesterova et al. (2011) found that the nature of the core material strongly affects the microcapsule stability and performance. Thus, experimental procedures developed for one core materials may not be suitable for encapsulation of another agent without modification.

To enhance the stability and durability properties of the microcapsules, some researcher proposed a double-layered shell microcapsule processing method (Li et al. 2008). In Li et al. (2008), polyurea microcapsules were firstly fabricated by interfacial polymerization as inner layer, on which UF resin was coated to form a protective outer layer by in-situ polymerization. These double-layered microcapsules were found to successfully prevent agglomeration and inter-capsule cross-linking and presented enhanced thermal stability.

2.3.3 Healing Agents

Four types of reaction mechanisms for healing agents can be identified based on number of components, delivery mechanism into the host matrix, and different conditions of reaction after release. While some agents require moisture, air, or heat to react and solidify (Figure 2-10 (a)

and (b)) or react with the components in the host matrix (Figure 2-10 (c) and (d)), other agents react with another component mixed in the host matrix (Figure 2-10 (e) and (f)) or provided by

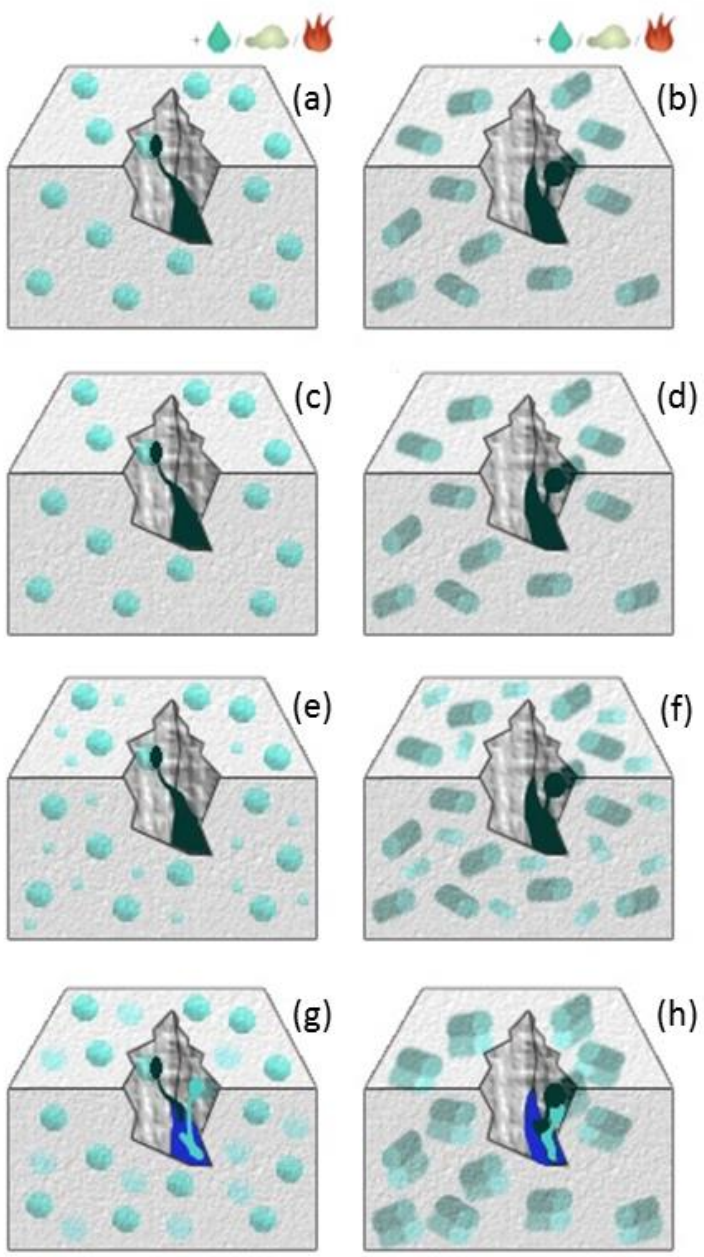


Figure 2-10: Microcapsules-Based Healing Reaction Mechanisms with Agents Encapsulated by Spherical/Cylindrical Microcapsules: (a)-(b) Reaction upon Contact with Moisture or Air or due to Heating; (c) (d) Reaction with the Cementitious Matrix; (e) (f) Reaction with a Second Component Mixed in the Matrix; or (g) (h) Reaction with a Second Component Provided by Additional Microcapsules (adapted from Tittelboom and Belie 2013)

additional microcapsules (Figure 2-10 (g) and (h)) (Tittelboom and Belie 2013). The healing agents could be encapsulated using spherical or cylindrical microcapsules in each of these cases.

Examples of the healing agents requires contact with external elements like the air, moisture and heating (Figure 2-10 (a) and (b)) include tung oil, $Ca(OH)_2$, methyl methacrylate, CA, and epoxy (Thao et al. 2009). In one of their concrete repairing mortar research, Cailleux and Pollet (2009) encapsulated tung oil or $Ca(OH)_2$ inside spherical microcapsules with a gelatin shell. It was observed that the microcapsule shell had viability issues and some of the capsules were broken during the mixing process. However, the remaining capsules were successfully ruptured by the crack propagation and, upon contact with the air, hardening of the tung oil and crystallization of the $Ca(OH)_2$ were identified. Dry (1994) investigated the mechanism in Figure 2-10 (b). Porous polypropylene capsules filled with MMA were waxed before being dispersed into the concrete matrix. After the damage was detected in the concrete beam, the beam was externally heated. The wax around the microcapsules melted and the MMA agent flowed out through the pores of the capsules into the cracks. In a subsequent work, cylindrical glass capsules were manufactured with CA as healing agent, which hardens upon contact with air (Dry 2000). However, it was reported that the CA encountered difficulties to flow out of the glass carriers under gravity and capillary force, and in some cases no healing agent could leak out of the capsules (Joseph et al. 2007).

Compared to agents needing external elements, self-healing agents that react with components of the host matrix (Figure 2-10 (c) and (d)) possess unique advantages in healing micro cracks inside of the material, which is the most likely case for microencapsulation-based self-healing applications. Su et al. (2013) encapsulated rejuvenators (dense, aromatic oils containing a high proportion of maltenes constituents) with methanol-melamine-formaldehyde

microcapsules for self-healing asphalt concrete applications. Once the rejuvenator was released from the capsules, it reacted with the aged asphalt and restored the original ratio of asphaltenes to maltenes of the asphalt, which reduced the formation of additional cracks (Garc á et al. 2011).

SS is another healing agent that reacts with components of the host matrix. The self-healing mechanism of the SS relies on two reactions with the cementitious components. The first reaction happens between SS with calcium hydroxide, which is naturally present in the concrete or in similar materials due to cement hydration (Nonat 2004). The second reaction occurs between sodium hydroxide and silica. A C-S-H product is formed due to these two reactions, which serves as the main mending agent (Huang and Ye 2011). In both reactions, the mending agent residing in an aqueous environment within the microcapsule is very important (Nonat 2004). Water enables further hydration of the damaged cement paste and allows better bonding of the mending agent with the host material. The products of both processes fill the cracks and subsequently contribute to the recovery of mechanical properties (Brown et al. 2005). The concept of microencapsulation-based self-healing concrete with SS as healing agent has been proven by various researchers (Huang and Ye 2011, Pelletier et al. 2011 and Gilford et al. 2013). Huang and Ye (2011) embedded microcapsules filled with SS into engineered cementitious composites (ECC). Recovery of flexural strength was successfully observed. Recovery of flexural strength and reduction of corrosion were also observed in Pelletier et al. (2011), in which SS was encapsulated with a PU shell. In Gilford et al. (2013), the parameters for SS microcapsule preparation were studied. In addition, experimental results showed significant self-healing effect in terms of recovery of the modulus of elasticity (detailed information regarding this research will be provided in a later section of this thesis).

One example of healing agents reacting with another component dispersed in the host matrix (Figure 2-10 (e) and (f)) is the epoxy-hardener system. This is a mechanically stimulated system with embedded healing agents using epoxy as encapsulated healing agent. In order to trigger the healing of the epoxy, a hardener has to be incorporated into the host matrix at the same time. When the crack propagation initiates the rupture of the microcapsules and releases the healing agent inside them, polymerization occurs upon contact of the epoxy with the hardener, which fills the cracks and accomplishes the healing procedure. This system has unique advantages for applications in composite materials since the healing agent is of the same material as the host matrix, which ensures good bonding between the agent and the matrix. In Yin et al. (2007), urea-formaldehyde microcapsules filled with epoxy and an imidazole-metal complex ($CuBr_2(2\text{-MeIm})_4$) hardener were embedded into a woven glass fabric/epoxy composite laminate. However, this system was not autonomous. 95% of the strength of the composite was regained after damage when the system was heated up to $130\,^{o}C$. However, this high temperature of activation makes this system not suitable for concrete or cementitious material applications.

The DCPD-Grubbs' catalyst system is another example of the self-healing mechanism shown in Figure 2-10 (e) and (f). It is a mechanically stimulated system where the encapsulated healing agent and the catalyst are dispersed into the host matrix at the same time. The triggering of the system requires the release and contact of the healing agent with the catalyst inside the crack's surface. The liquid form DCPD is used as the healing agent and usually encapsulated with UF polymer shells. The Grubbs' catalyst is a ruthenium based catalyst (first generation Grubbs' catalyst: Bis(tricyclohexylphosphine) benzylidine ruthenium dichloride) that initiates the ring opening metathesis polymerization (ROMP) of DCPD, the product of which is responsible for the healing of the cracks (Wu et al. 2008). This system has been the most successful and

extensively studied microencapsulation-based self-healing method since its proof of concept by White et al. (2001) in a self-healing epoxy material. Extensive research has shown its effectiveness in a wide range of self-healing materials, e.g., epoxy, structural composites, fiber-reinforced polymer, and concrete, for recovery of mechanical properties like rupture strength, fracture toughness, and stiffness (Kessler and White 2001, Kessler et al. 2002, Brown et al. 2002, Gilford et al. 2012).

Significant research has been performed to identify alternative healing agents for the Grubbs' catalyst system. Ethylidene norbornene was proposed for its significantly faster ROMP speed and lower solidification point (lower than $-78\,^{\circ}C$) than that of DCPD (which varies linearly with the purity of the resin between $-25\,^{\circ}C$ for a 75% DCPD content and $+30\,^{\circ}C$ for a 100% content (DOW 2014)) (Liu et al. 2006). However, DCPD remains the most commonly used healing agent in this system due to its relatively low cost for application in composite materials, wide range of availability, long shelf life, low volatility and viscosity, and its rapid polymerization at ambient conditions upon contact with a proper catalyst (Murphy and Wudl 2010). The major drawback of this system is the stability and cost issues of the Grubbs' catalyst. The first generation Grubbs' catalyst could be deactivated under prolonged exposure to air and moisture. It also loses its reactivity upon contact with diethylenetriamine, which is the agent used to cure the epoxy matrix (Jones et al. 2006). Wilson et al. (2008) conducted a comparison study between different catalysts, i.e., first-generation Grubbs' catalyst, second-generation Grubbs' catalyst, and second-generation Hoveyda-Grubbs' catalyst. The speed of the ROMP of DCPD was found to increase from the first-generation to the second-generation Grubbs' catalyst, and from the second-generation Grubbs' catalyst to second-generation Hoveyda-Grubbs' catalyst. The second-generation Hoveyda-Grubbs' catalyst stayed active, whereas the other two catalysts turned

deactivated upon exposure to DETA. However, the cost issues associated with using Grubbs' catalyst remains in the DCPD-Grubbs' catalyst system due to the limited world supply of Ru (Murphy and Wudl 2010), which makes it unsuitable for applications in cementitious materials, where the cost is the prime consideration due to the vast production of the materials itself.

The two-part epoxy system is the most extensively investigated self-healing mechanism. It consists of two separately encapsulated components (Figure 2-10 (g) and (h)). This system is based on the encapsulation and embedment of both components of the self-healing agent into the host matrix. The two components react and heal the damage of the materials upon contact after being released from the capsules by the triggering mechanism. In Yuan et al. (2008), an epoxy healing agent and a low temperature hardener were both encapsulated and then embedded into a composite material. Successful and rapid self-healing action was observed in the experiments and maximum healing happened when the ratio of the two capsules was kept equal to 1:1. Mihashi et al. (2000) utilized spherical capsules with formaldehyde formalin shells containing a two component epoxy healing agent in their self-healing concrete study. However, it was concluded that hardening of the agent was difficult to be achieved due to the insufficient mix of the two components within the cracks. In another self-healing cementitious material research, Feng et al. (2008) encapsulated a two component epoxy healing agent with spherical UF microcapsules. To promote the mixing of the two components, they added a diluent to the epoxy resin to adjust the viscosity. However, beneficial results were only obtained by thermal curing at $120\,^{\circ}C$.

SS was selected as the healing agent in this research on self-healing concrete because of the following considerations:

(1) The healing process does not require external elements like air, moisture, or heating. The main focus of this research is healing of microcracks inside of the concrete matrix

(2) It is one of the most cost-effective healing agents. Since the ultimate goal of the self-healing concrete research is the industrial application, which means vast production, the cost issue becomes one of the essential considerations.

(3) Previous research have shown more promising results for application of SS as a healing agent in the cementitious materials when compared to other types of agents (Huang and Ye 2011, Pelletier et al. 2011, Gilford et al. 2013).

2.3.4 Review of Applications

Microencapsulation has been object of significant research for its potential applications in construction materials, e.g., for mortar, lime, cement, marble, sealant, and paints (Boh and Sumiga 2008). Significant research has been performed to extend the application of microencapsulation in order to promote one or more material properties, e.g., fire resistance, hydration, degradation resistance, freeze-thaw resistance, expansion resistance, and decrease of water absorption (Kamoto et al. 1989, Parthy 2003, Boh and Sumiga 2008). Microencapsulation of healing agents was first introduced to heal microcracks in structural polymeric materials (White et al. 2001). A wide range of investigation has been conducted since then to explore its potential applications in composite materials, e.g., increasing fracture toughness, reducing fatigue crack propagation, and promoting healing efficiency of self-healing composite materials (Brown et al. 2002, 2006, Kessler et al. 2003). Considerable research has also been done to evaluate microencapsulation of healing agents as a self-healing mechanism in other self-healing material applications, e.g., self-healing coating systems (Zhao et al. 2011), self-healing and antifouling paints for corrosive and bio-corrosive environment (Szabó et al. 2011).

Self-healing concrete provides a proactive approach rather than a reactive countermeasure for cracks that develop within concrete structures. Self-healing concrete materials have been proven effective in terms of reduction of permeability (Reinhardt and Jooss 2003) and recovery of strength and stiffness (Li et al. 1998). As early as in 2001, Katsuhata et al. (2001) tested a capsule-based self-healing system in polymer modified concrete using an approach similar to the concept of microencapsulation. In this system, drops of one-part epoxy with a hardened shell and a liquid core were fabricated as the delivery system. The epoxy hardened after reacting with the alkalis and hydroxide ions after being released in the concrete matrix, which contributed to the healing of the cracks. Regain of mechanical properties of the mortar was successfully achieved using this system.

Various attempts have been made in recent years to introduce the microencapsulation technology into self-healing cementitious materials. Microcapsules with different shell materials and healing agents have been fabricated and applied in self-healing materials, for example cement, mortar and concrete. Yang et al. (2011) proposed a healing agent-catalyst embedment system with the healing agent and catalyst separately encapsulated in silica gel-shell microcapsules. MMA was chosen as the healing agent and an initiator containing triethylborane was used as catalyst. These two types of microcapsules were dispersed into the fresh cement mortar along with carbon microfibers, which was used to mitigate cracking at the micro scale. Permeability tests showed that the gas permeability coefficient of the mortar decreased by 50.2% and 68% at the age of 3 days and 30 days, respectively, after being loaded to 80% of its ultimate strength and healing for 24 hours. The fatigue tests also revealed improved crack resistance and toughness.

Li et al. (2013) proposed an innovative microcapsule for self-healing cementitious material applications. The proposed microcapsule is composed of an epoxy resin core (diglycidylether of bisphenol A epoxy resin) and a shell made of poly styrene-divinylbenzene. The microcapsule was first implemented in self-healing cement paste to test its self-healing capabilities and efficiency. Experimental results showed significant restoration of mechanical properties, e.g., flexural and compressive strength, as well as reduction of water permeability. Self-healing action was further proved by presence of the hardened epoxy within the cracks. In a recent research, Wang et al. (2013) reported successful implementation of an organic microcapsule in self-healing cementitious material. This organic microcapsule featured a UF shell containing epoxy as healing agent. Experimental studies on mortar specimens showed strength recovery up to 9% and a significant reduction of permeability.

Studies have also been conducted to investigate the use of SS as a healing agent for self-healing concrete applications. Huang and Ye (2011) used SS-core microcapsules for developing a self-healing engineering cementitious composite. Significant healing was achieved in terms of recovery of the flexural strength. In addition, the X-ray microanalysis revealed that the healing products formed in the cracks were composites of C-S-H and SS. These findings proved that the main mechanism of self-healing by SS is the crystallization of SS and its reaction with calcium cations. It was also noted that the concentration of the SS microcapsules is the main factor that affects the self-healing efficiency. Pelletier et al. (2011) utilized SS as the healing agent in their microencapsulation-based self-healing concrete research. The SS was encapsulated in PU microcapsules by an in-situ synthesis procedure using interfacial polymerization. The self-healing property was demonstrated in the flexural tests, where the strength recovery of the specimens with microcapsules was at least 10% more than the control specimens. It was also

noted by the authors that the presence of the microcapsules in the concrete did not affect its compressive strength and that the anticorrosive properties of the concrete were significantly enhanced.

While the results obtained in laboratory studies for self-healing concrete have been very encouraging, the results in field applications have not yet been as satisfactory, since it is very difficult to limit the size of the cracks in the concrete to less than 150 μm (size beyond which the self-healing mechanism cannot be activated, see Yang et al. 2009). An emerging research direction focused on improving the performance of self-healing concrete is the development of ECC that can limit the average crack size due to the intrinsic material properties (Yang et al. 2009). Another way to mitigate the propagation of cracks is through combining SMAs with existing self-healing system (Kirkby et al. 2009). It is envisioned that the SMA bars can bring the cracks back to a healable level after the load is removed, which may promote the healing efficiency of the system.

This research investigates another potentially cost-effective approach to limit the average crack size and thereby enhance the efficiency of the self-healing concrete, i.e., external confinement of self-healing concrete cylinders with FRP laminates.

2.4 FRP-Confined Concrete

2.4.1 Confinement Effect

FRP composites have found increasingly numerous applications in structural engineering due to their high strength-to-weight and stiffness-to-weight ratios, high corrosion resistance, and potentially high durability (Einde et al. 2003). One of these applications is the confinement of RC columns with FRP to improve their structural performance in terms of ultimate load bearing capacity and ductility (Nanni and Bradford 1995, Seible et al. 1997).

FRP confinement of RC columns presents numerous advantages when compared to other strengthening techniques, e.g., strengthening using steel jackets. Some of these advantages include small increase in structural size and weight, easy transportation, and good resistance to corrosion and other degradation processes due to harsh environmental conditions (Bakis et al. 2002). This strengthening method has been widely used in retrofitting of bridges and buildings in the past few decades (Flaga 2000, Pantelides et al. 2000, Mertz et al. 2003, Monti 2003, Motavalli and Czaderski 2007).

FRP-confined RC columns behave differently than steel-confined RC columns. In fact, while steel jackets provide a constant confinement after the yielding point of the confining material is reached, FRP jackets provide a linearly increasing confinement force, which better contrasts the expansion of the concrete in the radial direction and significantly reduces the volumetric expansion of the concrete. This phenomenon produces a significantly more ductile behavior of the concrete, which is evidenced by the distinct bilinear shape of the monotonic stress-strain curve (see Figure 2-11) with a smooth transition zone beginning at a stress level close to the strength of the unconfined concrete.

The use of FRP confinement for RC cylindrical columns derives from the fact that, when concrete is subjected to an axial compression load, the concrete tends to expand laterally and to load the FRP confining jacket in axial tension along the radial direction. Thus, the concrete core of the column becomes subjected to a 3D compressive stress condition, which can significantly increase the compressive strength and the ductility of otherwise brittle concrete (Bathe and Ramaswamy 1979). Figure 2-12 shows the failure surface of concrete when subjected to two-dimensional stress conditions. It is observed that the compressive strength of concrete subjected

to biaxial compressive loading (point 2 in Figure 2-12) is significantly higher than the corresponding strength of concrete subjected to uni-axial compression (point 1 in Figure 2-12).

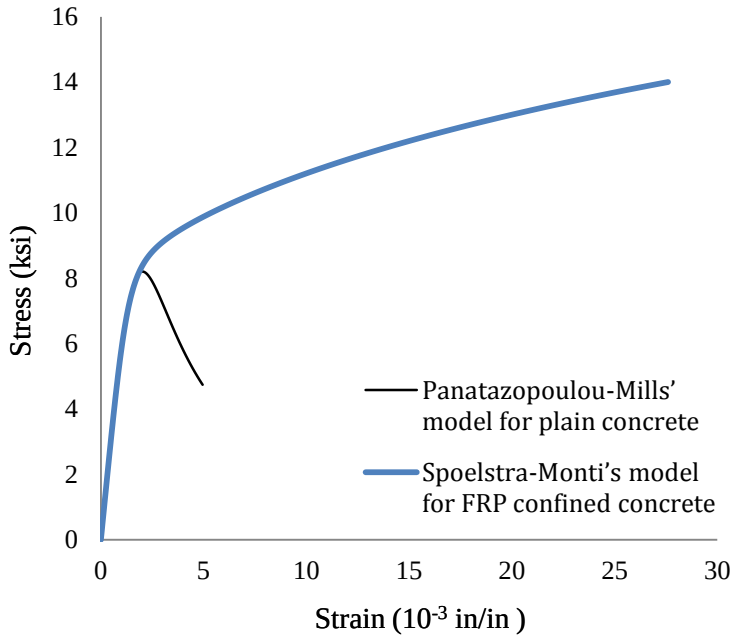


Figure 2-11: Stress-Strain Response for FRP Confined Concrete (Pantazopoulou and Mills 1995, Spoelstra and Monti 1999)

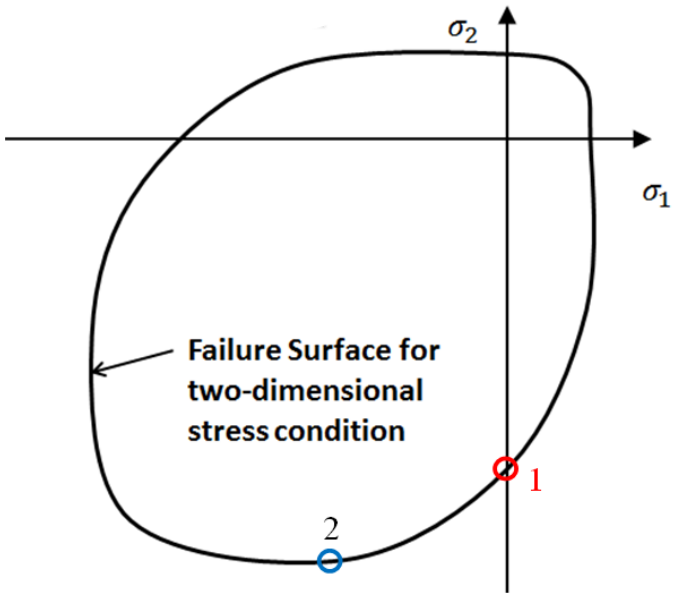


Figure 2-12: Multi-Surface Plasticity Model for Concrete Subjected to Biaxial Loading (adapted from Murray et al. 1979)

Candappa et al. (2001) conducted experimental research on strain-stress performance of concrete cylinders subjected to 3D compressive loading. The concrete cylinders were longitudinally loaded with confining pressure of 0, 4, 8 and 12MPa applied around the lateral direction. Two specimens were tested for each of the confining pressure levels. From the experimental results, the compressive strength increased greatly under 3D loading conditions: the strength of the concrete specimens subjected to axial loading with a confining pressure of 12MPa was 100MPa, i.e., about 2.5 times the strength of the specimens subjected to one-dimensional axial loading, which was equal to 40MPa. In addition, concrete exhibited a substantially improved ductility performance under 3Dstress conditions: the ultimate axial strain of the concrete specimens subjected to axial loading with a confining pressure of 12MPa was equal to 0.016, i.e., about 8 times the ultimate axial strain of the specimens subjected to one-dimensional axial loading, which was equal to 0.002.

It is noteworthy that, while extensive research is available to document the positive effects on strength and ductility due to FRP confinement of RC columns subjected to axial and bending actions, no information is available in the literature regarding the effects of FRP confinement on self-healing concrete. Thus, one potential benefit to confine the self-healing concrete with FRP sheet is to improve its self-repairing capability and efficiency.

2.4.2 Anticorrosive Effect

Concrete is widely used as a compressive construction material because of its low cost and excellent compressive performance. However, with an extremely small fracture energy when compared to that of mild steel (about $0.1\,kJ/m^2$ vs. $100\,kJ/m^2$), concrete is known to be inherently brittle and to crack under tensile stress (Yang et al. 2011). Once micro-cracks form within the concrete matrix, it is very difficult to detect and repair these cracks in time using existing

techniques before they develop into macro-cracks, which can significantly hinder the performance of concrete structures, e.g., by reducing the strength and the stiffness of the material and inducing corrosion problems. The most severe corrosion problems in RC structues are mainly caused by chloride contamination in marine structures and deicing salts used in winter for specific structures, e.g., bridges (Pantazopoulou et al. 2001). Expansive forces are generated in concrete because of the expansion of the corrosion products, which leads to spalling of the cover and further accelerates the steel reinforcement disintegration. While the mechanical properties of the concrete can be restored by other techniques, corrosion can destroy concrete structures from inside and can substantially shorten their service life.

FRP confinement is one of the most cost-effective approaches among the different techniques available to protect RC structures from corrosion. The anti-corrosion effect of FRP confinement was proven and investigated for different RC elements by various researchers (Lee et al. 2000, Badawi and Soudki 2005, Masoud and Soudki 2006). Masoud and Soudki (2006) suggested that the reinforcement mass loss can be reduced by up to 16% using FRP confinement (Figure 2-13). In a long-term study (3 years) by Suh et al. (2007), the metal loss and corrosion rate of FRP-wrapped specimens were found significantly lower than those of un-wrapped ones. In Lee et al. (2000), damaged FRP-confined and unconfined concrete cylinders were subjected to the same accelerated corrosion regime. Experimental results showed that FRP confinement greatly reduced the rate of corrosion after the FRP confinement was applied, resulting in a 50% decrease of the rate of corrosion. No additional loss of strength or stiffness and only a slight reduction in the ductility were observed in the FRP-confined specimens.

Wootton et al. (2003) studied the effect of several design variables, including type of epoxy resin, FRP fiber orientation, and number of confinement layers, on the anti-corrosive

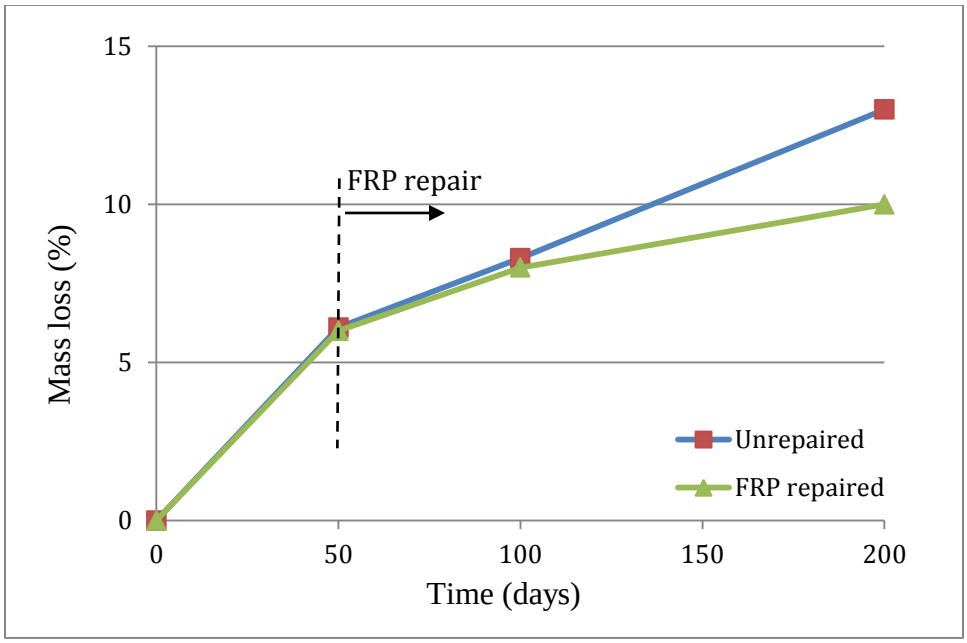


Figure 2-13: Average Reinforcement Mass Loss for Unconfined and FRP-Confined Specimens (adapted from Masoud and Soudki 2006)

performance of carbon FRP-confined concrete cylinders. Experimental results showed that the type of epoxy can significantly affect the resistance of RC specimens to accelerated corrosion in terms of extending life, decreasing overall rate of reinforcement mass loss, and reducing concrete chloride content. Increasing the number of laminates and applying the FRP along the hoop direction also promoted the anti-corrosive performance of RC structures. Spainhour and Wootton (2008) indicated that the type of epoxy has a stronger impact over the thickness of the confinement on the corrosion resistance ability of RC, while Gadve et al. (2009) found that confinement with glass FRPs worked better than confinement with carbon FRPs in reducing the corrosion of the reinforcement, which was explained based on higher electrical resistance of glass fibers when compared to carbon fibers. In addition, it was reported that grouting the voids between the FRP laminates and the core material surface with either conventional or expansive grouts enhances the anti-corrosive properties of this system (Pantazopoulou et al. 2001).

Therefore, an additional benefit of confining the self-healing concrete with FRP laminates is to increase its corrosion resistance capabilities. These improved capabilities can significantly prolong the service life of the self-healing concrete, and prohibit the corrosive components from infiltrating into the cracks, when structural damage happens. In this way, a preferable reaction environment is provided for the self-healing mechanism, which ensures the sealing of the cracks and thereby the healing of the concrete.

2.4.3 Behavior of FRP-Confined Concrete

Significant research has been performed to investigate the behavior of FRP-confined RC columns with square or rectangular cross-sections, for which a lower level of confinement efficiency can be reached (Micelli and Modarelli 2013). This reduced confinement efficiency depends on the geometry of the column, corners' radii, and cross-sectional aspect ratio (defined as the depth (longer side)/width (shorter side) of the cross-section of prismatic members), which can cause non-uniform distribution of the stress in the FRP confinement. The square or rectangular sections lead to a variation in lateral confining pressure distribution from a maximum at the corners to a minimum in between, which is in contrast to the even confining pressure observed for circular columns in order to achieve the full confinement effect (Rahul and Urmil 2013). The unevenness of the distribution of confining stress is proportional to the corner radius or corner radius ratio (which is defined in the literature for square sections as the ratio between the corner radius and the side length, and ranges between 0 and 0.5 (Wang and Wu 2008)) and the cross-sectional aspect ratio, which explains the fact that the corner radius (ratio) is proportional to the increase of strength in confined concrete columns, and that the confinement effectiveness decreases as the aspect ratio increases (Wang and Wu 2008, Wu and Wei 2010).

Commonly used FRPs include carbon, glass, and aramid FRP composites (CFRP, GFRP and AFRP). Among these FRPs, GFRP and CFRP are the most cost-effective and, thus, the most commonly used FRP products. A few new FRPs, such as polypara-phenylene-benzo-bis-oxazole, polyethylene terephthalate/polyester, dyneema, and basalt, have gradually found application in recent years. When compared to CFRPs, GFRPs generally show a lower tensile strength, but a significantly larger ultimate strain. Therefore, RC columns confined with GFRP present a lower load bearing capacity, but a higher ductility performance when the same thickness of confining material is applied. In addition, the orientation of the fibers inside of the FRP composites can dramatically change the behavior of the confined RC columns. Experimental studies showed that, for FRP-confined concrete columns, specimen performance is optimized when fibers are aligned at 90° with respect to the principal axis of the column and the performance diminishes with decreasing fiber angle (Vincent and Ozbakkaloglu 2013). The study reported in this thesis is based on the behavior of concrete cylindrical specimens confined using GFRP sheets with their fibers aligned along the hoop direction of the cylinders (i.e., oriented at 90° with respect to the principal axis of the cylinder).

During the last decade, numerous analytical studies were performed to predict the mechanical behavior of FRP-confined concrete as well as important properties, such as ultimate strength and ductility. These studies provide a better understanding of how certain variables can affect the behavior of FRP-confined concrete when it is subjected to axial compression. A uniaxial model for concrete confined with FRP was introduced by Spoelstra and Monti (1999). This model explicitly accounts for the continuous interaction with the confining device due to the lateral strain of concrete. The relation between the axial and lateral strains is derived through equilibrium between the (dilating) confined concrete and the confining device, which allows one

to trace the state of strain in the jacket and to detect its failure. Shao et al. (2006) developed a constitutive model that includes cyclic rules for loading and unloading, plastic strains, as well as stiffness and strength degradation. This model can be used to predict the behavior of FRP-confined concrete under uniaxial cyclic compression. In Hu (2012), a frame finite element (FE) was developed to accurately estimate the load-carrying capacity and ductility of FRP-confined RC circular columns subjected to axial load only, or both axial and lateral load. These numerical models were used to estimate the performance of the FRP-confined self-healing concrete in the present research.

2.5 Previous Work by Other Researchers at LSU on Microencapsulation-Based Self-Healing Concrete

Previous research conducted within the same research group by another researcher at LSU explored the application of DCPD and SS as healing agents in microencapsulation-based self-healing concrete (Gilford et al. 2013). The research focus was the proof of concept for microencapsulation-based self-healing concrete and a parametric study for fabrication of microcapsules filled with DCPD or SS. The effects of preparation parameters, namely temperature, agitation rate, and pH, on the shell thickness and size (diameter) of the microcapsules was thoroughly evaluated and discussed. Based on the results of the experiments, the optimum microcapsule preparation parameters to control the shell thickness and size of the microcapsules were identified as: (1) temperature = 55 ℃, agitation = 250-550rpm depending on the desired average size of the microcapsules, and pH = 3.1 for DCPD microcapsules; and (2) temperature = 55 ℃, agitation = 350 rpm, and pH = 3.1 for SS microcapsules.

The effectiveness of the self-healing mechanism for self-healing concrete was evaluated with variations of microcapsules produced under different pH values and different microcapsule contents (Gilford et al. 2013). For SS, improvement in the modulus of elasticity of the concrete

before and after healing was observed at a pH value of 3.1 (see Figure 2-14) and SS content of 5.0% (see Figure 2-15).

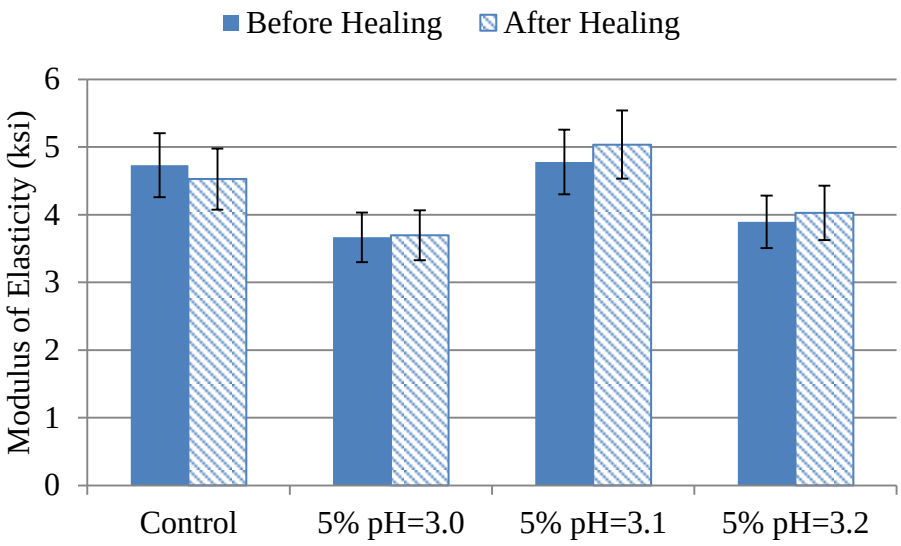


Figure 2-14: Effect of Preparation pH of Microcapsules on Concrete Modulus of Elasticity before and after Healing (adapted from Gilford et al. 2013)

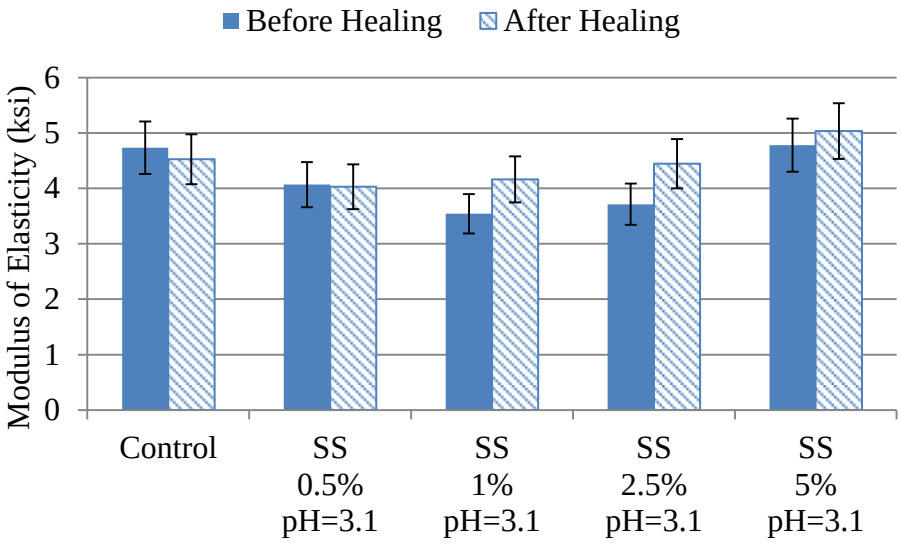


Figure 2-15: Effect of Amount of Microcapsules (% of Cement Weight) on Concrete Modulus of Elasticity before and after Healing (adapted from Gilford et al. 2013)

At other pH values, the effect of the SS microcapsules on the concrete performance was negligible. The research presented in this thesis was performed using SS microcapsules produced using the optimum microcapsule preparation parameters derived in Gilford et al. (2013) and reported above.

2.6 Application of SEM Technology in Concrete Research

Electron microscopes (EM) are instruments that examine objects on a very fine scale utilizing a beam of highly energetic electrons. EM examinations can yield diverse information about the microstructure of materials, e.g., morphology (shape and size of the micro-particles composing the object), topography (surface features of an object), composition (elements and compounds that the object is composed of and the relative amounts of them), and crystallographic information (atom structure of the object) (Reed 2005). EMs function exactly as their optical counterparts, except that they use a focused beam of electrons instead of light to produce an "image" of the specimen and gain information regarding its microstructure and element composition. The basic working theory of EMs can be briefly described as follows (Voutou et al. 2008, see Figure 2-16):

(1) A fine probe of electrons with energies typically of up to 40 keV is formed under high vacuum condition from the electron guns.

(2) This stream is accelerated towards the specimen while it is confined and focused using metal apertures and magnetic lenses into a thin, focused, monochromatic beam.

(3) The sample is irradiated by the beam and interactions occur inside the irradiated sample, affecting the electron beam.

(4) These interactions and effects are detected and transformed into an image or other analysis results.

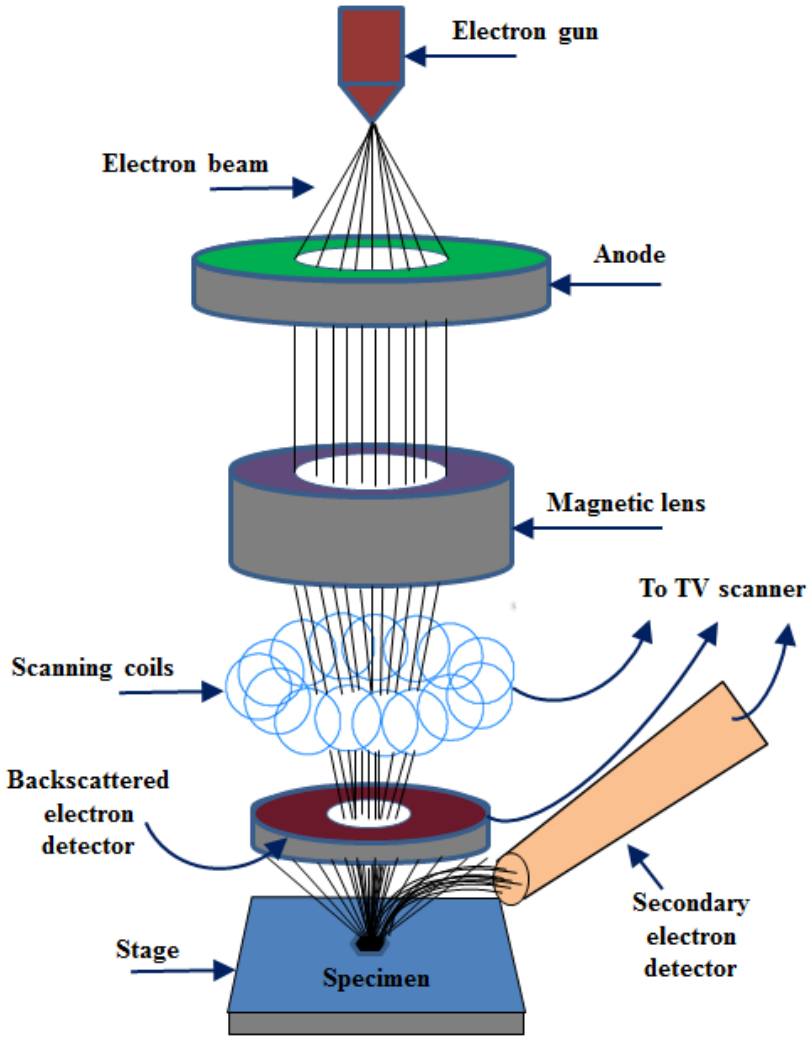


Figure 2-16: Working Mechanism of SEMs (adapted from Voutou et al. 2008)

Two basic types of EMs can be identified: transmission electron microscopes (TEMs) and SEMs. The difference between SEM and TEM is the electron reactions exploited between the electron beam and the specimens. The reactions exploited in the TEMs are unscattered electrons, elastically scattered electrons, and inelastically scattered electrons, while the SEM involves reactions of secondary electrons, backscattered electrons, and relaxation of excited atoms (Reed 2005). TEM was the first type of EM and was developed by Knoll and Ruska in 1931 (Voutou et al. 2008). The first SEM, as it is known today, was described and developed in 1942 by

Zworykin with a resolution of 50nm (Goldstein et al. 2003). In 1960, Everhart and Thornley greatly improved the SEM technology by refining the secondary electron detection process (Goldstein et al. 2003). The first commercially available SEM machine was produced in 1965, which was based on the SEM V experimentally developed by Pease and Nixon in 1963 (Breton 1999). As of today, the SEM technology has become one of the most powerful instruments in materials and life science.

SEMs can be used for different types of analyses. Among these analyses, X-ray spectroscopy analysis, which is obtained by attaching an X-ray spectrometer to the SEM, is noteworthy. The X-ray spectrometer yields information about the element composition of the specimens by detecting and analyzing X-rays produced by bombardment of a solid by electrons (Reed 2005). There are two types of X-ray spectroscopy analyses: energy-dispersive X-ray spectroscopy (EDX) and wavelength-dispersive X-ray spectroscopy. Although wavelength-dispersive X-ray spectroscopy is capable of yielding better spectral resolution, EDX is faster, more convenient to use, and more common. The energy-dispersive spectrometers simultaneously record X-rays of all energies and produce an output in form of a plot of intensity versus X-ray photon energy, which allows the analyst to identify chemical elements from the peaks of the plot.

Since its invention, the SEM technology has been a very valuable tool in the development of scientific theories in industries like chemistry, molecular science, physical science and technology, and materials science. Applications of the SEM in concrete studies date back to the 1990s. Since then, the SEM has been widely used to examine the mechanical and chemical properties of concrete materials in the micro- and nano-scale. Jacobsen et al. (1995) conducted SEM observations of the concrete's microstructure after frost deterioration and autogenous healing. The results showed that crack width due to freeze/thaw ranged from 1-10 μm. Closing

of several cracks was successfully observed after autogenous healing with C-S-H hydration products traversing at several locations. Another application of SEM in concrete materials is to monitor the hydration of and micro-crack propagation within the cement. Direct imaging of hydraulic cements by SEM can yield a complete picture of both bulk and surface phase compositions of hydraulic cement (Stutzman 2004). Micro-cracks of the drying cement can be observed using environmental scanning electron microscopy (ESEM) at a relative humidity ranging from 0 to 100% (Kjellsen and Jennings 1996). Other applications of the SEM in concrete studies include fracture analysis, identification of deteriorating minerals in concrete matrix, and observations on dedolomitization of carbonate concrete aggregates (Nemati 1997, Gregerová and Všianský 2009, Princic et al. 2013).

In addition to investigating intrinsic concrete properties, the SEM technique can also be employed in examining the status of additive materials in modified concrete materials. An example is the use of SEM to observe the crystal structure at the aggregate-cement interfacial transition zone of fiber-reinforced concrete (Sun et al. 2009, Palmquist et al. 2011). In addition, Wang et al. (2008) conducted SEM, ESEM, and EDX analysis to monitor the morphology and chemical composition change of fly ash particles in fly ash modified concrete. Similar to this idea, in the present research, SEM imaging tests were performed to examine the presence of SS microcapsules in the concrete matrix, and EDX tests were performed to investigate the element composition of healed and non-healed specimens.

3 EXPERIMENTAL EVALUATION OF SELF-HEALING MECHANISM

3.1 Introduction

The first phase of this research consisted of obtaining experimental data to support the hypothesis that composite action due to FRP confinement can improve the self-healing properties of self-healing concrete. An experimental plan was developed consisting of three sets of tests: (1) a set of preliminary stiffness/strength tests, which were needed to evaluate the stiffness and strength of the concrete specimens and to define the loading protocol for subsequent tests; (2) a set of stiffness tests under cyclic loading separated by self-healing periods (referred to as self-healing stiffness test in the remainder of this thesis), which were used to identify any self-healing effect; and (3) a set of strength tests, which were used to identify any effect of the self-healing agent on the concrete strength.

3.2 Experimental Equipment

3.2.1 Concrete Compression Strength Testing Machine

The concrete strength test machine used in this research for both the preliminary and the additional strength tests was an ELE ACCU-TEK TM 350 compression test machine with a capacity of 350 kips (1,500 KN). This equipment is shown in Figure 3-1 (a). ELE ACCU-TEK TM 350 meets the requirements of ASTM C39 and AASHTO T-22 for the brick and concrete cylinder compression test. The compression test machine is load-controlled and is powered by the hydraulic pump connected. The reading unit on the top of the machine serves as both the digital controller and the result displayer. Test parameters, such as the test mode (compression test or beam bending test), specimen type, section properties, and loading pace rate, can be controlled from the digital reading unit. The loading pace rate for the tests performed in this research was set to 440 lb/s, according to ASTM C39 (ASTM 2004). The concrete cylinders

were capped with 70 Duro neoprene pads inside of the retainer rings at both ends before being tested, as shown in Figure 3-1 (b). The output obtained from the equipment included the sample peak load, sample peak stress, and loading pace rate.

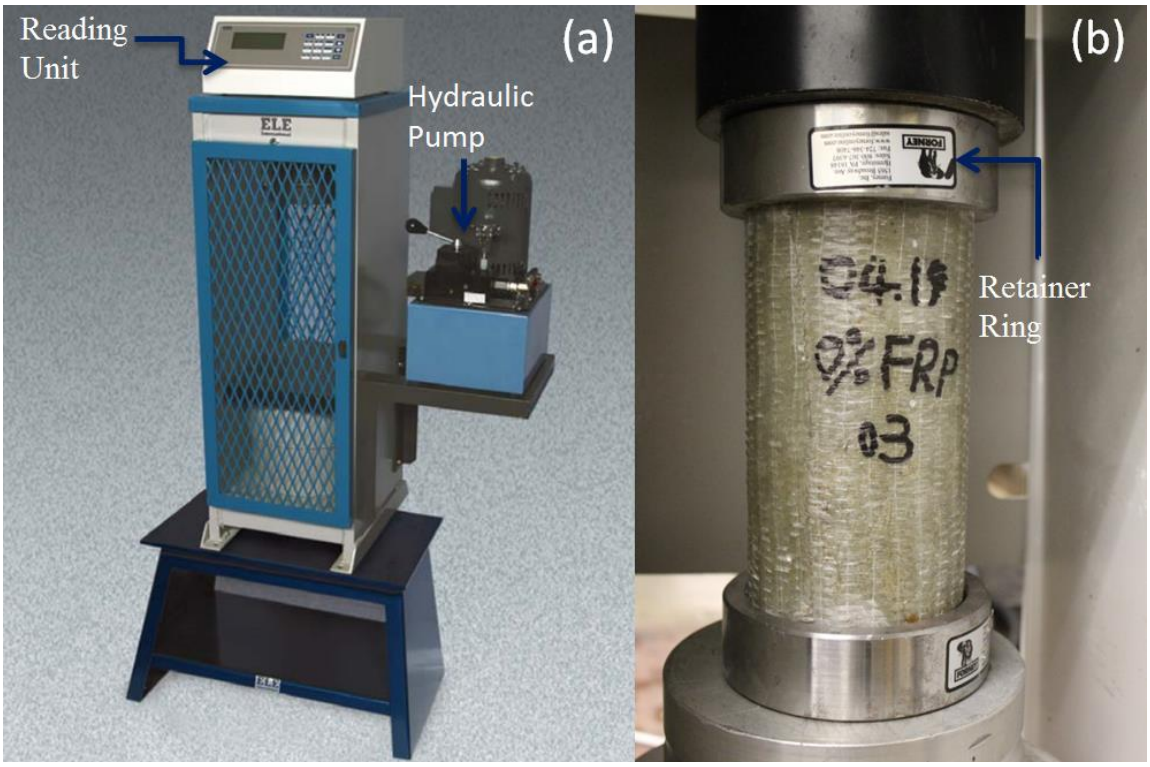


Figure 3-1: Concrete Compression Strength:
(a) Test Machine, and (b) Test Setup

3.2.2 Concrete Stiffness Test Machine

The concrete stiffness test was performed utilizing an MTS machine with a capacity of 550 kips (2,500 KN) (see Figure 3-2), which meets the requirements of ASTM C469 (ASTM 2010). The MTS machine is digitally controlled by the controller, from which the loading procedure can be modified. A loading cell with a capacity of 110 kips was introduced between the MTS machine and the concrete cylinder in order to record the loading history. In order to obtain the stress-strain response of the specimen, it was assumed that the load was uniformly applied to the circular surface of the cylindrical specimen.



Figure 3-2: MTS Machine and Stiffness Test Setup:
(a) MTS Machine, (b) MTS Controller,
and (c) Stiffness Test Setup

3.2.3 Vertical Displacement Measurement System

The vertical displacement of the concrete cylinders was measured using a compressometer and a linear variable differential transformer (LVDT) aligned along the vertical direction as shown in Figure 3-3. The compressometer meets the requirements of ASTM C469 (ASTM 2010). According to ASTM C469 specifications, when the fixed points are in the middle of the LVDT and the pivot rod as in the case of this experimental campaign (see Figure 3-3), the vertical displacement of the concrete cylinder is given by

$$d_c = \frac{d_{LVDT}}{2} \tag{3.1}$$

in which d_c denotes the relative displacement of the loading point on the top of the concrete specimen with respect to the fixed base, and d_{LVDT} denotes the relative displacement of the two ends of the LVDT.

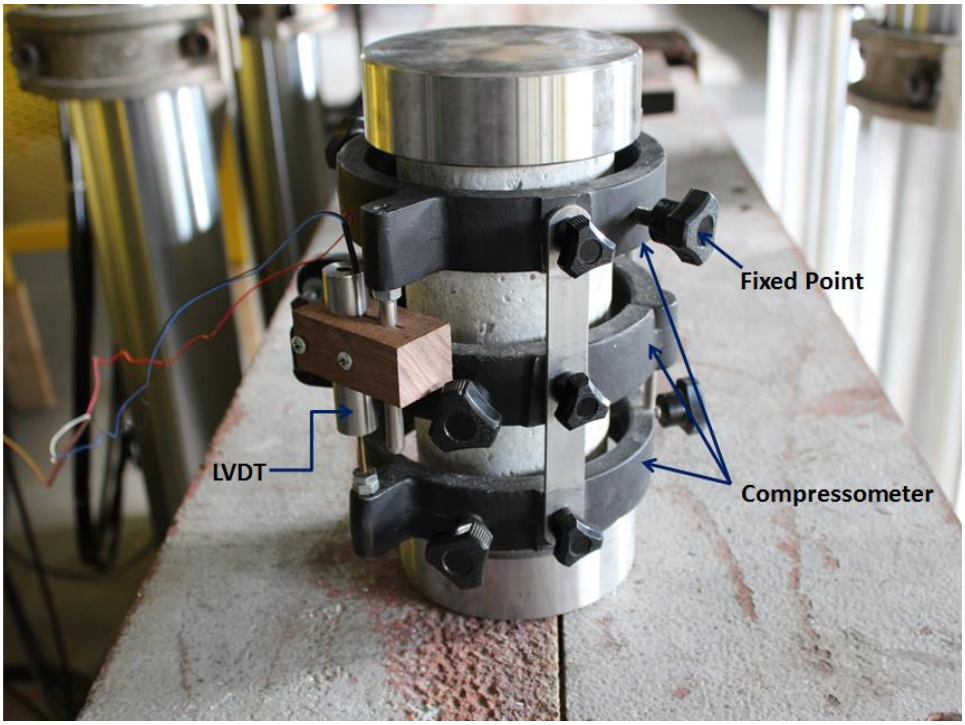


Figure 3-3: Vertical Displacement Measurement System

The strain of the concrete cylinder can be obtained as

$$\varepsilon = \frac{d_c}{L_{eff}} \tag{3.2}$$

in which ε denotes the axial strain of the cylindrical concrete specimen, and L_{eff} denotes the effective length of the compressometer. In this research, $L_{eff} =$ 5.25 in (13.3 cm).

3.2.4 Data Acquisition System (DAQ)

Figure 3-4 shows the DAQ used in this research, which included a NI9205 DAQ module, an external power supply, and a computer with LabVIEW (LabVIEW 2003). The NI9205 features 16 single-ended analog voltage inputs, 16-bit resolution, 250 ks/s aggregate sampling rate and

±10 V programmable input ranges. The loading time history from the loading cell and the displacement time history from the LVDT were read and processed through the DAQ system using the same (synchronized) time reference. These data were directly used to plot the strain-stress curves for the specimens. The external power supply featured an adjustable DC output. A 24 V DC was used to power the LVDT in this research. A graphical program was built under LabVIEW2013 to read output of the DAQ system with a frequency of 100 samples/second (s/s). Data were averaged over 20 samples to improve stability and five data points were saved per second.

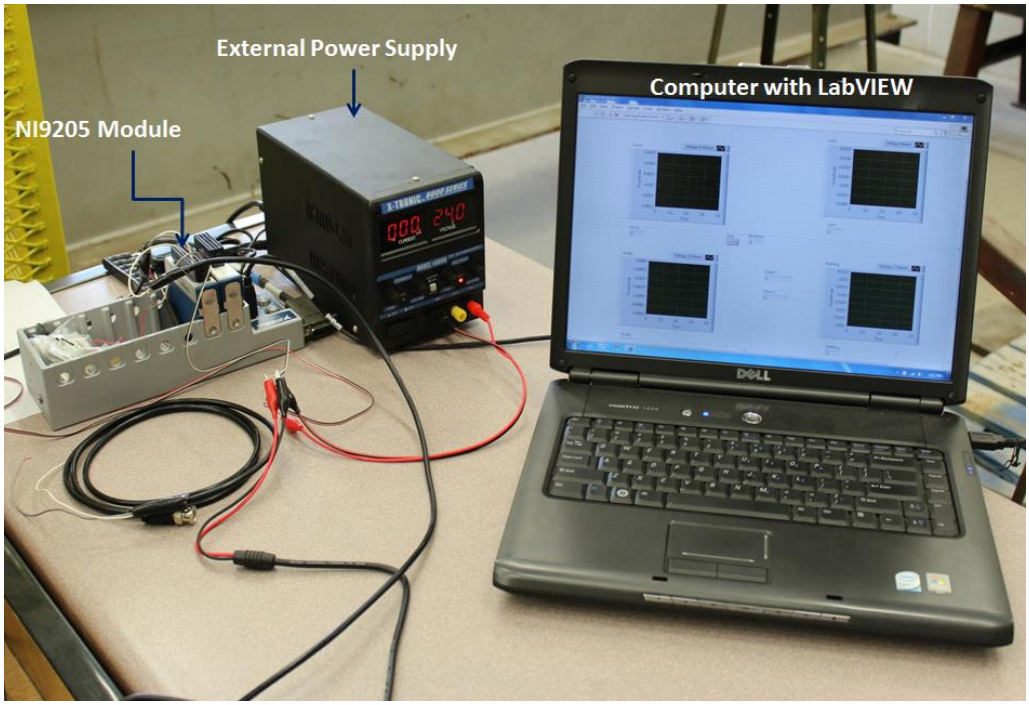


Figure 3-4: Data Acquisition System

3.3 Methodology

3.3.1 Test Materials and Specimen Preparation

The chemicals utilized in the preparation of the microcapsules using the in-situ polymerization method are listed in Table 3-1. The micro-encapsulation laboratory procedures

that were utilized in this study for preparation of SS microcapsules are presented in the Appendix. The concrete utilized in this research was QUIKRETE Pro Finish high strength concrete mix, with a nominal compressive strength of 5,000 psi. The FRP sheet used was SikaWrap Hex-100G uniaxial E-glass fiber fabric, which is designed specifically for structural strengthening. The properties of the fiber are listed in Table 3-2. SikaDur 300 impregnating resin was used as adhesive with a volume mixing ratio of Part A: Part B = 2.82:1.

Table 3-1: Required chemicals for interfacial polymerization synthesis

Chemical	Function	Manufacturer
Urea	Creates endothermic reaction in water	The Science Company
Ammonium Chloride	Assists with curing Process	The Science Company
Resorcinol (Technical Grade Flake)	Reacts with formaldehyde and is a chemical intermediate for the synthesis process	NDSPEC Chemical Corporation
ZeMac E60 Copolymer	Improves mechanical properties	Vertellus Specialties, Inc.
ZeMac E400 Copolymer	Improves mechanical properties	Vertellus Specialties, Inc.
Octanol	Prevents surface bubbles	Oltchim
Hydrochloric Acid	Lowers pH	The Science Company
Sodium Silicate	Reacts with $Ca(OH)_2$	The Science Company
Sodium Hydroxide	Increases pH	The Science Company
Formaldehyde	Reacts with urea during synthesis process	The Science Company
DETA (diethylenetriamine) Mix with EPON 828	Used in synthesis of catalysts, epoxy curing agent, and corrosion inhibitors	Huntsmann

Table 3-2: Cured FRP laminate properties with Sikadur Hex 300 (SikaWrap Hex-100G)

Tensile Strength (ksi/MPa)	Tensile Modulus (ksi/MPa)	Elongation (%)	Nominal Thickness (in./mm)
77.1/531.6	3426.3/23623.5	2.12	0.04/1.016

The concrete cylindrical specimens were prepared using the QUIKRETE Pro Finish concrete mix with a water/cement ratio of 0.5. SS microcapsules were added to the mixing water at a

carefully measured content of 1.0, 2.5, and 5.0% by weight of cement. The cylinders were de-molded after 24 hours and submerged into water at a temperature between 20-25 ℃ for 28 days to be fully cured. For the confined specimens, the concrete surface was carefully cleaned before being impregnated with the resin. One layer of glass fiber was fully impregnated with resin and then wrapped around the concrete cylinders with the glass fiber aligned along the hoop direction. To avoid anchorage rupture, an overlap length of a quarter of the circumference was adopted along the fiber direction, as recommended by the FRP producer.

3.3.2 Experimental Matrix

A total of 6 ordinary (non-self-healing) concrete and 24 self-healing concrete cylinders of 4-in (10.16 cm) diameter and 8-in (20.32 cm) height were prepared for uniaxial compression tests. For the preliminary test specimens, three specimens were left unconfined and three specimens were wrapped with one layer of FRP. For the self-healing concrete specimens, the content of SS microcapsules was varied as 0.0%, 1.0%, 2.5% and 5.0% of cement weight. Three unconfined specimens and three FRP-confined specimens were prepared for each level of SS content. Six specimens (three unconfined and three FRP-confined) of ordinary concrete were used for the preliminary stiffness/strength tests, while the remaining specimens were used for both the stiffness and strength tests.

Table 3-3 presents the test matrix followed in the first phase of this research. The specimens are identified using acronyms composed by three parts. The first part of the acronym is composed by two characters that indicate the type of test, i.e., PR = preliminary test (the specimens were subjected to cyclic loading to evaluate the stiffness and then monotonically loaded until failure to obtain the peak strength), and SH = self-healing test (the undisturbed specimens were subjected to cyclic loading, then left to heal for one week, and then subjected to

a second set of cycling loading). The second part of the acronym consists of two digits that indicate the SS content, i.e., 00 = 0.0% (ordinary concrete), 10 = 1.0% (self-healing concrete with SS content equal to 1.0% of cement weight), 25 = 2.5% (self-healing concrete with SS content equal to 2.5% of cement weight), 50 = 5.0% (self-healing concrete with SS content equal to 5.0% of cement weight). The third part of the acronym is composed by two or three characters that indicate the confinement type, i.e., PL = plain (unconfined) concrete and FRP = FRP-confined concrete.

Table 3-3: Experimental test matrix

Test type	Specimen ID	SS content	Confinement type	Number of specimens
Preliminary test	PR00PL	0.0%	Unconfined	3
	PR00FRP		FRP	3
Self-healing test	SH00PL	0.0%	Unconfined	3
	SH00FRP		FRP	3
Self-healing test	SH10PL	1.0%	Unconfined	3
	SH10FRP		FRP	3
Self-healing test	SH25PL	2.5%	Unconfined	3
	SH25FRP		FRP	3
Self-healing test	SH50PL	5.0%	Unconfined	3
	SH50FRP		FRP	3

3.3.3 Experimental Investigation Protocol

The preliminary strength test was conducted following the ASTM C39 standard (ASTM 2004). Before performing the preliminary strength test, the specimens were subjected to a set of three cycles of compressive loading, used to evaluate the initial stiffness of the concrete specimens according to ASTM C469 (ASTM 2010).

The self-healing stiffness test was performed in three phases: (1) a first set of cyclic loading, (2) a one-week period of self-healing during which the specimens were maintained in water between a temperature of 20 ℃ to 25 ℃, and (3) a second set of cyclic loading. The cyclic

loading was performed using an MTS machine following a modified version of ASTM C469 (ASTM 2010). The specimens were loaded and unloaded for one cycle up to 20% of their compressive strength (estimated from the results of the previously performed preliminary strength tests), for one cycle up to 40% of their compressive strength, and for three cycles up to 75% of their compressive strength. For each specimen, the stress time history was recorded from a loading cell and the strain time history was measured using an LVDT attached to the specimen through a compressometer. The tangent stiffness modulus (computed as the slope of the stress-strain curve between 2% and 10% of the estimated peak strength of the specimens) and the residual strain at end of each loading cycle (computed as the strain reached during unloading at 2% of the estimated peak strength of the specimens) were calculated before and after healing.

3.4 Experimental Results and Discussion

3.4.1 Results of the Preliminary Tests

The preliminary stiffness/strength test was performed to obtain the initial stiffness and the peak strength of the unconfined and confined concrete specimens. These tests were performed following ASTM standards, i.e., ASTM C469 for evaluation of the initial stiffness and ASTM C39 for evaluation of the peak strength.

The experimental results of the preliminary tests are presented in Table 3-4. The peak strength of the concrete (f_c) was calculated as the average of the failure loads of each set of specimens divided by the area of the cylinder. During the cyclic testing, the strain and stress history were recorded and then plotted. The initial tangent modulus (E_c) of the concrete was calculated as the average of initial tangent modulus from the three loading cycles. In order to get more information about the stress-strain curves of the concrete specimens subject to different loading cycles, the unconfined specimens of the preliminary tests (PR00PL) were loaded to

higher loading levels after completion of the stiffness test and before the strength test. One specimen (PR00PL #1) was broken during these tests, the strength of which was viewed as an outlier and therefore not considered in the calculation of the average strength.

Table 3-4: Results of the preliminary tests

Specimen ID	Specimen #	Strength (ksi)	Stiffness (ksi)	Average Strength (ksi)	Average Stiffness (ksi)
PR00PL	1	6.74(outlier)	7.09	Local failure	5.87
	2	8.27	4.92	8.18	
	3	8.09	5.59		
PR00FRP	1	10.72	6.34	10.7	6.38
	2	10.29	6.24		
	3	10.97	6.56		

The average strength of the ordinary concrete specimens was 8.18 ksi, which is much higher than the corresponding nominal strength (5 ksi). Due to limitations of the loading cell capacity, the specimens could not be loaded to failure using the MTS machine. Thus, in this research, the specimens' stiffness and strength were evaluated using the MTS machine and the concrete compressive test machine, respectively. The measured FRP confinement efficiency was low, with only 30% increase in terms of strength and 9% in terms of stiffness when compared to the unconfined specimens. This result could be due to the high strength of the concrete (Micelli and Modarelli 2013), poor workmanship in the application of the FRP, and geometric irregularities of the concrete specimens. Typical compression failure modes were observed for both the unconfined and FRP-confined specimens under uniaxial compressive load (see Figure 3-5).

A numerical study was performed to assess the modeling capabilities of existing material constitutive models for unconfined and FRP-confined concrete. The measured mechanical parameters were employed to model the stress-strain response of the concrete specimens using existing material constitutive models that are available in the general-purpose FE code

FEDEASLab (Filippou and Constantinides 2004), i.e., the Pantazopoulou-Mills' model for plain (unconfined) concrete (Pantazopoulou and Mills 1995) and the Spoelstra-Monti's model for FRP-confined concrete (Spoelstra and Monti 1999). The strain at the peak strength (ε_c) of the concrete was not experimentally measured and was assumed equal to 0.002 based on existing literature (Pantazopoulou and Mills 1995). The FRP mechanical properties used in the Spoelstra-Monti's model are listed in Table 3-2 and were taken from the FRP producer's specifications.

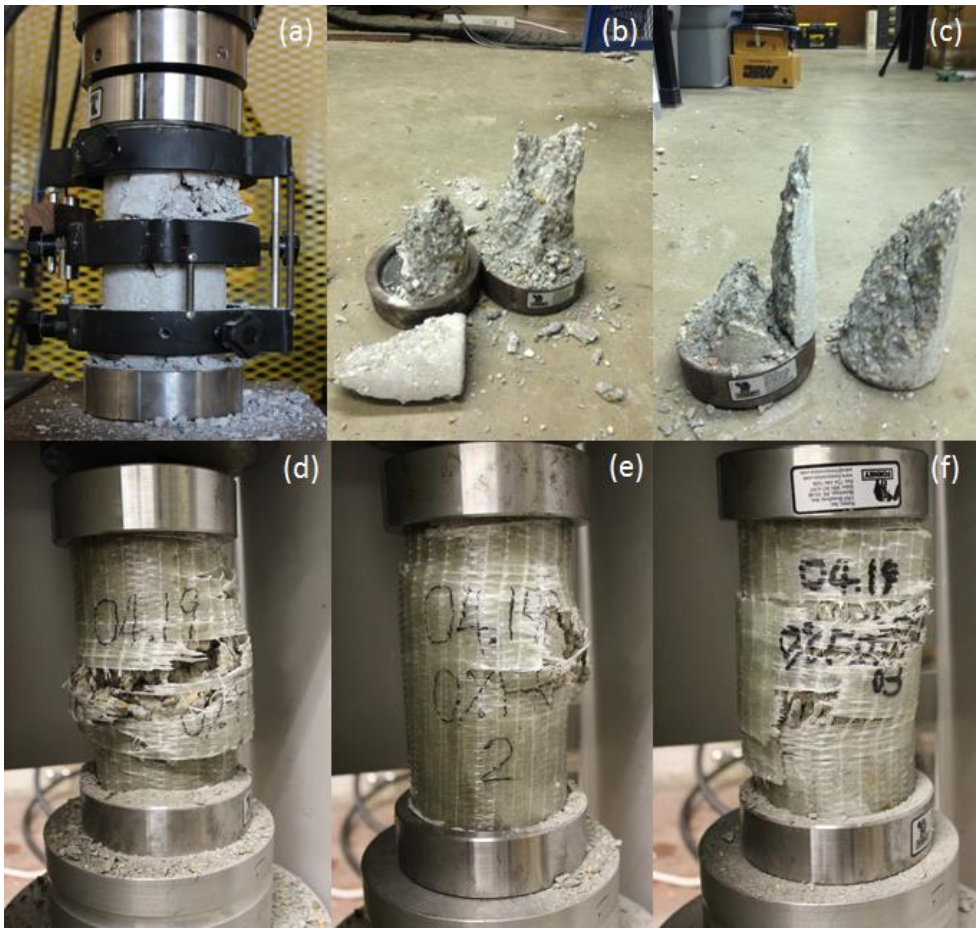


Figure 3-5: Failure Modes of the Specimens in the Preliminary Tests:
(a) PR00PL#1, (b) PR00PL#2, (c) PR00PL#3,
(d) PR00FRP#1, (e) PR00FRP#2, and (f) PR00FRP#3

The experimental stress-strain time histories were compared with the corresponding numerical results from monotonic loading in Figure 3-6 (specimen SH00PL #3 and

Pantazopoulou-Mills' model) and Figure 3-7 (specimen SH00FRP #2 and Spoelstra-Monti's model). A significant difference (about 30%) was observed between the experimentally

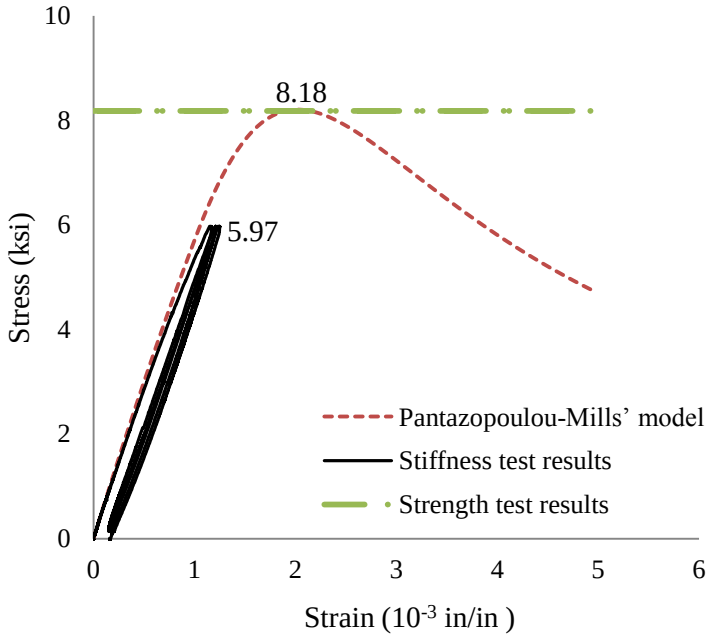


Figure 3-6: Stress-Strain Response for Unconfined Ordinary Concrete Specimens (Experimental Curve Corresponding to Specimen SH00PL #3)

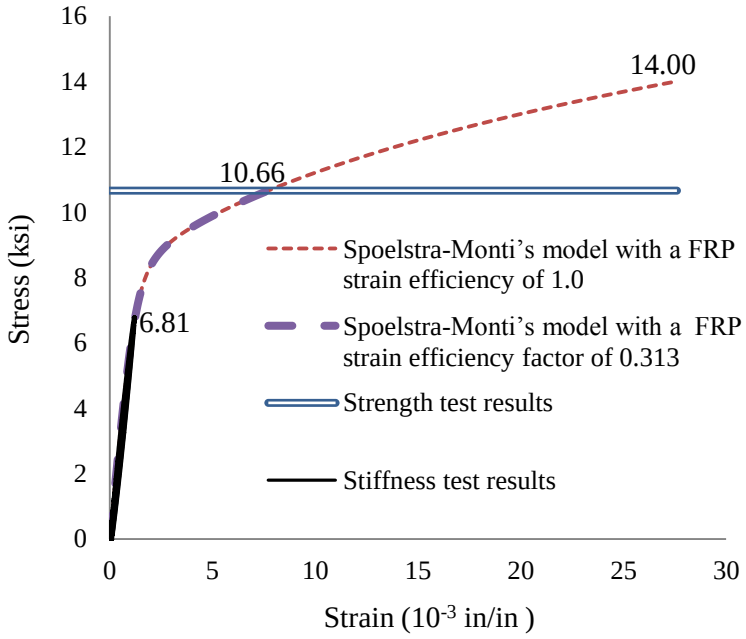


Figure 3-7: Stress-Strain Response for FRP Confined Ordinary Concrete Specimens (Experimental Curve Corresponding to Specimen SH00FRP #2)

measured strength and the strength obtained based on the Spoelstra-Monti's model for FRP-confined concrete when the FRP ultimate strain from manufacturer was used as input. As the ultimate strain of the FRP was not measured in the experiment, the FRP strain efficiency factor (defined as the ratio of hoop rupture strain of the FRP jackets in FRP-confined concrete and the ultimate material tensile strain) for the considered specimen was back calculated using the Spoelstra-Monti's model as 0.313. This value is relatively low compared with the average value of 0.624 found by Lam and Teng (2004). Possible causes of this difference may be errors of the model, poor workmanship, small specimen size (high curvature at the interface), and differences between the FRP products used in this research and in the references found in the literature (Wu and Jiang 2013).

The results from the preliminary experimental tests and their comparison with numerical modeling results were used to define the loading protocol for the self-healing tests. This protocol was defined by balancing the requirements of limiting the damage to the specimens while allowing the formation of micro-cracks in the concrete.

3.4.2 Results of the Self-Healing Stiffness Tests

The self-healing stiffness test was performed to investigate the basic hypotheses that (1) self-healing concrete is able to autonomously repair micro-cracks formed in the concrete matrix, and (2) the composite action provided by FRP-confinement can improve the self-healing properties of self-healing concrete. Micro-cracks in the concrete matrix are generated (among other causes) by loading of the concrete and can produce residual strain and stiffness reduction in the damaged concrete. The level of damage of the concrete matrix can be related with the residual strains after unloading of the damaged concrete. The repair of micro-cracks can be observed at a macroscopic scale from the recovery of stiffness of the concrete specimens. Thus, the residual strain measured

after unloading of the concrete can be considered a measure of the concrete damage and the amount of stiffness recovery measured between two different loading phases can be considered a measure of the self-healing effects. The self-healing test was used in this research to measure the residual strains and the stiffness variation of the concrete specimens.

Table 3-5 provides the residual ("Resid.") strains (the strain after unloading of the damaged concrete) and the maximum ("Max.") strains (the maximum strain measured during the loading period) for all load cycles of every concrete specimen tested as a part of the self-healing test. Two of the specimens (i.e., SH00PL #3 and SH01PL #3) were damaged and were not tested under cyclic loading. The results present a significant scatter. It is observed that the maximum strains before and after healing tend to be very similar. The maximum strains after healing are usually slightly larger than the corresponding strains before healing for the 20% and 40% loading cycles, while the maximum strains after healing are usually smaller than the corresponding strains before healing for the 75% loading cycles, with the exception of the specimens with 2.5% SS, for which the opposite is true. The strains corresponding to specimens with 1.0% SS are usually larger than the corresponding strains of specimens with other SS content. The combination of FRP-confinement and 5.0% SS seems to be particularly efficient in reducing both the residual and the maximum strains.

The self-healing test was also used to evaluate the self-healing effects in terms of stiffness variation, ΔE, after healing of the concrete. The stiffness variation is defined in this research as

$$\Delta E = \frac{E_h - E_d}{E_0} \tag{3.3}$$

in which E_h denotes the tangent stiffness modulus of the concrete specimens after healing (i.e., the average of the secant stiffness measured between 2% and 10% of the concrete strength in the

Table 3-5: Residual and maximum strains at each load cycle of tested concrete specimens

Load cycle			#1 (20%)		#2 (40%)		#3 (75%)		#4 (75%)		#5 (75%)	
ID	#	Healing	Resid.	Max.	Resid.	Max.	Resid.	Max.	Resid.	Max.	Resid.	Max.
			(10^{-3} in/in)		(10^{-3} in/in)		(10^{-3} in/in)		(10^{-3} in/in)		(10^{-3} in/in)	
SH00PL	1	Before	0.031	0.260	0.029	0.524	0.084	1.076	0.061	1.088	0.077	1.078
		After	0.071	0.290	0.070	0.571	0.083	1.081	0.091	1.090	0.105	1.090
	2	Before	0.038	0.260	0.052	0.548	0.117	1.108	0.133	1.156	0.145	1.160
		After	0.031	0.286	0.038	0.577	0.064	1.108	0.074	1.125	0.079	1.135
SH00FRP	1	Before	0.039	0.319	0.066	0.696	0.042	1.347	0.265	1.401	0.299	1.467
		After	0.044	0.354	0.059	0.718	0.107	1.251	0.129	1.280	0.150	1.322
	2	Before	0.032	0.299	0.044	0.640	0.112	1.196	0.133	1.237	0.154	1.267
		After	0.035	0.327	0.041	0.684	0.094	1.229	0.110	1.255	0.116	1.277
	3	Before	0.042	0.313	0.059	0.654	0.122	0.991	0.105	1.218	0.128	1.254
		After	0.030	0.315	0.031	0.658	0.070	1.159	0.081	1.190	0.092	1.220
SH10PL	1	Before	0.033	0.287	0.047	0.601	0.128	1.266	0.148	1.295	0.147	1.311
		After	0.035	0.320	0.048	0.652	0.098	1.248	0.117	1.279	0.131	1.299
	2	Before	0.037	0.294	0.060	0.630	0.196	1.409	0.097	1.336	0.123	1.372
		After	0.033	0.316	0.037	0.634	0.077	1.209	0.076	1.230	0.076	1.240
SH10FRP	1	Before	0.063	0.341	0.095	0.729	0.349	1.599	0.468	1.796	0.570	1.963
		After	0.065	0.448	0.105	0.937	0.275	1.735	0.357	1.869	0.351	1.958
	2	Before	0.043	0.337	0.079	0.718	0.052	1.511	0.345	1.628	0.280	1.728
		After	0.060	0.404	0.102	0.857	0.186	1.503	0.215	1.607	0.260	1.681
	3	Before	0.057	0.346	0.089	0.739	0.243	1.464	0.304	1.572	0.351	1.650
		After	0.057	0.365	0.084	0.777	0.191	1.424	0.228	1.487	0.261	1.540
SH25PL	1	Before	0.036	0.227	0.047	0.472	0.100	0.951	0.113	0.968	0.129	0.988
		After	0.030	0.286	0.039	0.592	0.087	1.235	0.091	1.244	0.104	1.286
	2	Before	0.032	0.240	0.047	0.507	0.112	1.032	0.129	1.053	0.137	1.059
		After	0.034	0.292	0.044	0.598	0.105	1.266	0.123	1.299	0.118	1.342
	3	Before	0.027	0.277	0.035	0.575	0.102	1.176	0.113	1.201	0.115	1.208
		After	0.038	0.295	0.056	0.643	0.109	1.243	0.137	1.300	0.153	1.334

(Table 3-5 continued)

Load cycle			#1 (20%)		#2 (40%)		#3 (75%)		#4 (75%)		#5 (75%)	
SH25FRP	1	Before	0.041	0.327	0.062	0.680	0.135	1.219	0.158	1.281	0.166	1.299
		After	0.046	0.350	0.062	0.710	0.098	1.252	0.113	1.284	0.118	1.295
	2	Before	0.046	0.334	0.066	0.692	0.127	1.258	0.144	1.297	0.171	1.334
		After	0.048	0.371	0.064	0.749	0.109	1.317	0.122	1.345	0.132	1.370
	3	Before	0.026	0.306	0.027	0.639	0.085	1.186	0.100	1.205	0.102	1.221
		After	0.050	0.353	0.065	0.722	0.097	1.246	0.105	1.276	0.118	1.298
SH50PL	1	Before	0.049	0.267	0.063	0.552	0.121	1.076	0.134	1.090	0.139	1.096
		After	0.042	0.285	0.038	0.568	0.050	1.068	0.052	1.073	0.058	1.076
	2	Before	0.027	0.253	0.027	0.518	0.059	1.030	0.065	1.038	0.048	1.071
		After	0.032	0.267	0.035	0.541	0.053	1.012	0.052	1.013	0.052	1.012
	3	Before	0.042	0.256	0.049	0.534	0.082	1.053	0.087	1.058	0.093	1.069
		After	0.033	0.286	0.035	0.557	0.057	1.046	0.069	1.061	0.073	1.062
SH50FRP	1	Before	0.055	0.297	0.067	0.628	0.086	1.129	0.098	1.148	0.106	1.164
		After	0.047	0.336	0.043	0.665	0.069	1.132	0.075	1.135	0.084	1.149
	2	Before	0.076	0.310	0.095	0.676	0.119	1.160	0.088	1.142	0.097	1.153
		After	0.046	0.339	0.053	0.682	0.075	1.167	0.086	1.183	0.105	1.206
	3	Before	0.062	0.272	0.117	0.590	0.225	1.078	0.287	1.138	0.316	1.157
		After	0.043	0.329	0.041	0.649	0.058	1.109	0.067	1.122	0.079	1.140

second and third loading cycles of the second loading phase), E_d denotes the tangent stiffness modulus of the damaged concrete specimens (i.e., the average of the secant stiffness measured between 2% and 10% of the concrete strength in the last two loading cycles of the first loading phase), and E_0 denotes the tangent stiffness modulus of the undamaged concrete specimens (i.e., the average of the secant stiffness measured between 2% and 10% of the concrete strength in the second and third loading cycles of the first loading phase).

The stiffness variation of the self-healing stiffness tests is presented in Table 3-6. Figure 3-8

Table 3-6: Stiffness variation of the self-healing stiffness tests

	Specimen #	E_0 (ksi)	E_d (ksi)	E_h (ksi)	ΔE (%)	Average ΔE (%)	Standard deviation
SH00PL	1	-	-	-	-	Local failure	
	2	6.31	5.93	5.65	-4.44	-2.82	2.29
	3	5.95	5.64	5.57	-1.20		
SH00FRP	1	6.66	6.19	6.13	-0.91	1.30	7.75
	2	6.91	6.45	6.09	-5.11		
	3	6.86	6.08	6.76	9.92		
SH10PL	1	-	-	-	-	Local failure	
	2	5.54	4.95	5.07	2.11	2.29	0.25
	3	5.55	4.99	5.13	2.47		
SH10FRP	1	6.20	5.11	4.71	-6.35	-0.78	6.91
	2	6.16	5.36	5.18	-2.95		
	3	5.96	5.30	5.71	6.96		
SH25PL	1	7.31	6.80	5.51	-17.69	-10.47	11.62
	2	6.93	6.64	5.48	-16.65		
	3	5.65	5.34	5.50	2.93		
SH25FRP	1	6.28	6.21	6.14	-0.99	-2.62	2.07
	2	6.41	6.13	5.81	-4.95		
	3	6.61	6.24	6.11	-1.90		
SH50PL	1	6.04	5.88	5.71	-2.78	-0.39	4.68
	2	6.32	6.21	5.99	-3.39		
	3	6.04	5.62	5.92	5.00		
SH50FRP	1	6.85	6.59	6.52	-1.08	-9.64	11.63
	2	6.93	6.57	6.23	-4.95		
	3	8.67	8.52	6.53	-22.88		

shows the averages of E_0, E_d, and E_h obtained at low levels of stress from each set of three specimens considered in this research. In general, the specimens with FRP-confinement were stiffer than the corresponding unconfined specimens, with the exception of the specimens with 2.5% SS. In terms of stiffness recovery, a similar behavior was observed for both unconfined and FRP-confined specimens. A non-negligible variability of the results was observed, from 10.47% of stiffness loss for the SH25PL group and the SH50FRP group to 2.29% of stiffness recovery for the SH10PL group. However, only a null or minimal stiffness recovery (i.e., 1.30% for SH00FRP group, 2.29% for SH10PL group, and no recovery for other groups) was found after a one-week healing period for the specimens. This observation indicates that (1) the self-healing mechanism was not activated in this phase of the research, and (2) other variables determined the stiffness recovery behavior rather than the presence of FRP-confinement.

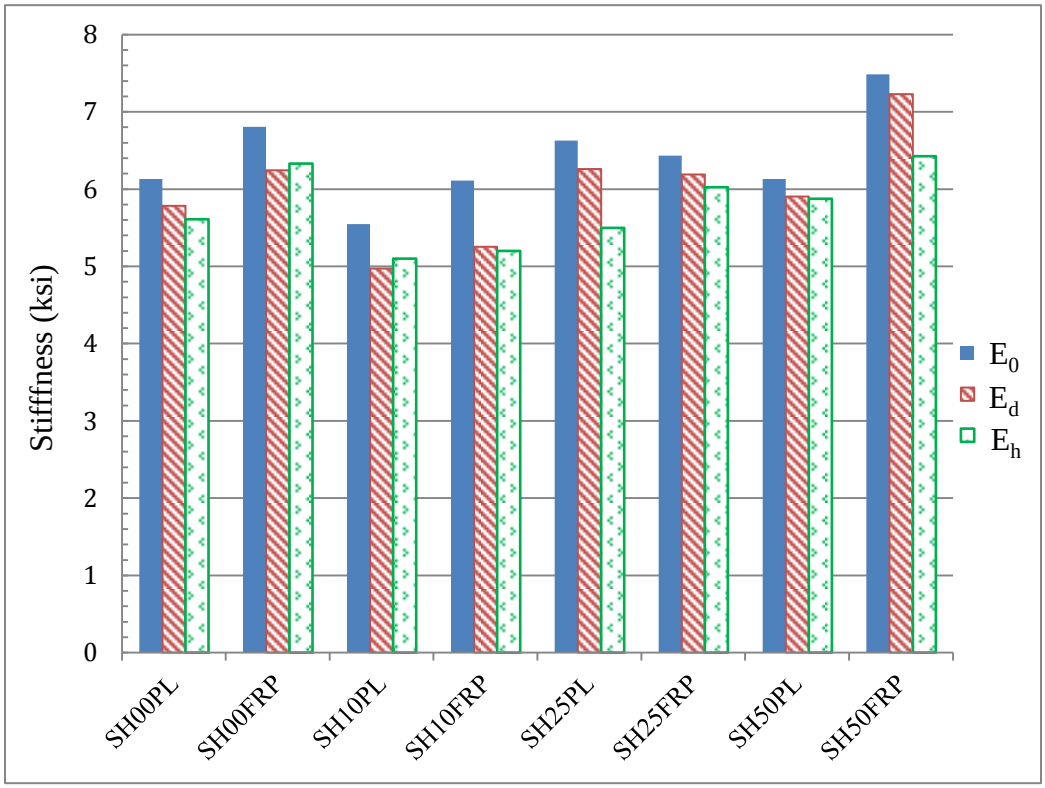


Figure 3-8: Concrete Stiffness Before and After Healing

Figure 3-9 through Figure 3-12 compare the stress-strain response before and after healing of one unconfined and FRP-confined specimen for each SS content level considered in this study. It is observed that, in general, the stress-strain curves after healing and before healing are closer when FRP-confinement is employed rather than when the concrete is unconfined. In addition, the specimens with 1.0% SS reached a higher level of damage when compared to specimens with other SS content. In contrast, the specimens with 5.0% SS are the least damaged among all the specimens. In addition, the stress-strain curves before and after healing are most similar for the specimens with 5.0% SS. These observations seem to suggest that the addition of 1.0% SS decreases the strength and stiffness of the concrete, whereas the addition of 5.0% SS increases the strength and stiffness of the concrete.

3.4.3 Results of the Strength Test

A strength test was performed after the self-healing test in order to analyze the effects of SS content and FRP-confinement on the strength of the concrete specimens after healing. Since one cylinder from each of the SH00PL group and the SH10PL group (SH00PL #1 and SH10PL #1) was already broken during the self-healing stiffness tests, the concrete strength for these two groups was evaluated using only one cylinder. For the other groups considered in this research, two out of three cylinders were monotonically loaded up to failure to obtain the compressive strength (one specimen of each group was preserved to be used for the second phase of this research and further investigation of the results). The compressive strength of the concrete was calculated in the same way as the preliminary strength tests.

Table 3-7 presents results obtained in the strength tests. Figure 3-13 presents the average strength of all the specimens tested in each group. The maximum and minimum strength in each group are also marked on the graph.

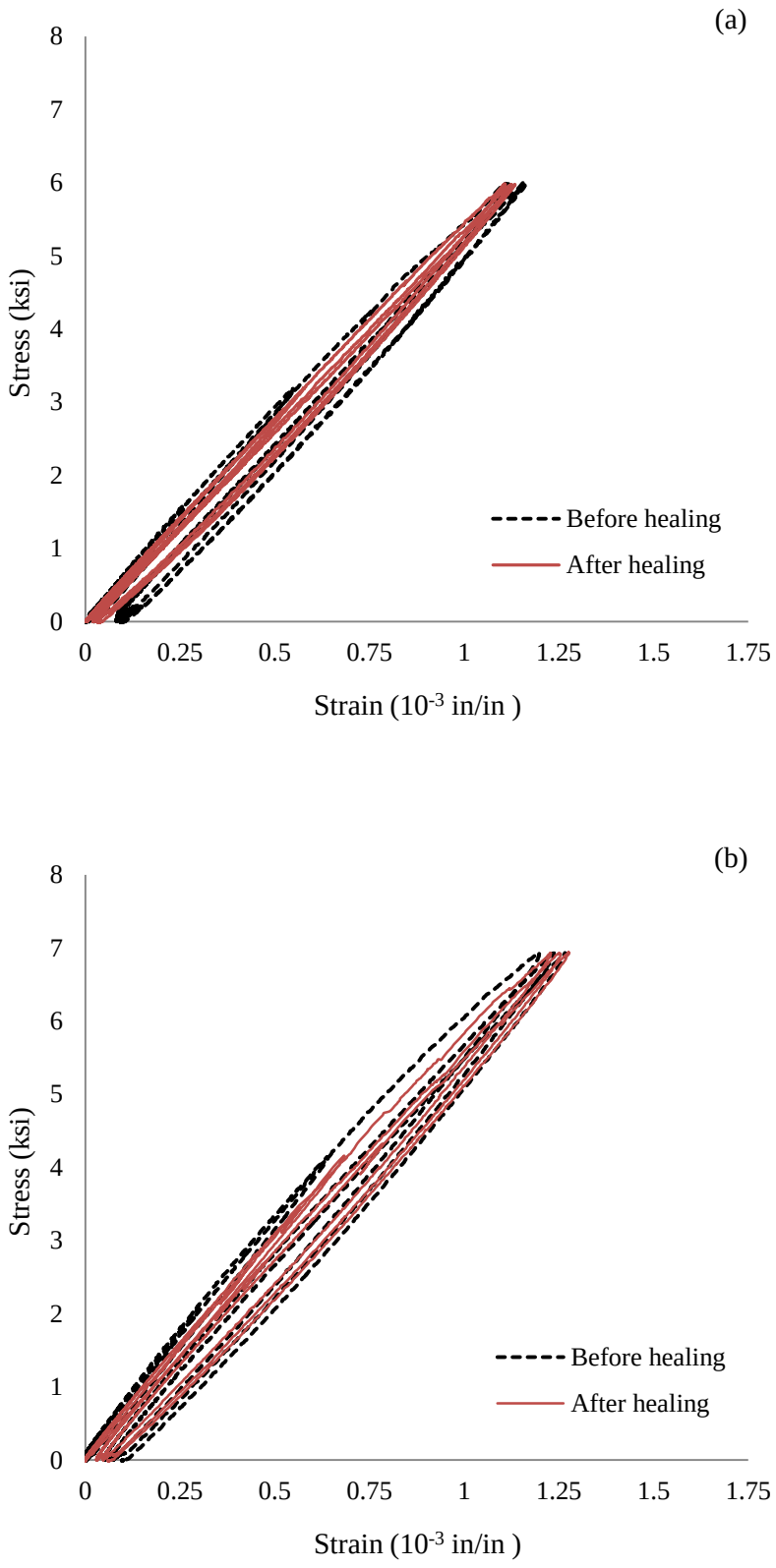


Figure 3-9: Stress-Strain Response for Ordinary Concrete Specimens: (a) Unconfined, and (b) FRP-Confined

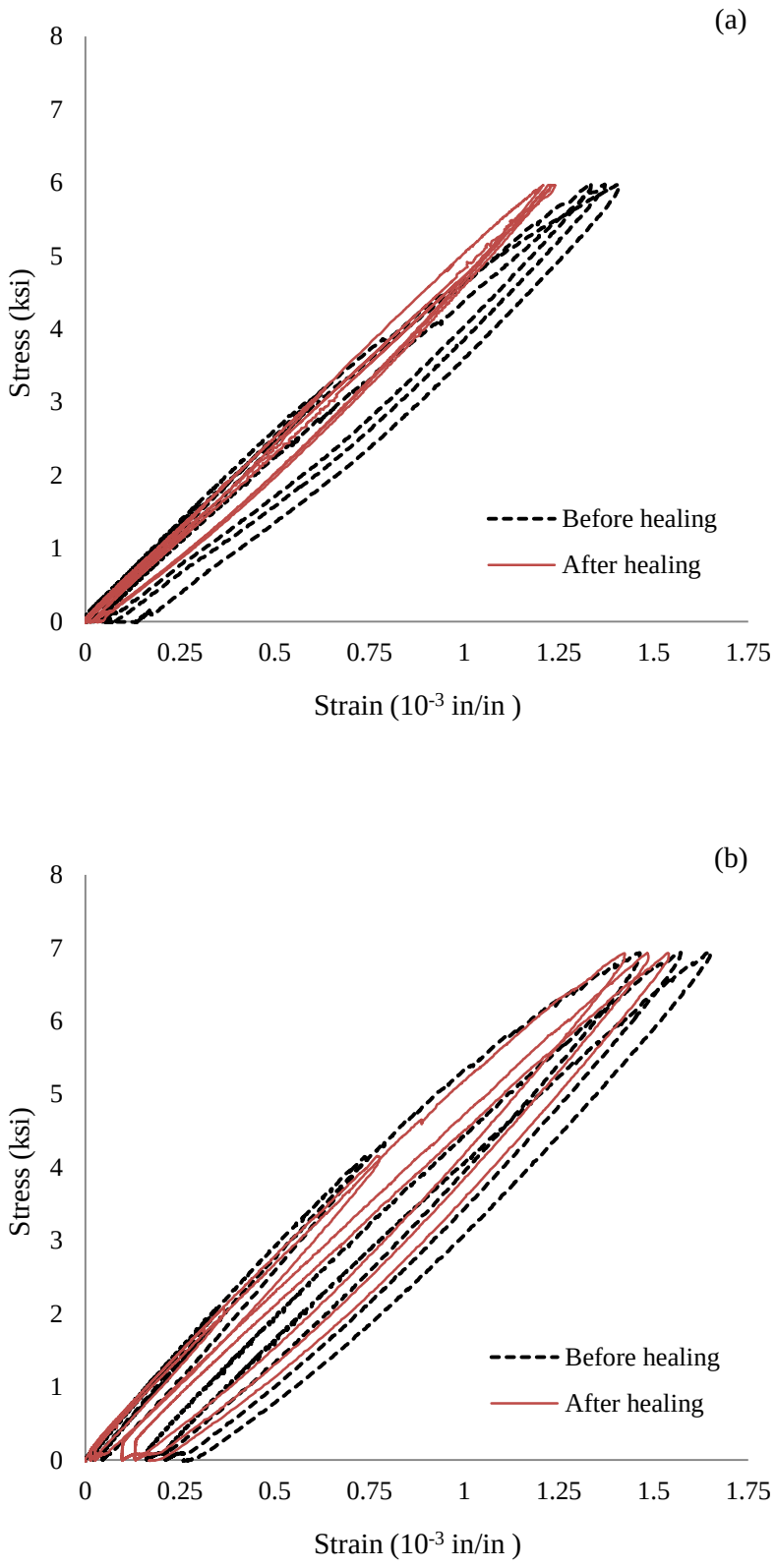


Figure 3-10: Stress-Strain Response for Concrete Specimens with 1.0% SS: (a) Unconfined, and (b) FRP-Confined

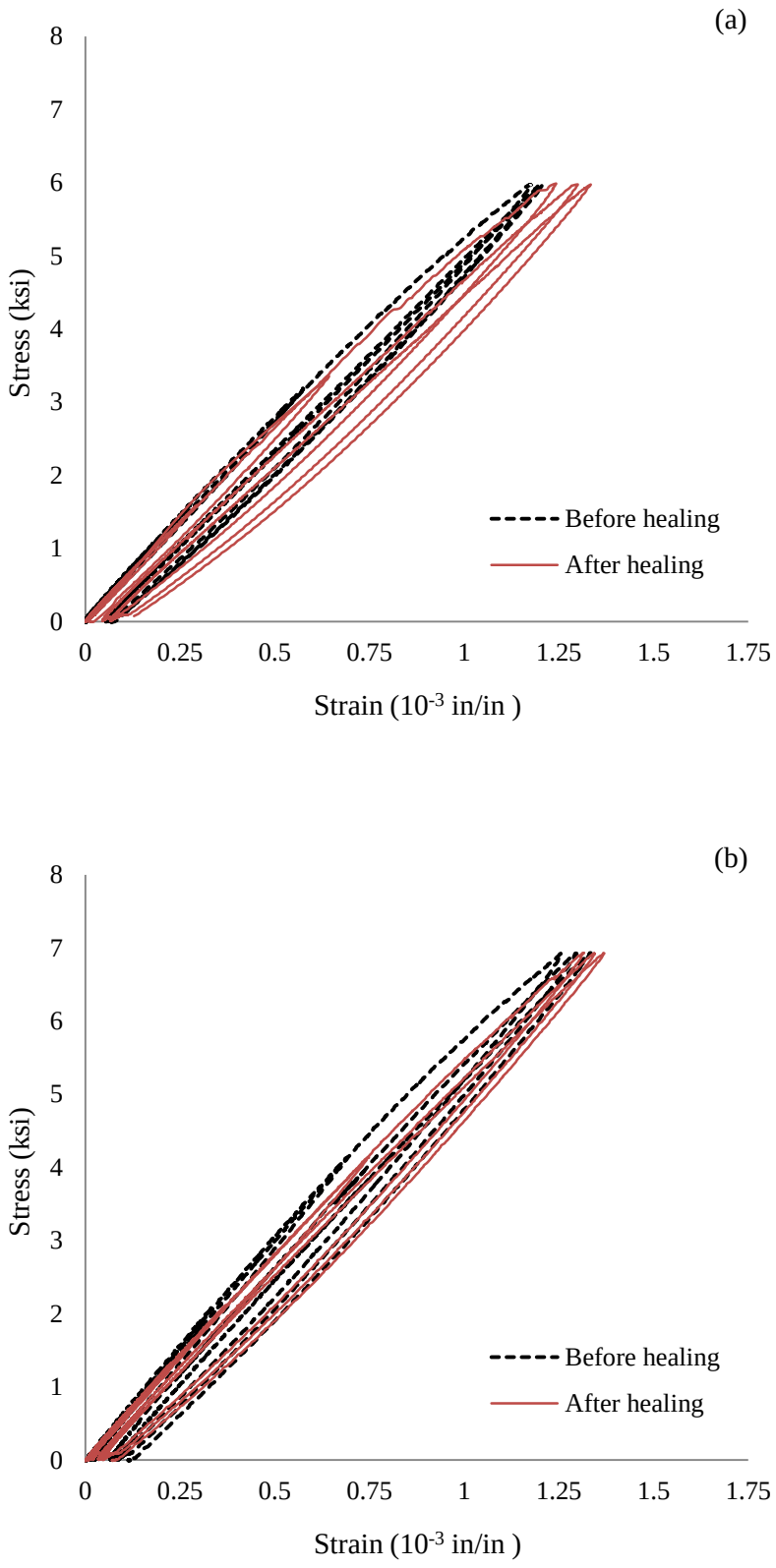


Figure 3-11: Stress-Strain Response for Concrete Specimens with 2.5% SS: (a) Unconfined, and (b) FRP-Confined

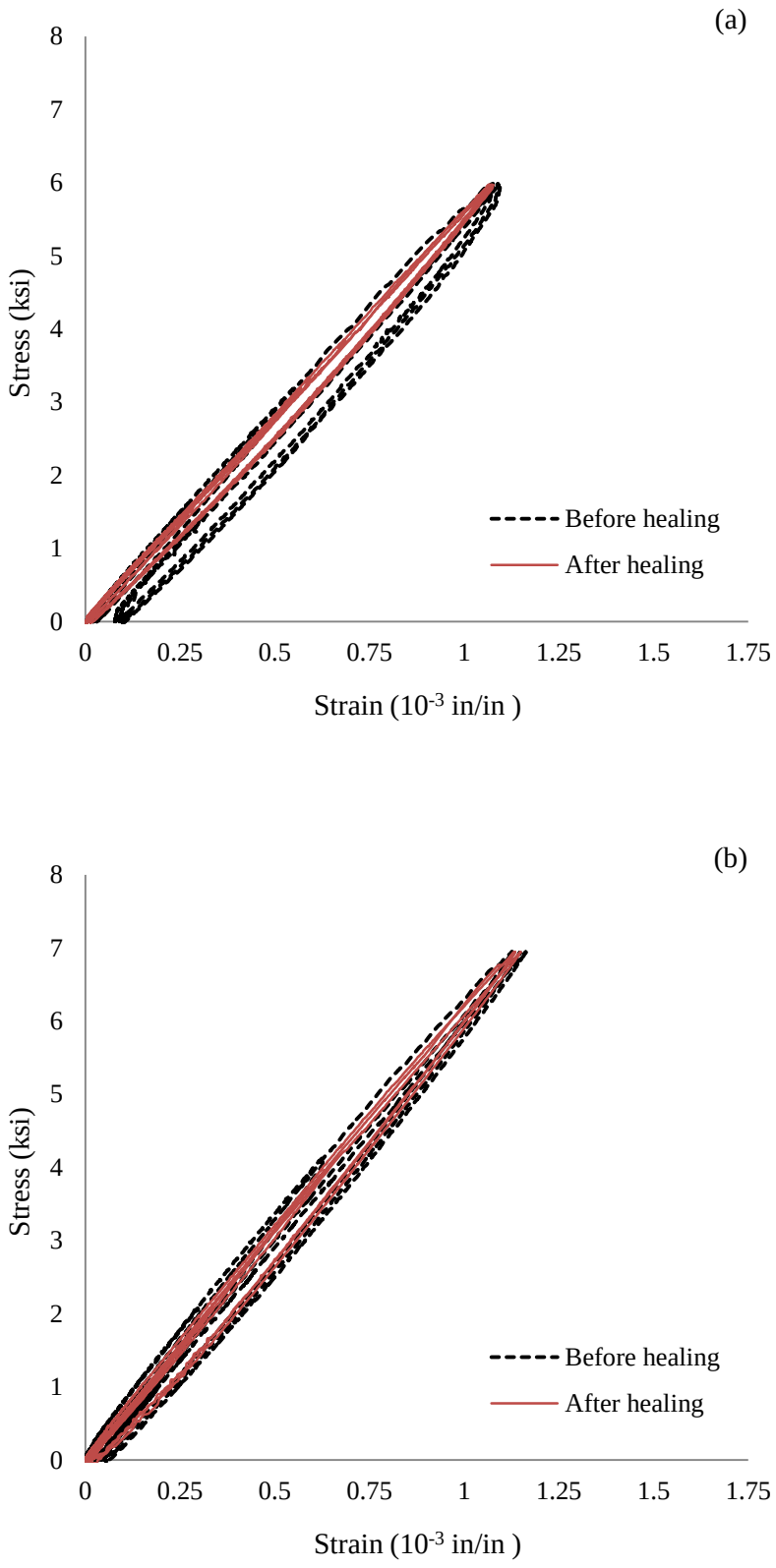


Figure 3-12: Stress-Strain Response for Concrete Specimens with 5.0% SS: (a) Unconfined, and (b) FRP-Confined

Table 3-7: Concrete strength test results

Specimen ID	Specimen #	Strength (ksi)	Average Strength (ksi)	Standard Deviation
SH00PL	1	98.98	98.98	-
	2	Local Failure	-	
SH00FRP	1	125.50	137.60	17.11
	2	149.70		
SH10PL	1	90.92	90.92	-
	2	Local Failure	-	
SH10FRP	1	144.50	142.00	3.54
	2	139.50		
SH25PL	1	97.52	98.96	2.04
	2	100.40		
SH25FRP	1	143.30	139.40	5.52
	2	135.50		
SH50PL	1	107.90	107.50	0.57
	2	107.10		
SH50FRP	1	118.70	119.70	1.41
	2	120.70		

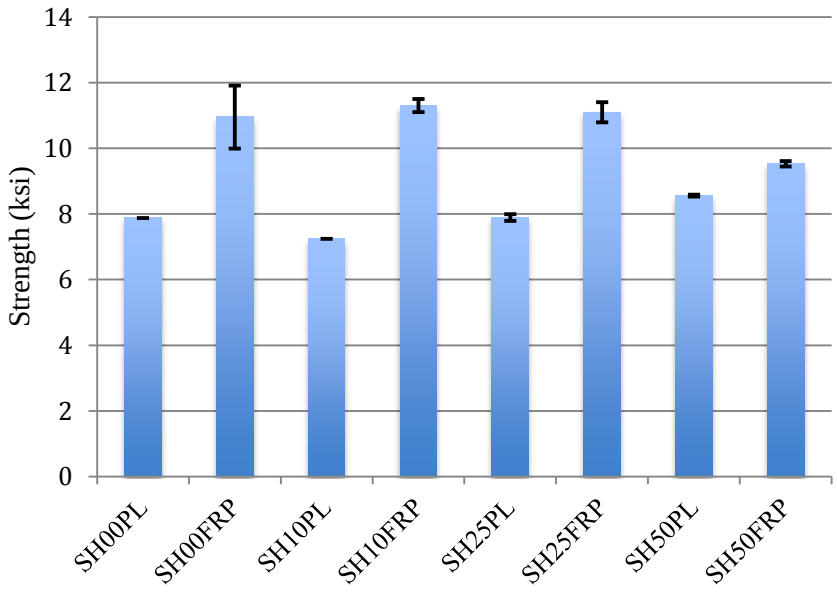


Figure 3-13: Concrete Strength Test Results

A small variance is found between the strength of the specimens within each group. For the unconfined concrete specimens, a strength drop is observed between the SH00PL group and the SH10PL group. The strength of the unconfined concrete specimens increases from SH10PL to SH50PL. This observation suggests that the content of the SS microcapsules affects the strength of the concrete material. For the FRP-wrapped specimens, the average strength is almost the same for the SH00FRP, SH10FRP and SH25FRP groups, whereas the average strength of the SH50FRP group is significantly lower than the other groups. Since the strength of the SH50PL groups is higher than the strength of other groups with lower SS content, this observation suggests that the strength of the FRP-wrapped specimens depends on the quality of the FRP confinement application rather than on the SS content.

3.5 Conclusions Regarding the Tested Hypothesis Based on Self-Healing Stiffness and Strength Tests

The results obtained in the self-healing stiffness tests are insufficient to prove or disprove the hypothesis that composite action due to FRP confinement can increase the efficiency of self-healing mechanisms in the concrete. In fact, the experimental results from the self-healing stiffness tests indicate that the self-healing mechanism was not activated both in the unconfined and confined specimens. However, the experimental results obtained from the strength tests indicate that the presence of SS microcapsules affects the strength of the concrete for unconfined specimens.

The obtained results indicated that additional experiments and analysis were needed to gain additional insight into the problem at hand, and that a modified research plan was needed to reliably test the hypothesis that composite action can improve the self-healing properties of self-healing concrete. To this end, the research presented in this thesis was extended to shed light on the reasons of non-activation of the self-healing mechanism in the experimental campaign

presented in this chapter. The hypotheses made to explain the non-activation of self-healing mechanism and the additional tests performed to test these hypotheses are presented in the next chapter of this thesis.

4 FURTHER INVESTIGATION OF THE RESULTS

4.1 Proposed Hypotheses

The results presented in Chapter 3 of this thesis were inconclusive in proving or disproving the hypothesis that composite action due to FRP confinement can improve the self-healing properties of self-healing concrete. The reason of this inconclusiveness was that the self-healing mechanism was not activated during the self-healing stiffness test. However, the strength test results indicated that the SS content affected the strength of the concrete specimens. Thus, a set of new hypotheses were proposed and investigated in order to understand the reasons of the non-activation of the self-healing mechanism. The proposed hypotheses were:

Hypothesis #1: The experimental test was affected by quality control issues (e.g., improper mixing of the self-healing concrete, errors in the execution of the self-healing stiffness test).

Hypothesis #2: The loading level reached in the self-healing stiffness test was insufficient to damage the concrete and trigger the self-healing mechanism. If the loading level reached in the test was too low to damage the concrete, the micro-cracks formed in the concrete would be too small to break the SS microcapsules and to release the self-healing material into the concrete. In this case, the self-healing concrete behavior would not be affected by the SS content.

Hypothesis #3: The healing procedure used in the self-healing stiffness test (i.e., submerging the concrete specimens in water with a temperature between 20 ℃ to 25 ℃ for a one-week period) was not sufficient to trigger the self-healing mechanism of the self-healing material. If the healing procedure was insufficient, the content of the SS microcapsules would not react with the concrete components to close the micro-cracks. In this case, improving the self-healing process (i.e., repeating it using water at a higher temperature and/or waiting a longer period of time) would activate (at least partially) the self-healing mechanisms.

Hypothesis #4: The manufacturing process of SS microcapsules was affected by quality control problems. If the SS was not successfully encapsulated, no stiffness recovery could be achieved even if the self-healing mechanism was triggered. In this case, the self-healing concrete composition would be different from that of the specimens used in the previous research performed at LSU (Gilford et al. 2013), for which self-healing of the concrete was successfully achieved.

Hypothesis #5: The SS microcapsules' outer shell was too thick to be broken by the stress concentration near the cracks produced by the loading. In this case, the micro-cracks in the concrete would propagate around the SS microcapsules without breaking them and without releasing the self-healing agent. In this case, the concrete specimens would contain undamaged SS microcapsules.

Hypothesis #6: The SS microcapsules suffered durability problems in the concrete environment. If the microcapsule outer shell decayed in the alkaline environment constituted by the concrete, the content of the microcapsules would have reacted with the concrete before the loading was applied. In this case, undamaged microcapsules would not be found within the self-healing concrete specimens.

Testing of hypothesis #1 would require repeating the entire experimental campaign. Funding limitations made impossible to repeat the investigation for this research project.

Hypothesis #2 was also quickly eliminated based on the results obtained in research previously performed by other researchers at LSU (Gilford et al. 2013), which showed that the self-healing mechanisms for SS microcapsules was activated at load levels that were even lower than the ones considered in the present research. In addition, the stress-strain curves obtained in this research for the self-healing specimens showed non-negligible plastic damage in the

concrete matrix. These results also support the elimination of hypothesis #2 as a possible explanation of the non-activation of the self-healing mechanism.

Based on the previous considerations, hypotheses #3 through #6 were further investigated.

4.2 Investigation of Hypothesis #3

Investigation of hypothesis #3 was performed by completing an additional self-healing stiffness test with a modified healing procedure. In research previously performed by other researchers at LSU (Gilford et al. 2013), the healing procedure was described as a curing period of 48 hours in 80 ℃ water, which was proven effective to trigger the self-healing mechanism of the self-healing concrete. It is noted here that higher temperature of the water bath and extended healing time promote the reaction of the self-healing agent with the concrete. Thus, the new self-healing procedure was obtained by submerging a select set of self-healing concrete specimens from the previous phase of this research in a water bath at a temperature of 65 ℃ (i.e., the maximum temperature that could be reached with the available facilities) for six days.

The select set of self-healing concrete specimens consisted of the three SH50PL cylinders (i.e., the unconfined concrete specimens with 5% SS microcapsules), for which a more significant reaction of the self-healing agent with the concrete could be expected due to the higher content of SS. The specimens were submerged in the bath of hot water and an additional set of self-healing stiffness tests were performed before completing the strength tests for the subject specimens. The ASTM C469 standard (ASTM 2010) was used to evaluate the stiffness of the specimens after the second healing period, by subjecting the specimens to a third set of cyclic loading (four loading cycles up to 40% of the specimens' compressive strength). A second set of stiffness variations ($\Delta E^{'}$), as well as the tangent stiffness moduli of the concrete specimens after healing ($E_h^{'}$) and the tangent stiffness moduli of the damaged concrete specimens ($E_d^{'}$), were

calculated and are presented in Table 4-1. A stiffness variation similar to that observed after the first healing procedure was observed also after the modified healing procedure, i.e., also in this case a negligible or null stiffness recovery was observed.

Table 4-1: Stiffness variation of SH50PL cylinders

Specimen ID	Specimen #	E_0 (ksi)	E_d (ksi)	E_h (ksi)	E_d' (ksi)	E_h' (ksi)	ΔE (%)	Average ΔE (%)	$\Delta E'$ (%)	Average $\Delta E'$ (%)
SH50PL	1	6.04	5.88	5.70	5.58	5.28	-2.97	-0.18	-0.05	-0.07
	2	6.33	6.21	6.09	6.18	5.55	-1.80		-0.10	
	3	6.12	5.62	5.88	5.75	5.45	4.24		-0.05	

Figure 4-1 compares the stiffness results of the self-healing stiffness test performed in the first phase of this research and of the third set of cyclic loading performed after the modified

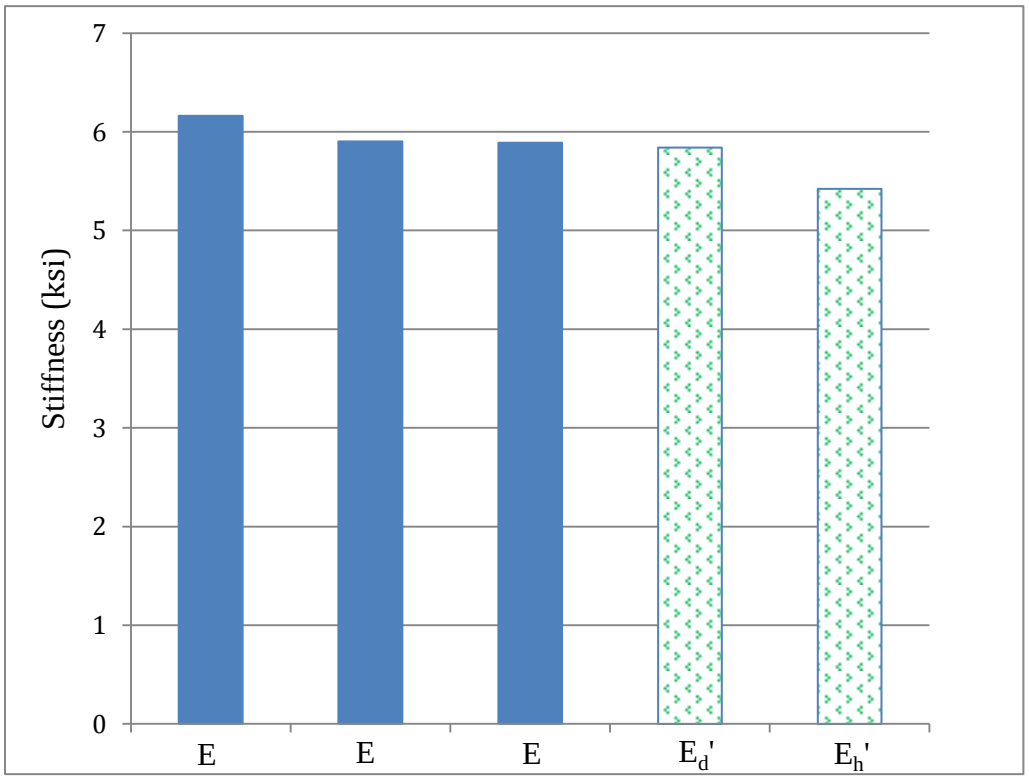


Figure 4-1: Results of the Third Set of Stiffness Test for SH50PL Cylinders

healing procedure for the three SH50PL cylinders. These results indicate that: (1) no significant stiffness recovery was achieved after the first healing period; (2) a small stiffness loss was observed after the second set of cyclic loading (i.e., $E_d^{'}$ is slightly E_h); and (3) no stiffness recovery was achieved either after the self-healing concrete specimens were treated with the modified healing procedure. In addition, a non-negligible stiffness loss is observed in Figure 4-1 between $E_d^{'}$ and $E_h^{'}$. Based on these results (i.e., no stiffness recovery was achieved after the modified healing procedure), it was concluded that hypothesis #3 is not valid, i.e., that the non-activation of the self-healing mechanism was not due to an insufficient healing procedure.

4.3 Investigation of Hypotheses #4 to #6

The investigation of hypotheses #4 through #6 was performed by conducting SEM tests (i.e., imaging and EDX) on both the self-healing concrete specimens that were tested in the present research (referred to as "non-healed specimens" in the following), and the specimens that were tested in the previous research performed by other researchers at LSU (Gilford et al. 2013) (referred to as "healed specimens" in the following). The SEM/EDX tests were used to identify: (1) if healed and non-healed specimens were characterized by different element compositions, which would suggest the validity of hypothesis #4, i.e., that the manufacturing process of SS microcapsules was affected by quality control problems; (2) if complete microcapsules were present inside the non-healed specimens, which would suggest the validity of hypothesis #5, i.e., the SS microcapsules outer shell was too thick to be broken by the cracks generated by the loading; (3) if no SS microcapsules were found within the concrete matrix of both the healed and non-healed specimens, which would suggest the validity of hypothesis #6, i.e., the microcapsules broke before the stiffness test due to the durability problems of outer shell of SS microcapsules in the concrete alkaline environment.

4.3.1 Experimental Matrix of SEM Test

The experimental matrix followed in the SEM tests is shown in Table 4-2. The specimens are identified using the same acronyms as in the self-healing stiffness tests with the addition of a final portion used to identify if the specimen successfully healed or not, i.e., H = healed specimens (specimens from the previous research performed by other researchers at LSU (Gilford et al. 2013) for which significant stiffness recovery was observed after the healing procedure), and NH = non-healed specimens (specimens from the present research for which no consistent stiffness recovery was observed after the healing procedure).

Table 4-2: Experimental matrix for the SEM tests

Specimen ID	Healing condition	SS content	Confinement type	Number of specimens	Number of samples
SH00PL-H	Healed	0.0%	unconfined	1	9
SH50PL-H		5.0%	unconfined	1	9
SH00PL-NH	Non-healed	0.0%	unconfined	1	9
SH50PL-NH		5.0%	unconfined	1	9
SH00FRP-NH	Non-healed	0.0%	FRP	1	9
SH50FRP-NH		5.0%	FRP	1	9

4.3.2 Sample Preparation of SEM Tests

A sampling scheme was designed to take a sufficient amount of samples from different locations in each concrete cylinder in order to be representative of the properties of the entire specimen. The sampling method followed in this research to prepare the samples for the SEM tests is shown in Figure 4-2. As shown in the experimental matrix, six cylinders were selected for the SEM tests and nine samples were cut from each cylinder. Although any sample type can be examined by SEM imaging, the best use of the SEM imaging requires flat, polished surfaces

(Stutzman 1991). In particular, sawn unpolished surfaces appear to be the best for SEM investigation of concrete (Marusin 1995). Thus, all cylinders were cut using fine diamond-impregnated wire saw without using any coolant to prevent contamination of the samples. Three sample sections with a thickness of 0.25 in (5 mm) were cut from each cylinder at the vertical quarter positions (see Figure 4-2). Three 0.4 in × 0.4 in (10 mm × 10 mm) square samples were then cut out of each sample section. The sample sections from specimen SH00PL-H are shown in Figure 4-3 (a), whereas the final square samples that were used for the SEM tests are shown in Figure 4-3 (b).

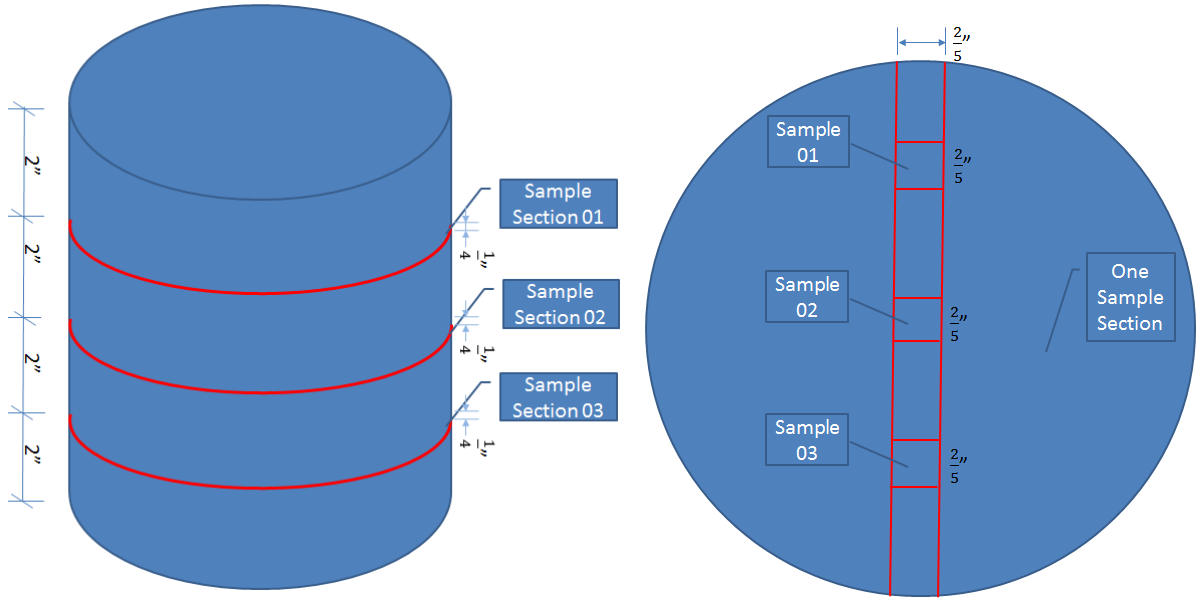


Figure 4-2: Sample Preparation Method for SEM Tests

After the completion of the sample cutting, all the samples were dried under a vacuumed environment. To prevent charging of the specimens with an electron beam under high vacuum and high voltage SEM mode, all samples were sputter coated with platinum shortly before being tested.

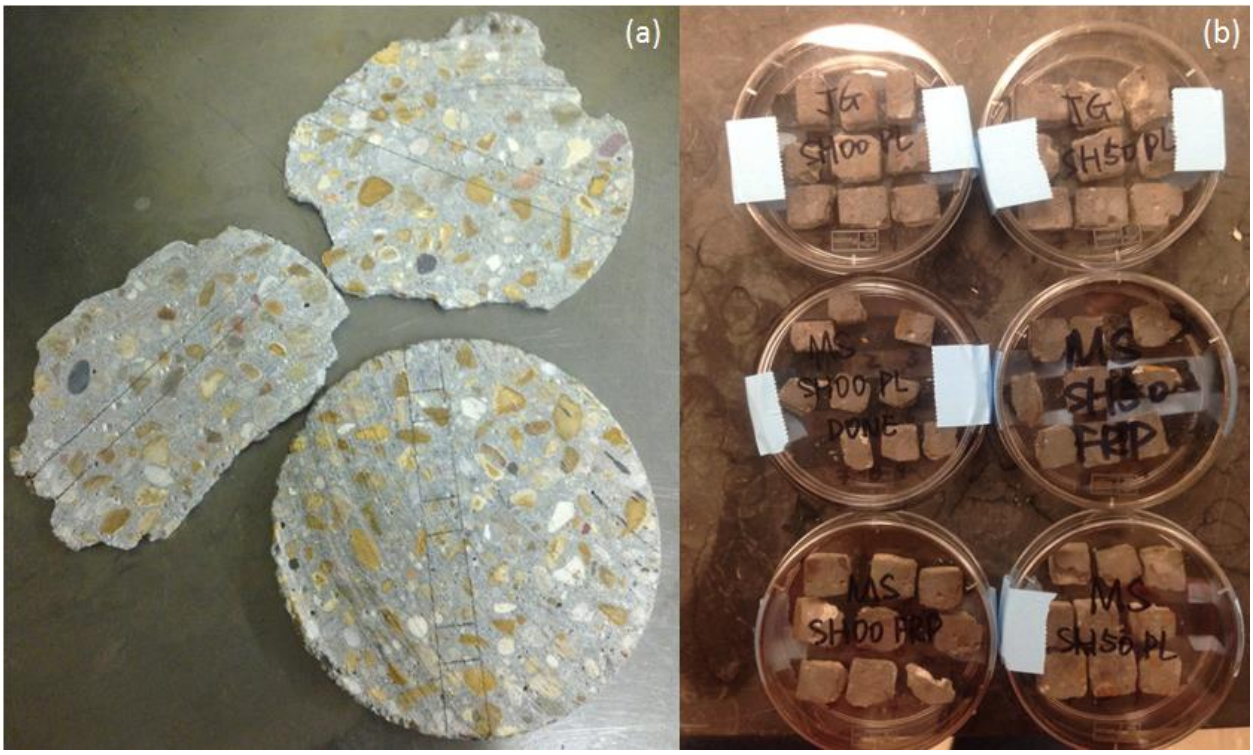


Figure 4-3: Concrete Samples for SEM Tests: (a) Sample Sections and Locations of Samples for SEM Tests; and (b) Final Samples

4.3.3 Experimental Methodology

Three sets of SEM tests were performed to investigate hypothesis #4 through #6:

SEM test #1: a large scale EDX analysis was performed to investigate hypothesis #4. The SEM parameters were set as following: electron column voltage 20 kV, electron beam spot size 6, high vacuum environment, filament voltage 1.36 V, and magnification × 160. EDX tests results provided the element composition of the concrete material for both the healed and non-healed specimens. Since the same concrete mix was used to pour both the healed and non-healed specimens, validity of hypothesis #4 would require a significantly lower silicon and/or sodium content in the element composition of the non-healed specimens when compared to the healed specimens.

SEM test #2: SEM imaging and EDX analysis focused on particles having similar external appearance of SS microcapsules (possible microcapsules) were performed to investigate hypothesis #5 and #6. Possible microcapsules were searched and imaged within the concrete matrix of each SEM sample. A small scale EDX analysis was performed focusing on these possible microcapsules. The SEM parameters were set to be the same as in SEM test #1, except for: electron beam spot size 3, and magnification × 10000~20000. A high percentage of the sodium element would suggest that the identified possible microcapsule could be actual SS microcapsules. The presence of a statistically significant number of SS microcapsules in the concrete matrix would suggest the validity of hypothesis #5 over hypothesis #6.

SEM test #3: focused ion beam slope cutting and SEM imaging were performed to further investigate hypothesis #5 and #6 by examining the inner condition of the possible microcapsules. The SEM parameters were set as in the previous SEM test #2. Some of the identified potential microcapsules were selected and cut using an ion beam. SEM imaging was performed over the cut sections to further examine the microstructure of the possible microcapsules (i.e., to identify the existence or lack thereof of an outer shell) in the concrete matrix. Results of this test were needed to confirm or refute the results obtained using focused EDX analysis.

4.3.4 Results of the SEM Test #1 (Large Scale EDX Analysis)

Figure 4-4 through Figure 4-9 present typical continuous X-ray spectra obtained from the scale EDX analysis of one of the nine samples corresponding to each of the specimens listed in Table 4-2. In these figures, the horizontal axis represents the incident electron energy (X-ray photon energy) expressed in keV (1 keV = approximately 1.6×10^{-16} joule), which results from the interactions between bombarding electrons and atomic nuclei and varies by element type. A qualitative analysis of the compositional elements in the target sample can be obtained by

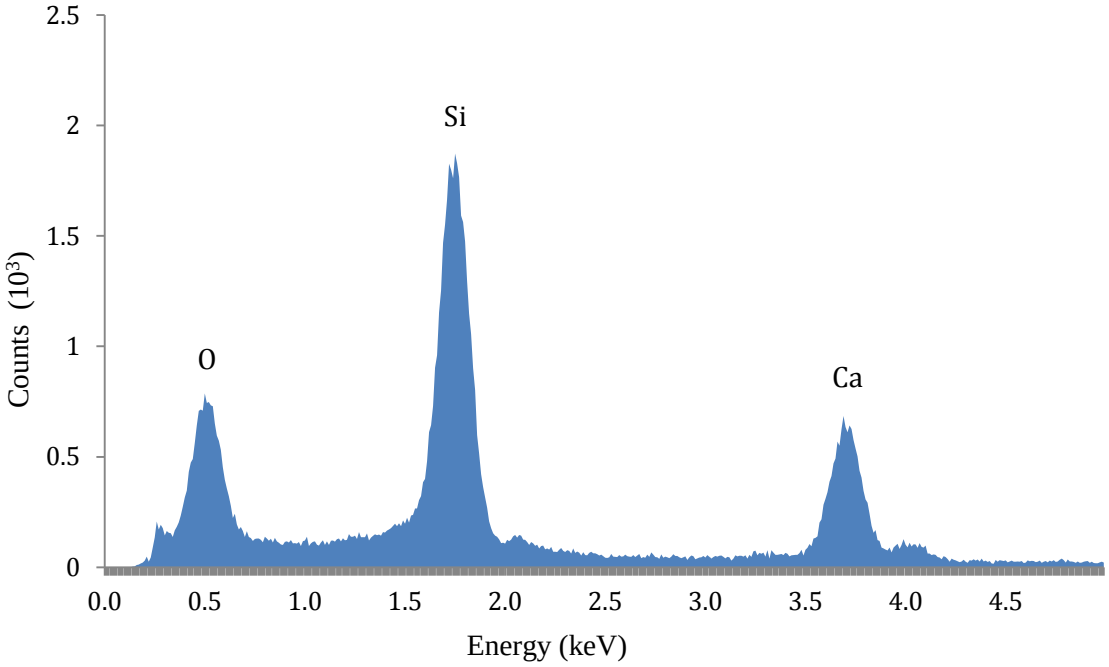


Figure 4-4: EDX Response of SH00PL-H Sample

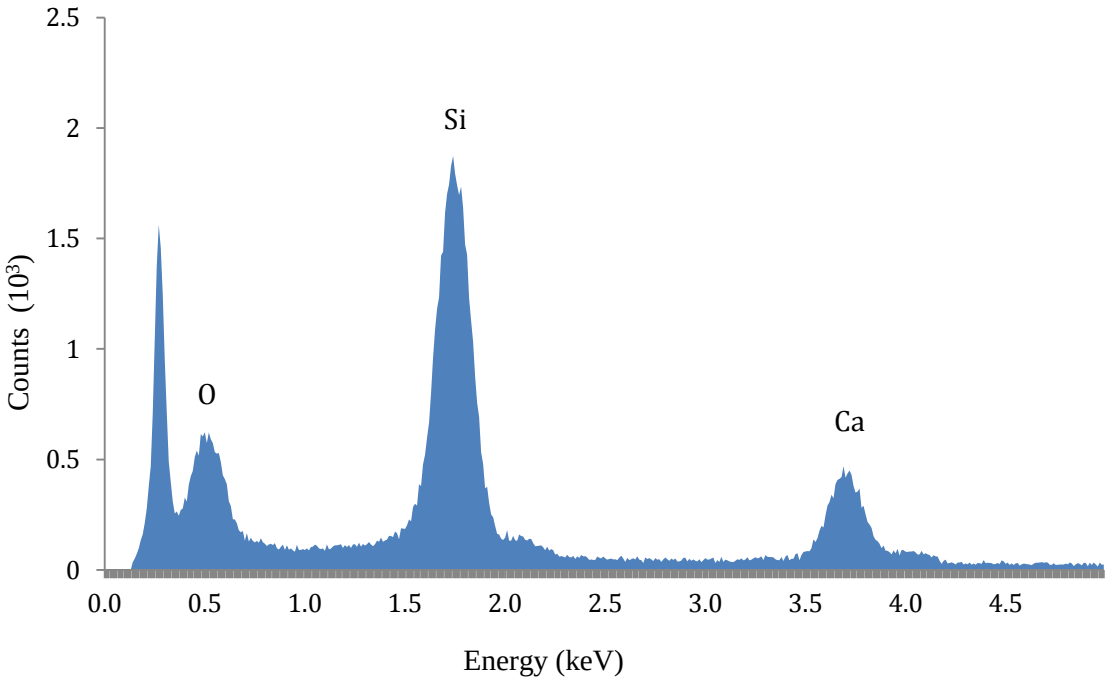


Figure 4-5: EDX Response of SH00PL-NH Sample

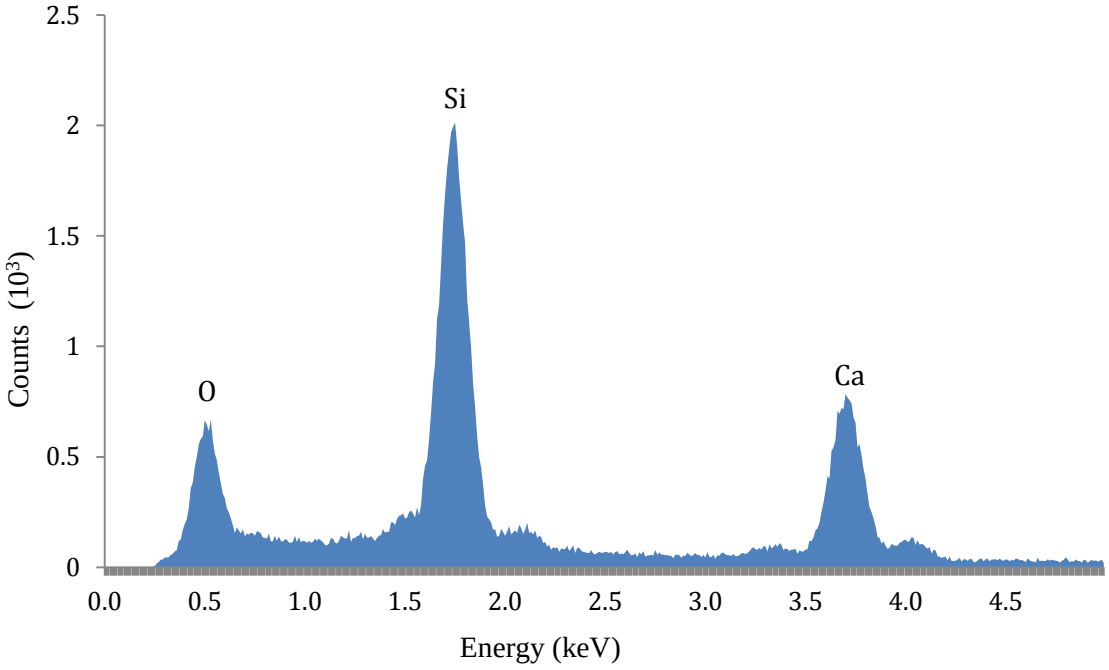


Figure 4-6: EDX Response of SH00FRP-NH Sample

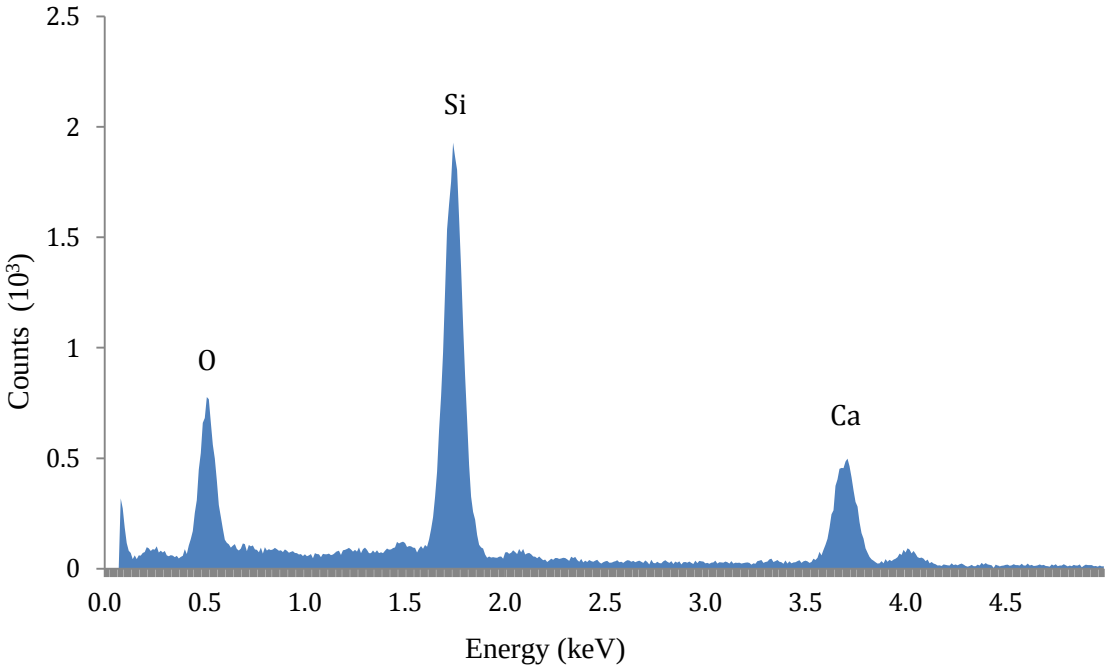


Figure 4-7: EDX Response of SH50PL-H Sample

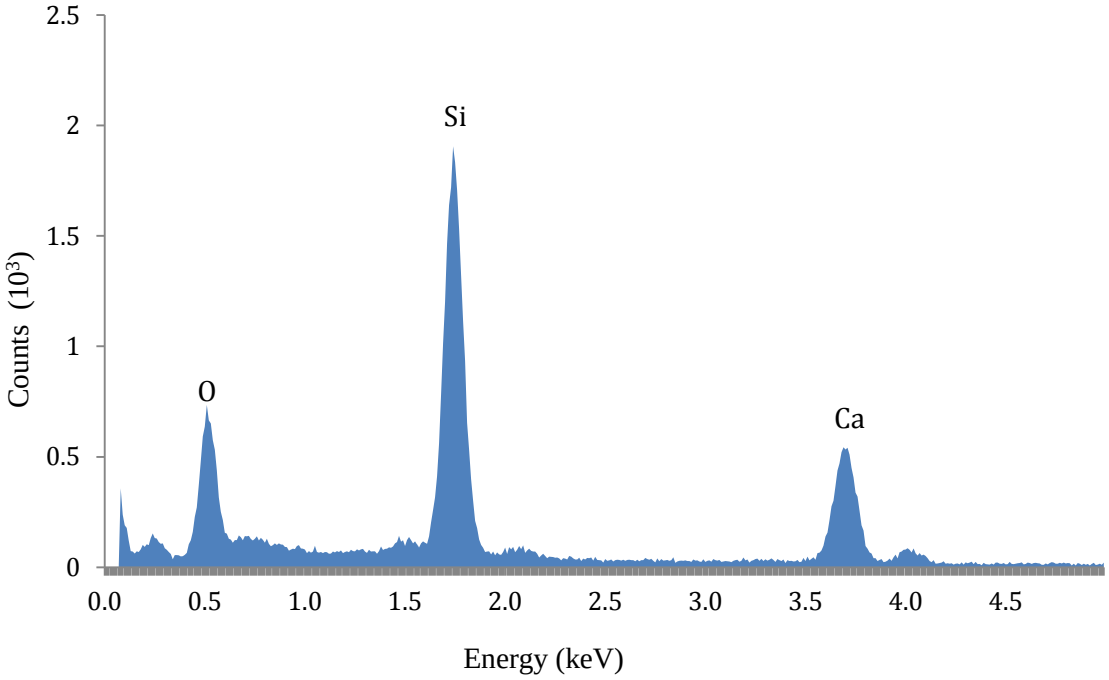


Figure 4-8: EDX Response of SH50PL-NH Sample

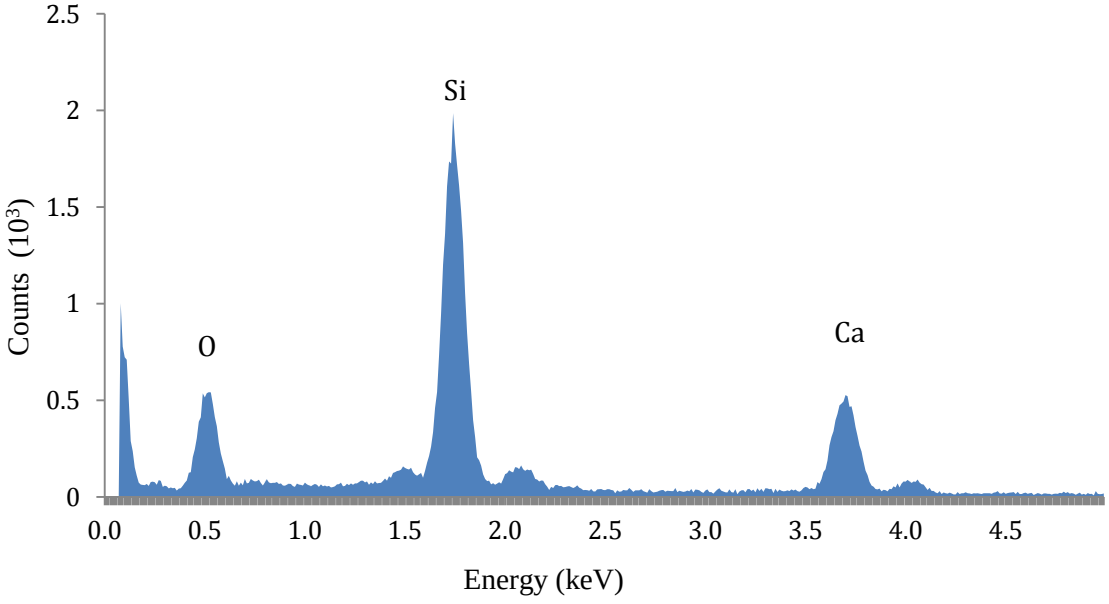


Figure 4-9: EDX Response of SH50FRP-NH Sample

identifying these energies (Reed 2005). The vertical axis represents the element concentrations in term of counts of pulses (current) of specific values of photon energy, which is an indication of a specific atom type. A quantitative analysis of the element composition can be performed by comparing the obtained element intensities corresponding to the samples to be analyzed with those emitted from standard samples (made of pure elements or compounds of know composition).

Figure 4-4 through Figure 4-6 presents the spectral responses of ordinary concrete samples (with 0.0% SS microcapsules) corresponding to SH00PL-H, SH00PL-NH, and SH00FRP-NH, respectively. Figure 4-7 through Figure 4-9 presents the spectral responses of self-healing concrete samples (with 5.0% SS microcapsules) corresponding to SH50PL-H, SH50PL-NH, and SH50FRP-NH, respectively. Except for the initial reflection peak and the peak corresponding to platinum (Pt) (the coating material) and located immediately after the silicon peak in the figures (i.e., at energy slightly higher than that corresponding to silicon), mainly three element peaks were observed: (1) the oxygen (O) peak, (2) the silicon (Si) peak, and (3) the calcium (Ca) peak. For a few locations in some of the samples, carbon (C) and/or aluminum (Al) peaks were also observed.

From the results presented in these figures, similar spectral responses were observed within the SH00 group and the SH50 group of specimens, respectively, which indicates that the concrete material had the same element composition within each group. Compared to the SH00 group specimens, the spectra of the SH50 specimens show a stronger response of silicon (which is a component of sodium silicate and of the silicate naturally present in the aggregate of the concrete), which is consistent with the fact that SS microcapsules in a quantity equal to 5.0% of the cement weight were added to the SH50 specimens, while the same concrete mix was used for

both SH00 and SH50 specimens. Sodium response was not found in any of the large scale EDX analysis spectrums. A possible explanation of this finding is that the sodium content in the concrete matrix is relatively low when compared to the content of other materials (i.e., the amount of sodium is below the EDX resolution).

At least 18 locations (two locations per sample) were chosen and analyzed for each cylinder. Table 4-3 summarizes the results of the large scale EDX analysis over the element composition of the concrete material. An increased content of silicon was considered as indication of the presence of SS microcapsules in the concrete matrix, even though sodium was not detected. The concrete material of the healed and non-healed specimens was found to have a very similar element composition for the unconfined concrete specimens within both the SH00 group and the SH50 group.

Table 4-3: Results of the large scale EDX analysis

Specimen ID	Sample spots	Weight (%)			Atom (%)		
		O	Si	Ca	O	Si	Ca
SH00PL-H	19	57.81	28.56	13.63	72.69	20.46	6.85
SH00PL-NH	18	56.71	28.38	14.90	71.93	20.51	7.57
SH00FRP-NH	21	50.16	28.64	21.19	66.92	21.78	11.29
SH50PL-H	19	53.34	34.80	11.86	68.46	25.38	6.16
SH50PL-NH	18	52.94	35.39	11.26	67.50	26.18	5.82
SH50FRP-NH	18	47.14	34.12	18.74	63.65	26.25	10.11

However, the FRP-confined specimens showed a lower percentage of oxygen and a higher percentage of calcium when compared to the unconfined concrete specimens. This observation can be explained by considering that the external FRP wrap can obstruct the interaction of the concrete with the air, which can lead to a lower level of concrete oxidation of the FRP-confined specimens when compared to the unconfined concrete specimens. In addition, the SH50 group

contained about 6% more silicon in terms of weight ratio, and about 5% more silicon in terms of atom percentage when compared to the SH00 group.

Thus, it was concluded that the concrete of the SH50 specimens contained SS microcapsules, which were successfully added to the concrete matrix and increased the content of silicon. Furthermore, the silicon content in the healed and non-healed specimens from both the SH00 and SH50 groups was very similar, i.e., about 28.5% by weight for the SH00 group, and about 34.8% by weight for the SH50 group. Based on the fact that the same concrete mix was used to produce both the healed and non-healed specimens, it was concluded that the composition of the microcapsules used to manufacture the healed and non-healed specimens was practically same. Thus, the non-activation of the self-healing mechanism cannot be explained as a quality control problem in the SS microcapsules' manufacturing process, and hypothesis #4 must be refuted.

4.3.5 Results of the SEM Test #2 (Small Scale EDX Analysis Focused on Potential Microcapsules)

For the SEM test #2, SEM imaging was employed to identify possible microcapsules (referred to as particles in the following), i.e., specific components within the samples that had an approximately spherical morphology similar to that of SS microcapsules. For each of the SH50 cylinders considered in Table 4-2, at least 18 particles (i.e., two particles per sample) were identified and analyzed with the EDX machine. A few particles in one of the ordinary concrete specimens (SH00FRP-NH) were also examined using the EDX machine in order to obtain a baseline comparison for the self-healing specimens.

Figure 4-10 through Figure 4-13 present a selected subset of the SEM images of the identified particles. The particles were easily distinguished from the base material in terms of brightness, shape, and/or texture. The external appearance of these particles is very irregular, which is consistent with the expected morphology of the SS microcapsules after they have been

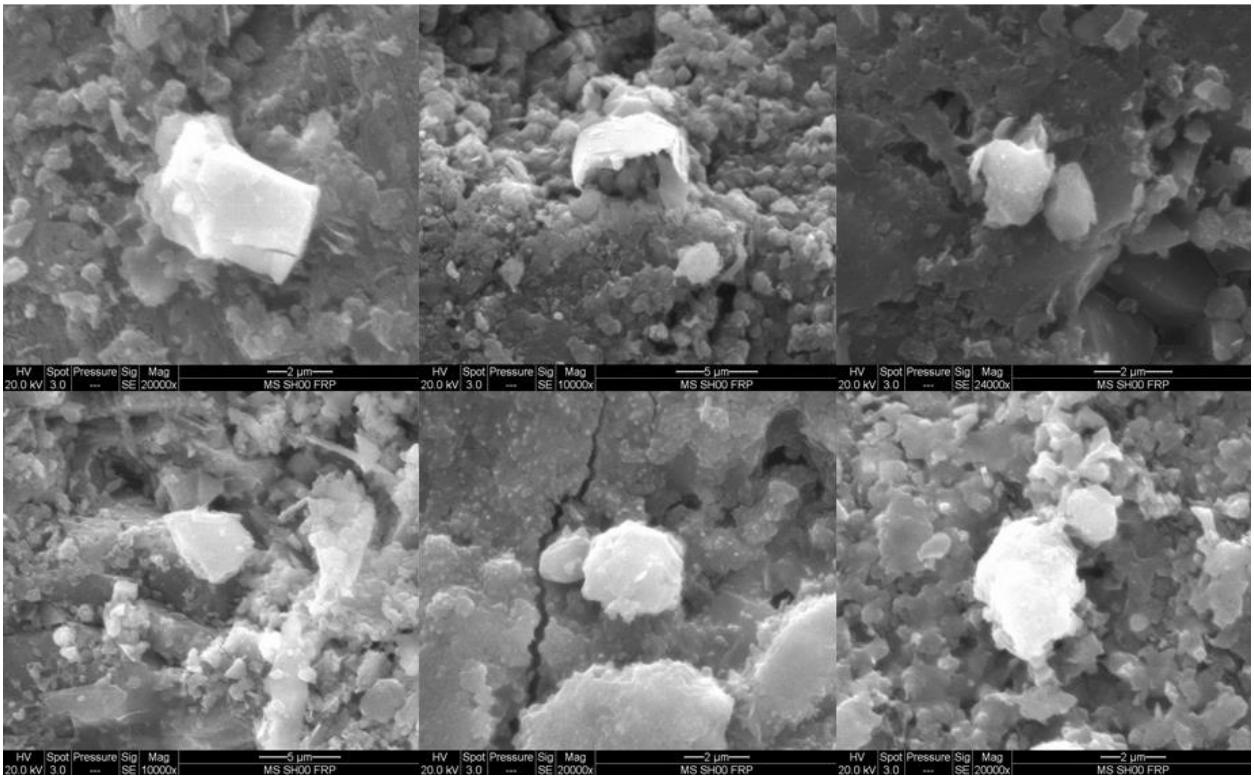


Figure 4-10: SEM Imaging of Particles from SH00FRP-NH Samples

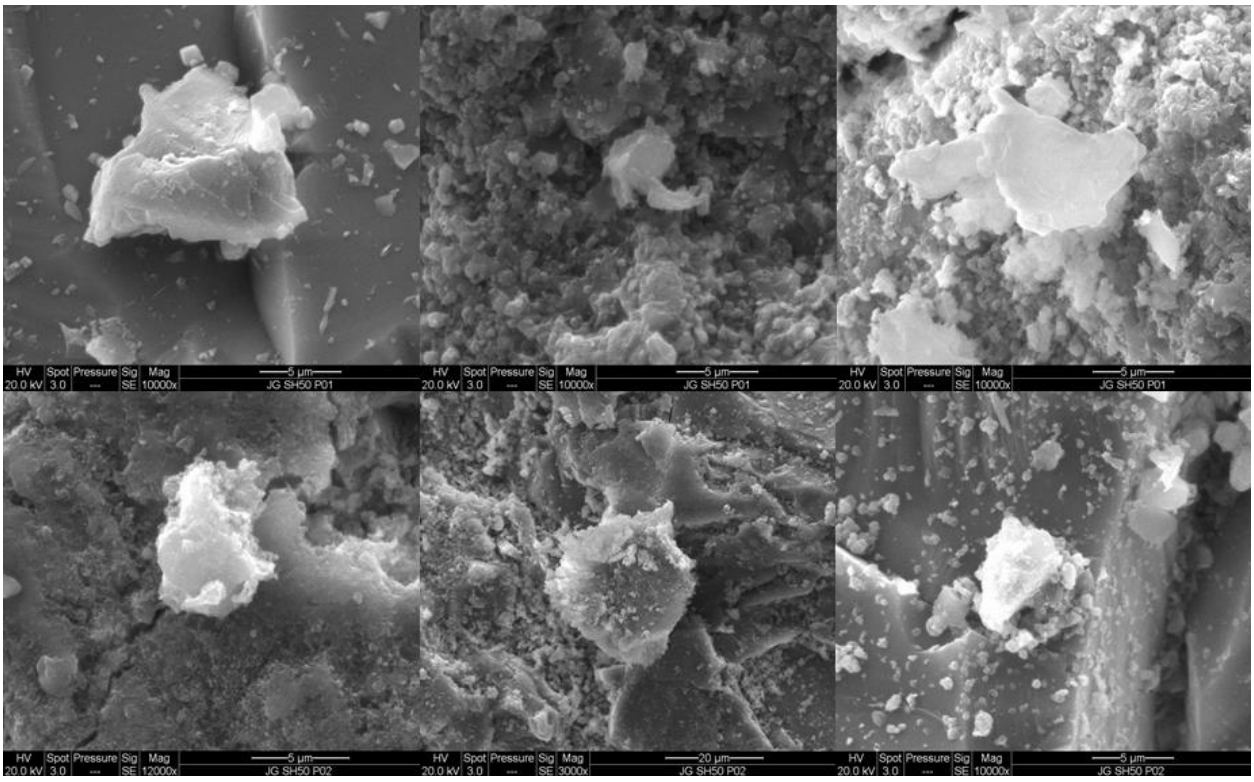


Figure 4-11: SEM Imaging of Particles from SH50PL-H Samples

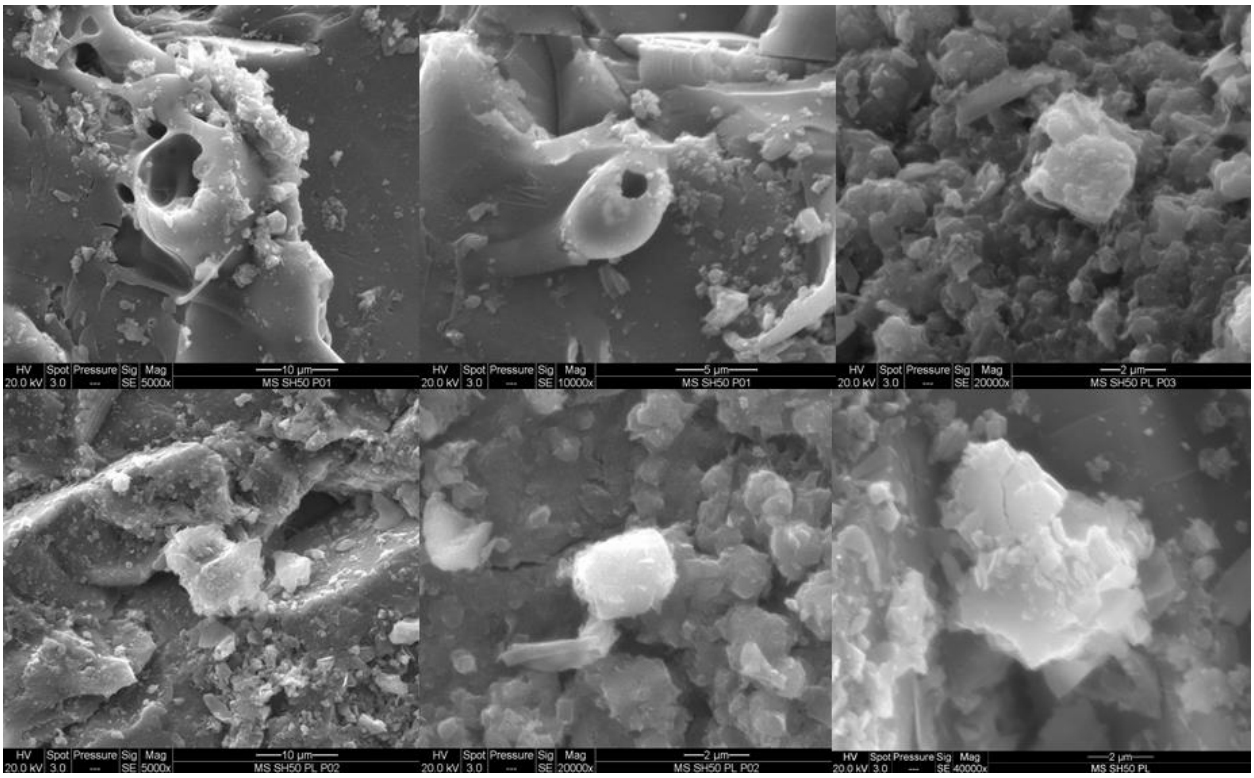


Figure 4-12: SEM Imaging of Particles from SH50PL-NH Samples

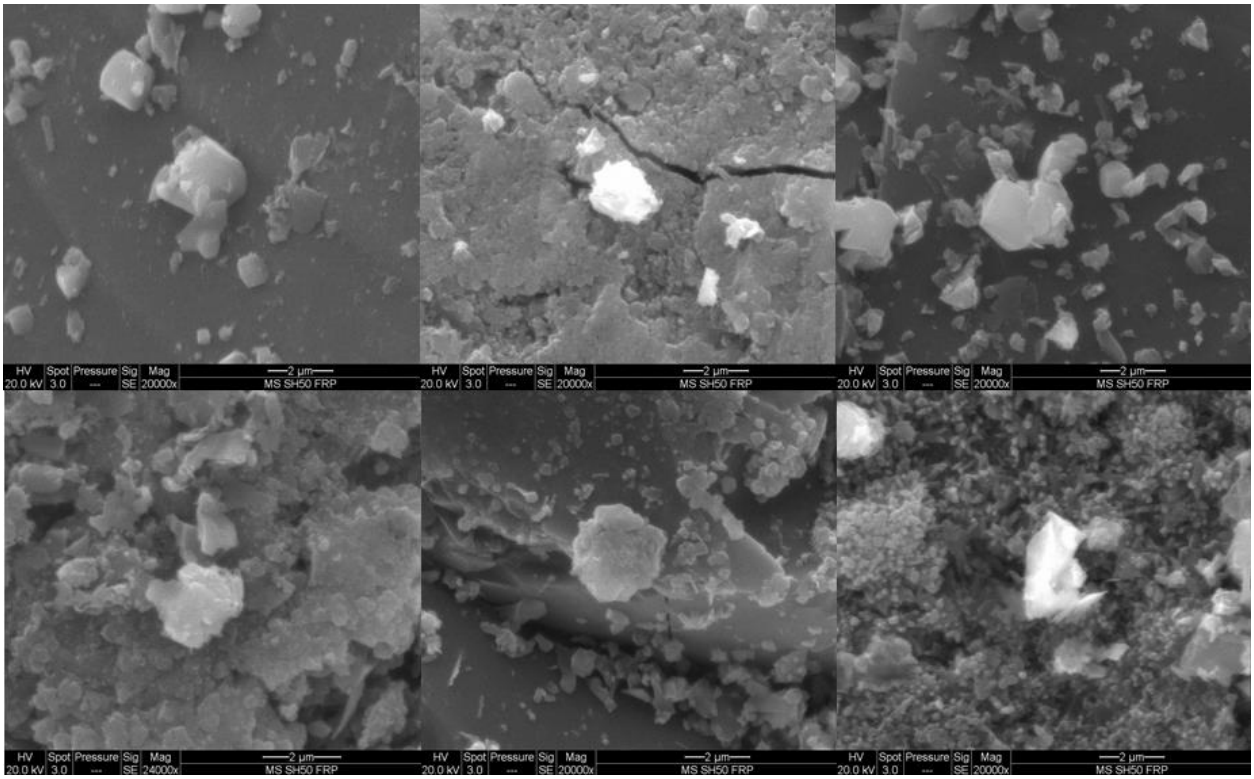


Figure 4-13: SEM Imaging of Particles from SH50FRP-NH Samples

mixed into the concrete. No significant difference was found in terms of external characteristics between the particles from the ordinary concrete specimen and the particles from the self-healing specimens. The SEM imaging tests were insufficient to determine whether a particle was an SS microcapsule or a different component of the concrete matrix. Thus, an EDX analysis was also conducted with the electron beam focused on each of the particles found.

Selected examples of the small scale EDX results are shown in Figure 4-14 through Figure 4-17. The small scale EDX spectra obtained in correspondence of the particles show large variability: some of the spectra are similar to the corresponding spectra obtained from the large scale EDX tests; some spectra show an extremely high percentage of silicon or calcium; and some other spectra show a miscellaneous element composition. The inconsistency of the particle compositions suggests that most of the identified particles are not actual SS microcapsules,

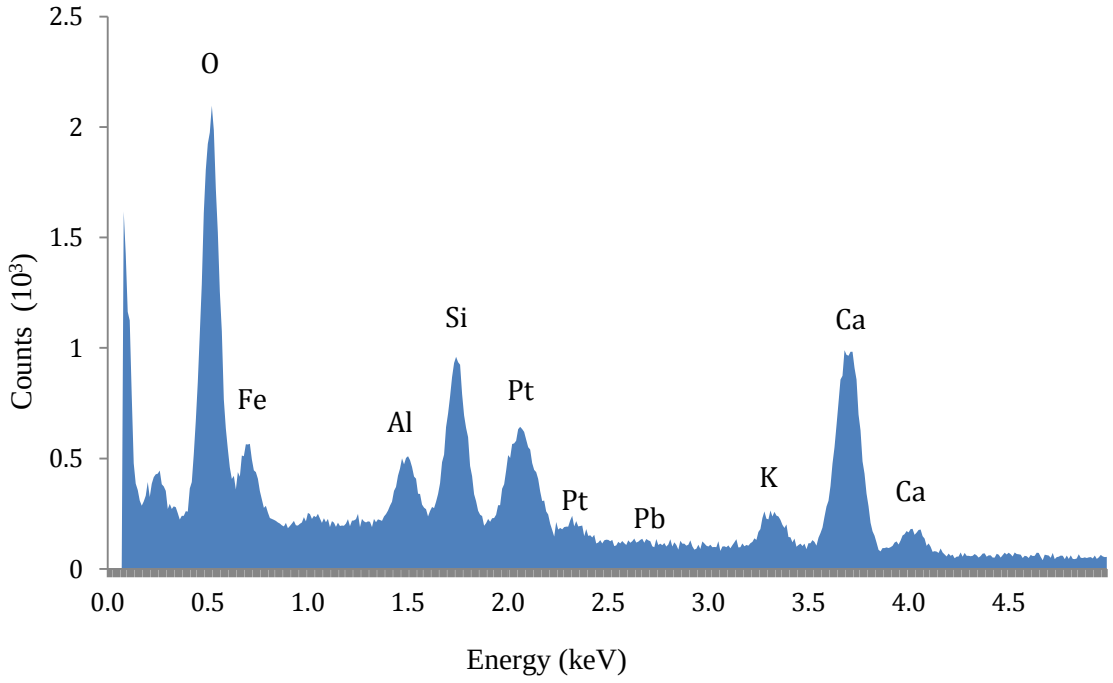


Figure 4-14: EDX Response of a Particle Selected from SH00FRP-NH

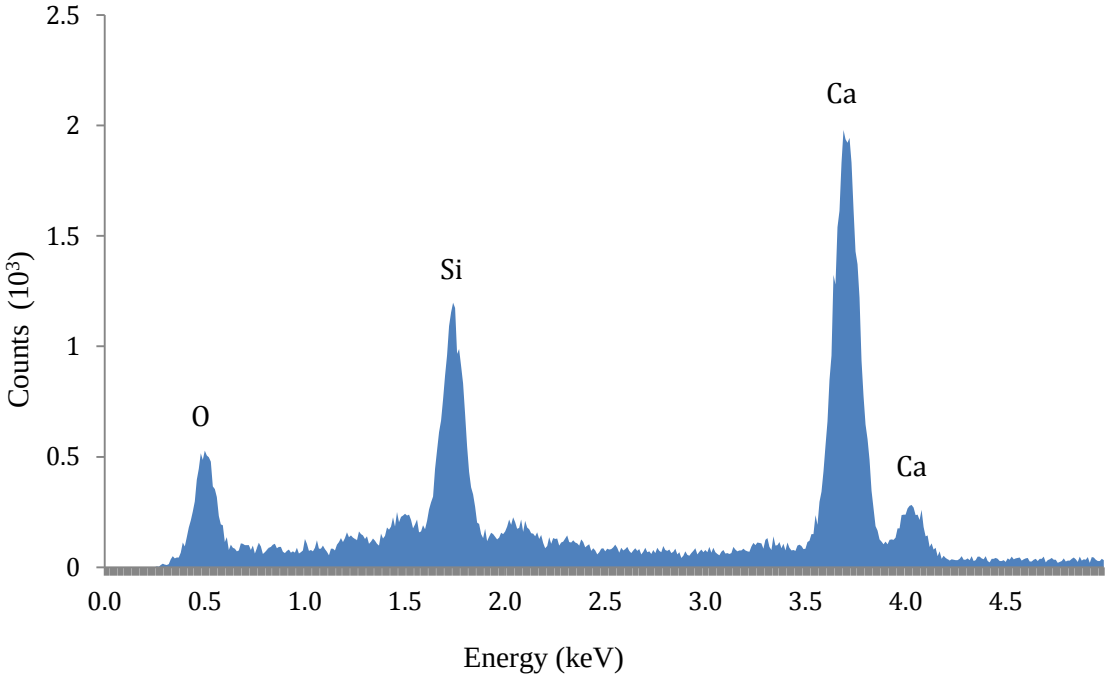


Figure 4-15: EDX Response of a Particle Selected from SH50PL-H

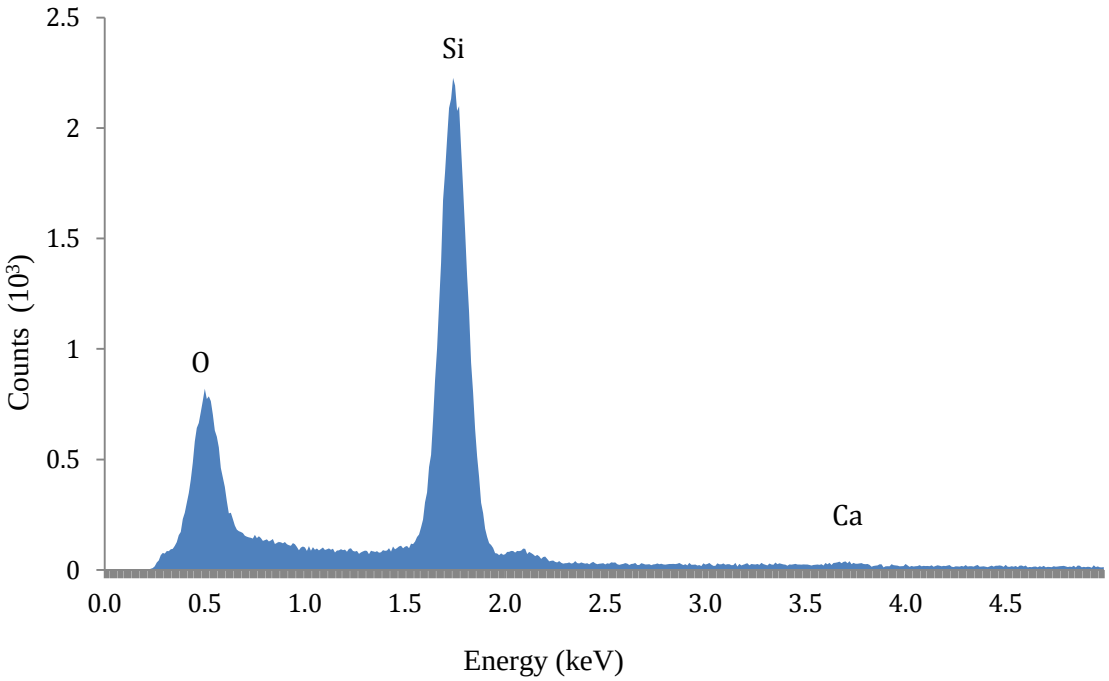


Figure 4-16: EDX Response of a Particle Selected from SH50PL-NH

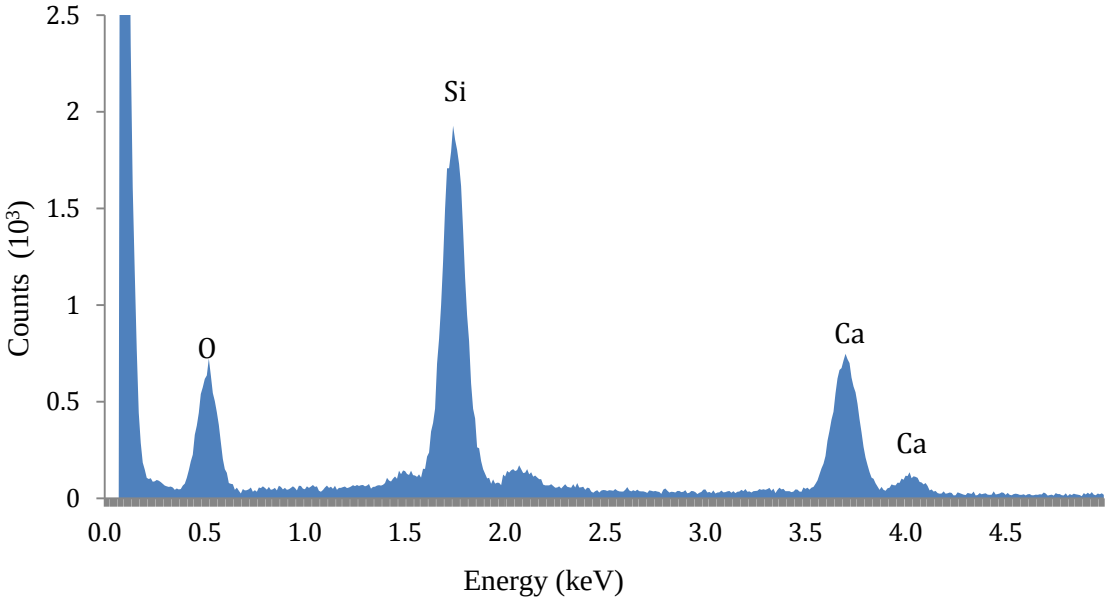


Figure 4-17: EDX Response of a Particle Selected from SH50FRP-NH

because the SS microcapsules would have had similar element compositions with a relatively large concentration of sodium.

Figure 4-18 through Figure 4-20 present the EDX spectra for the identified particles containing sodium for two ordinary concrete samples (Figure 4-18 and Figure 4-19) and for one self-healing concrete sample (Figure 4-20), respectively. The insets of these figures also provide the SEM image of the corresponding particle. It is noteworthy that, among the EDX analysis results obtained from all particles, sodium was found only in two SEM samples of ordinary concrete and in one SEM sample of self-healing concrete (out of the total of 50 particles identified inside all the considered samples). From the results presented in Figure 4-18 through Figure 4-20, it is observed that these three particles have similar element compositions. The fact that similar particles were found both in the ordinary and self-healing concrete samples suggests that these particles are not SS microcapsules, but other components already contained in the concrete mix.

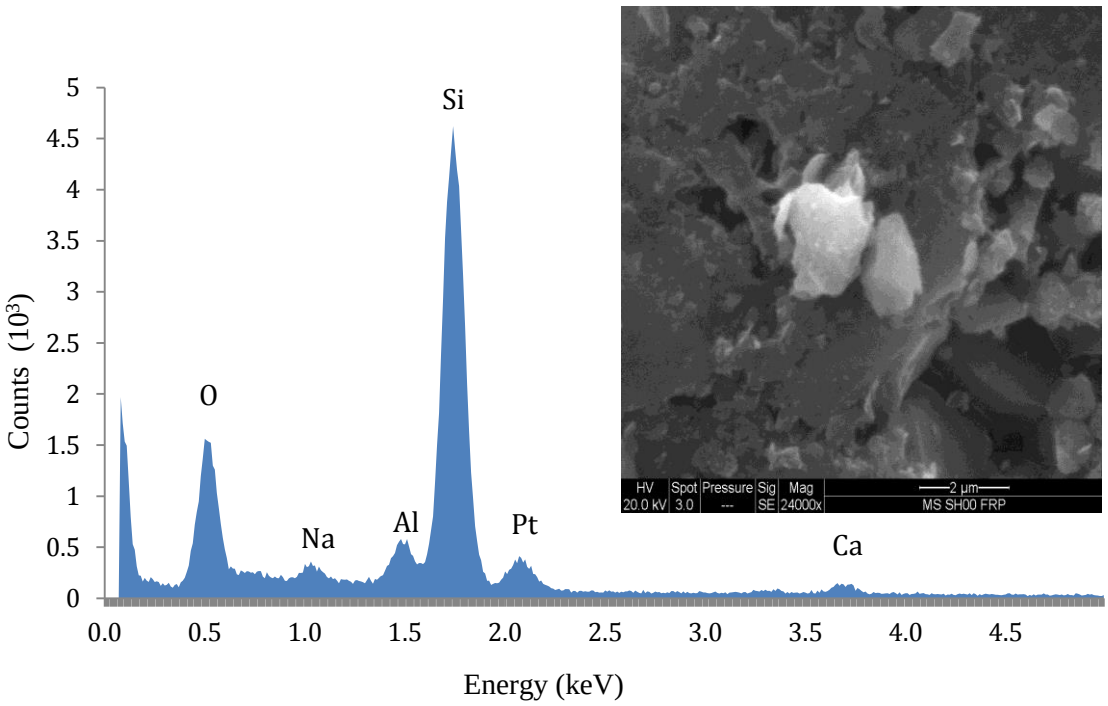


Figure 4-18: SEM Imaging and EDX Response of the Particle with Sodium from SH00FRP-NH Sample #1

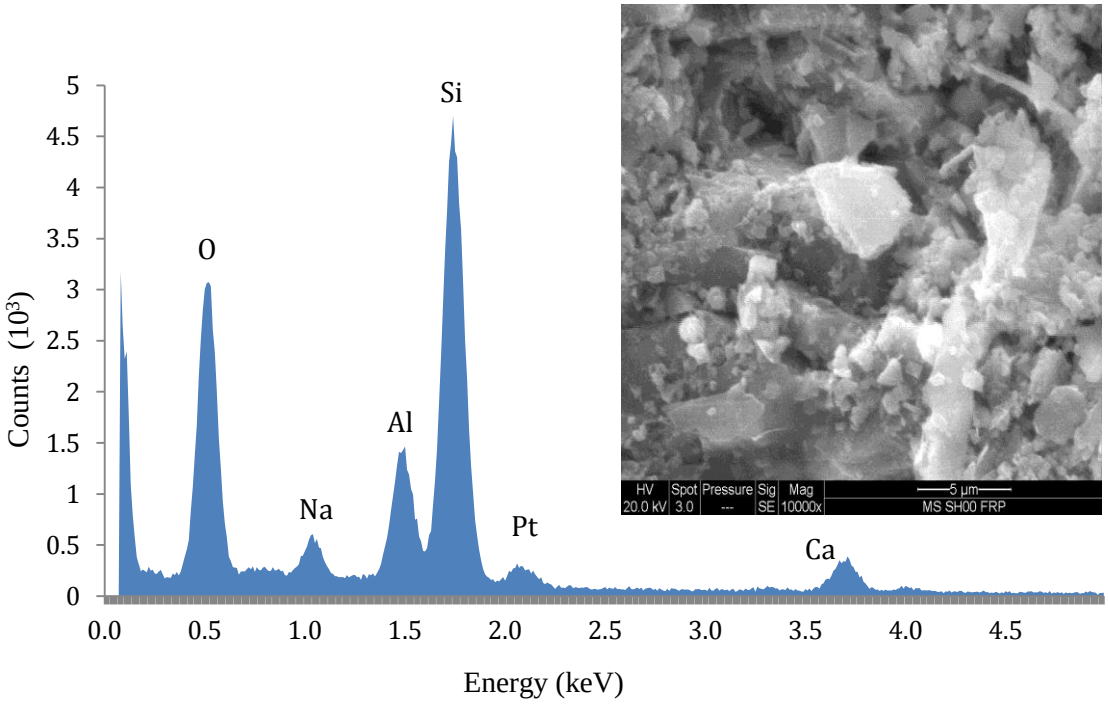


Figure 4-19: SEM Imaging and EDX Response of the Particle with Sodium from SH00FRP-NH Sample #4

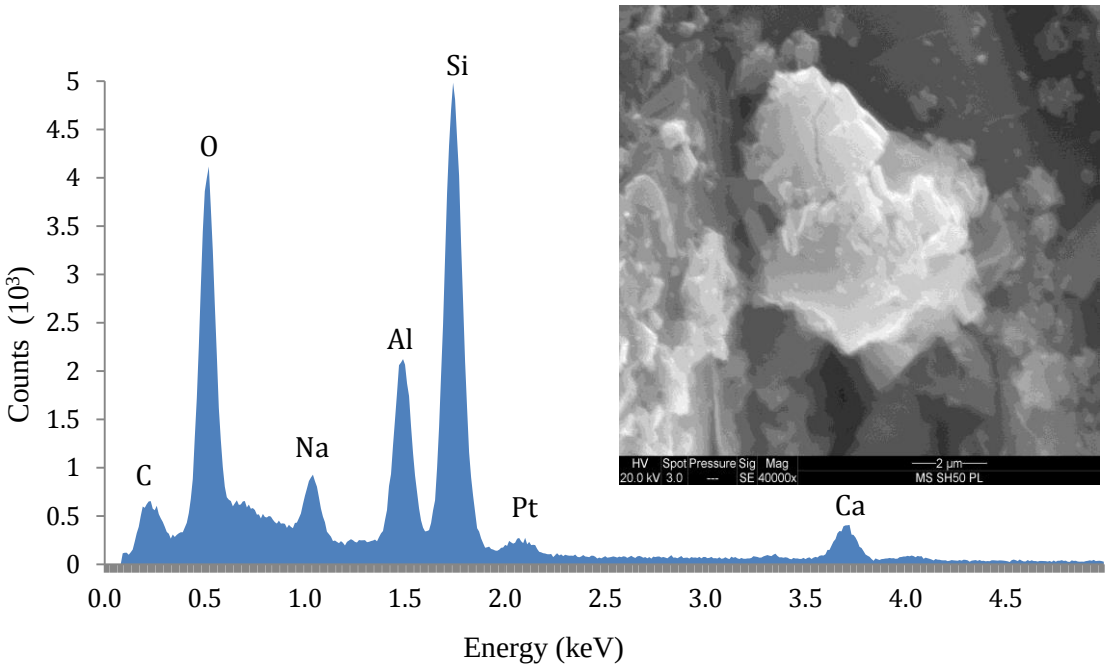


Figure 4-20: SEM Imaging and EDX Response of the Particle with Sodium from SH50PL-NH Sample #8

Table 4-4 shows the EDX analysis results for the three particles containing sodium. The weight percentage of sodium in each of these three particles is less than 4.5%, and the percentage of sodium atoms is less than 4.0%. According to molecular weight calculations, the weight percentage of sodium in an SS microcapsule is expected to be about 37.7%, and the percentage

Table 4-4: EDX analysis results of particles with sodium

Item	Specimen ID	Sample ID	O	Si	Ca	C	Na	Al
Weight (%)	SH00FRP-NH	1	44.95	**47.84**	0.00	0.00	**2.85**	4.37
	SH00FRP-NH	4	51.59	**32.43**	2.95	0.00	**4.39**	8.64
	SH50PL-NH	8	49.07	**17.52**	1.72	19.67	**4.00**	8.01
Atom (%)	SH00FRP-NH	1	58.55	**35.50**	0.00	0.00	**2.58**	3.37
	SH00FRP-NH	4	64.96	**23.26**	1.48	0.00	**3.85**	6.45
	SH50PL-NH	8	52.49	**10.68**	0.73	28.03	**2.98**	5.08

of sodium atoms is expected to be about 33.3%. However, the EDX analysis results provided values of the sodium percentage that are too low to be consistent with the presence of SS microcapsules, thus, further suggesting that the identified particles are not SS microcapsules.

4.3.6 Results of the SEM Test #3 (SEM Imaging Tests Using Focused Ion Beam Cuts)

In order to further validate the results obtained from the small scale EDX analysis, a select number of particles were cut using the ion beam. SEM imaging tests were performed over the cut sections of the particles. Figure 4-21 through Figure 4-23 present the results of the focused ion beam tests. Figure 4-21 (a) through Figure 4-23 (a) show a top view of the particle before cutting, Figure 4-21 (b) through Figure 4-23 (b) present the view of the cut section, and Figure 4-21 (c) through Figure 4-23 (c) illustrate the top view from the ion beam after cutting of the particle. It is observed that the morphology of the cut particles is inconsistent with the presence of an SS microcapsule, since these particles have only one texture and no outer shell can be identified for any of them. This finding indicates that intact SS microcapsules cannot be found in the self-healing concrete and confirms that hypothesis #5 (i.e., that the SS microcapsules' outer shell was too thick to be broken by the stress concentration near the cracks produced by the loading) must be rejected.

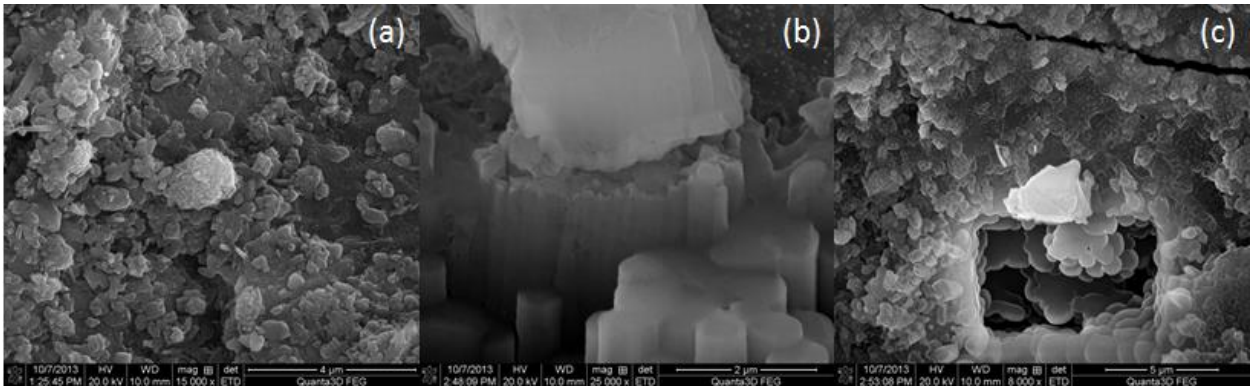


Figure 4-21: SEM Imaging Results Using Ion Beam Cuts for SH50PL-H Particle #1: (a) Top View , (b) Cut Section View, and (c) Top View of Ion Beam

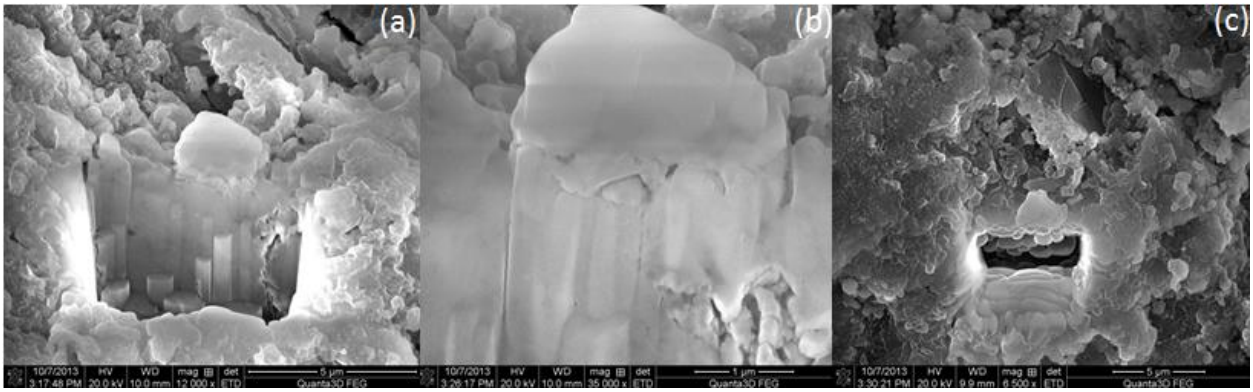


Figure 4-22: SEM Imaging Results Using Ion Beam Cuts for SH50PL-H Particle #2:
(a) Top View, (b) Cut Section View, and (c) Top View of Ion Beam

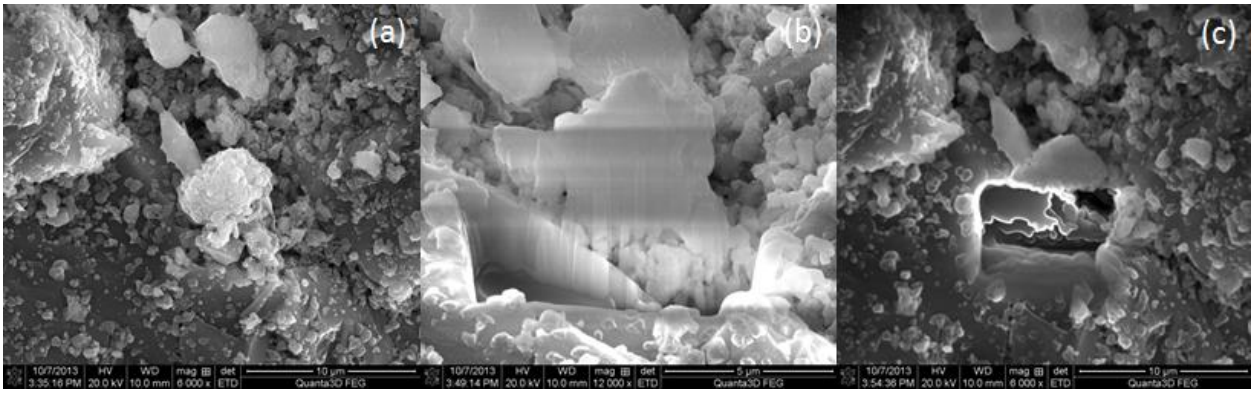


Figure 4-23: SEM Imaging Results Using Ion Beam Cuts for SH50PL-H Particle #3:
(a) Top View , (b) Cut Section View, and (c) Top View of Ion Beam

The results of the SEM imaging and EDX tests for more than 50 particles, together with the results of the ion beam slope cutting tests, indicate that SS microcapsules could not be found throughout the self-healing concrete matrix. However, it is possible that microcapsules were not found because of the low density of the SS microcapsules in the concrete matrix (i.e., the test results are insufficient to determine if any undamaged microcapsule was still present in the concrete matrix). Thus, these results are not sufficient to prove or disprove hypothesis #6(i.e., that the SS microcapsule shell durability problem was the cause of the non-activation of the self-healing mechanism). Further investigation is needed to draw a definitive conclusion regarding

the reasons that caused the non-activation of the self-healing mechanism in the research presented in this thesis.

5 CONCLUSIONS AND RECOMMENDATIONS

The objective of this research project was to test the hypothesis that composite action due to confinement with fiber reinforced polymers (FRP) of reinforced concrete structures can drastically improve the self-repairing properties of self-healing concrete materials. A first experimental campaign was conducted based on self-healing stiffness and strength tests of unconfined and FRP-confined ordinary concrete and concrete with different content of sodium silicate (SS) microcapsules.

The results obtained in the self-healing stiffness tests were insufficient to prove or disprove the hypothesis that composite action due to FRP confinement can increase the efficiency of self-healing mechanisms in the concrete. In fact, the experimental results from the self-healing stiffness tests indicated that the self-healing mechanism was not activated both in the unconfined and confined specimens. However, the experimental results obtained from the strength tests indicated that the presence of SS microcapsules affected the strength of the concrete in unconfined specimens.

Since the results of the first experimental campaign were inconclusive, a series of six hypotheses were proposed to explain why the self-healing mechanism was not activated in the self-healing stiffness test. The proposed hypotheses were: (1) the experimental test were affected by quality control issues; (2) the loading level reached in the self-healing stiffness test was insufficient to damage the concrete and trigger the self-healing mechanism; (3) the healing procedure used in the self-healing stiffness test was not sufficient to trigger the self-healing mechanism of the self-healing material; (4) the manufacturing process of SS microcapsules was affected by quality control problems; (5) the SS microcapsule outer shell was too thick to be broken by the stress concentration near the cracks produced by the loading; and (6) the SS

microcapsules suffered durability problems in the concrete environment. Hypothesis #1 could not be tested in this research due to funding limitations. Hypothesis #2 was discarded based on a review of the existing literature and previous work conducted by other researchers at LSU. A second experimental campaign was designed and performed to investigate hypotheses #3 to #6. The conclusions of this second experimental campaign were:

(1) Hypothesis #3 (insufficient healing procedure) was rejected based on the results of additional self-healing stiffness tests performed using a modified healing procedure.

(2) Hypothesis #4 (i.e., quality control issues in the manufacturing of SS microcapsules) was rejected based on the results of large scale scanning electron microscopy (SEM) tests and energy-dispersive X-ray spectroscopy (EDX) tests.

(3) Hypothesis #5 (SS microcapsule outer shell too thick to be broken) was rejected based on the results of small scale SEM and EDX tests.

(4) The results of the SEM imaging and EDX analysis were insufficient to prove or disprove hypothesis #6 (i.e., durability problems of the SS microcapsules in the concrete).

Further investigation is needed to investigate hypotheses #1 and #6, as well as to investigate the main hypothesis made in this research (i.e., that composite action due to FRP confinement can significantly improve the self-healing properties of self-healing concrete). The durability of SS microcapsules can be tested, e.g., by preparing a highly alkaline environment similar to the concrete environment, and by measuring the survival rate of the microcapsules at the end of controlled time intervals. After additional information is obtained regarding the durability of SS microcapsules in concrete and, if needed, the microencapsulation methodology is modified to account for this additional information, the experimental tests performed in this research should

be repeated with a very strict quality control, in order to avoid possible quality control issues and to test the main hypothesis of this research.

6 REFERENCES

Aldea, C. M., Song, W. J., Popovics, J. S., and Shah, S. P. (2000). Extent of healing of cracked normal strength concrete. Journal of Materials in Civil Engineering, 12: 92-96.

American Society for Testing and Materials (ASTM). (2004). Standard test method for compressive strength of cylindrical concrete specimens. C 39/C 39M – 04a. West Conshohocken, Pa.

American Society for Testing and Materials (ASTM). (2010). Standard test method for static modulus of elasticity and Poisson's ratio of concrete in compression. C469/C469M-10, West Conshohocken, Pa.

Araki, Y., Endo, T. Omori, T., Sutou, Y., Koetaka, Y., Kainuma, R., and Ishida, K. (2011). Potential of superelastic Cu-Al-Mn alloy bars for seismic applications. Earthquake Engineering and Structural Dynamics, 40: 107-115.

Badawi, M. and Soudki, K. (2005). Control of corrosion-induced damage in reinforced concrete beams using carbon fiber-reinforced polymer laminates. Journal of Composites for Construction, 9: 195-201.

Bakis, C. E., Bank, L. C., Brown, V. L., Cosenza, E., Davalos, J. F., Lesko, J. J., Rizkalla, S. H., and Triantafillou, T. C. (2002). Fiber-reinforced polymer composites for construction-state-of-the-art review. Journal of Composites for Construction, ASCE, 6(2): 73-78.

Bang, S. S., Galinat, J. K., and Ramakrishnan, V. (2001). Calcite precipitation induced by polyurethane-immobilized bacillus pasteurii. Enzyme and Microbial Technology, 28: 404-409.

Bathe, J. K. and Ramaswamy, S. (1979). On three-dimensional nonlinear analysis of concrete structures. Nuclear Engineering and Design, 52: 385-409.

Boh, B. and Sumiga, B. (2008). Microencapsulation technology and its applications in building construction materials. Materials and Geoenvironment, 55(3): 329-344.

Breton, P. J. (1999). From microns to nanometers: early landmarks in the science of scanning electron microscope imaging. Scanning Microscopies, 13(1): 1-6.

Brochu, A. B, Chyan, W. J., and Reichert, W. M. (2012). Microencapsulation of 2-octylcyanoacrylate tissue adhesive for self-healing acrylic bone cement. Journal of Biomedical Materials Research Part B, 100B: 1764-1772.

Brown, E. N., Kessler, M. R., Sottos, N. R., and White, S. R. (2003). In-situ poly(urea-formaldehyde) microencapsulation of dicyclopentadiene. Journal of Microencapsulation, 20: 719-730.

Brown, E. N., Sottos, N. R., and White, S. R. (2002). Fracture testing of a self-healing polymer composite. Experimental Mechanics, 42(4): 372-379.

Brown, E. N., Sottos, N. R., and White, S. R. (2006). Fatigue crack propagation in microcapsule-toughened epoxy. Journal of Materials Science, 41: 6266-6273.

Brown, E. N., White, S. R. and Sottos N. R.. (2005). Retardation and repair of fatigue cracks in a microcapsule toughened epoxy composite-Part I: Manual infiltration. Composites Science and Technology, 65(15-16): 2466-2473.

Brown, E. N., White, S. R. and Sottos, N. R. (2005). Retardation and repair of fatigue cracks in a microcapsule toughened epoxy composite-Part II: in-situ self-healing. Composites Science and Technology, 65(15-16): 2474-2480.

Buehler, W. and Wiley, R. (1961). The properties of TiNi and associated phases. Rep. NOLTR 61-75 [AD 266607], U.S. Naval Ordnance Laboratory, White Oak, MD.

Cailleux, E. and Pollet, V. (2009). Investigations on the development of self-healing properties in protective coatings for concrete and repair mortars. In Proceedings of 2nd International Conference on Self-Healing Materials, Chicago, IL, USA, 28 June–1 July.

Candappa, D. C., Sanjayan, J. G., and Setunge, S. (2001). Complete triaxial stress-strain curves of high-strength concrete. Journal of Materials in Civil Engineering, 13: 209-215.

Cho, S. H., Andersson, M., White, S. R., Sottos, N. R., and Braun, P. V. (2006). Polydimethylsiloxane-based self-healing materials. Advanced Materials, 18: 997-1000.

Dong, J. H., Cai, C. S., and Okeil, A. M. (2011). Overview of potential and existing applications of shape memory alloys in bridges. ASCE Journal of Bridge Engineering, 3: 305-315.

Dow Chemical Company (DOW). Dicyclopentadiene products: a guide to product handling and use. Form No. 778-04301. Available online: http://msdssearch.dow.com/PublishedLiteratureDOWCOM/dh_046d/0901b8038046d43a.pdf?filepath=aromatics/pdfs/noreg/778-04301.pdf&fromPage=GetDoc (accessed on Jan 14th, 2014).

Dry, C. (1990). Alteration of matrix permeability, pore and crack structure by the time release of internal chemicals. In: Proceedings of advance in cementitious materials. American Ceramic Society: Gaithersbury, Maryland, 729-68.

Dry, C. (1994). Matrix cracking repair and filling using active and passive modes for smart timed release of chemicals from fibers into cement matrices. Smart Materials and Structures, 3(2): 118-23.

Dry, C. (2000). Three design for the internal release of sealants, adhesives and waterproofing chemical into concrete to release. Cement Concrete Research, 30: 1969-77.

Dry, C. and McMillan, W. (1996). Three-part methylmethacrylate adhesive system as an internal delivery system for smart responsive concrete. Smart Materials and Structures, 5(3): 297-300.

Duerig, T. W., Melton, K. N., Stockel, D., and Wayman, C. M. (1990). Engineering aspects of shape memory alloys, Butterworth-Heinemann, London.

Edvardsen, C. (1996). Water permeability and self-healing through cracks in concrete. Deutscher Ausschuss fur Stahlbeton Bull (Berlin): 455.

Edvardsen, C. (1999). Water permeability and autogenous healing of cracks in concrete. ACI Materials Journal, 96(4): 448-454.

Einde, L. V. D., Zhao, L., and Seible, F. (2003). Use of FRP composites in civil structural applications. Construction and Building Materials, 17(6-7): 389-403.

Fan, C. J. and Zhou, X. D. (2010). Influence of operating conditions on the surface morphology of microcapsule s prepared by in-situ polymerization. Colloid and Surfaces A, 363: 49-55.

Feng, X., Zhuo, N., Ningxu, H., Biqin, D., Xuexiao, D., Zhan, H., and Ming, Z. (2008). Self-healing mechanism of a novel cementitious composite using microcapsules. In Proceedings of International Conference on Durability of Concrete Structures, Hangzhou, China.

Filippou, F. C., and Constantinides, M. (2004). FEDEASLab getting started guide and simulation examples. Technical Report NEESgrid-2004-22. www.neesgrid.org.

Flaga, K. (2000). Advances in materials applied in civil engineering. Journal of Materials Processing Technology, 106(1): 173-183.

Gadve, S., Mukherjee, A., and Malhotra, S. N. (2009). Corrosion of steel reinforced embedded in FRP wrapped concrete. Construction and Building Materials, 23: 153-161.

García, A., Schlangen, E. and Ven, M. V. D. (2011). Properties of capsules containing rejuvenators for their use in asphalt concrete. Fuel, 90: 583-591.

Gilford III, J., Hassan, M. M., Rupnow, T., Barbato, M., Okeil, A., and, Asadi, S. (2013). DCPD and sodium silicate microencapsulation for self-Healing of concrete. ASCE Journal of Materials in Civil Engineering, DOI: 10.1061/(ASCE)MT.1943-5533.0000892.

Glanville, W. H. (1931). The permeability of portland cement concrete. Building Research, Technical Paper 3: 1-61.

Goldstein, J., Newbury, D. E., Joy, D. C., Lyman, C. E., Echlin, P., LIfshin, E., Sawyer, L., and Michael, J. R. (2003). Scanning electron microscopy and X-ray microanalysis, 3rd ed. Plenum Press, New York.

Gregerová, M. and Všianský, D. (2009). Identification of concrete deteriorating minerals by polarizing and scanning electron microscopy. Materials Characterization, 11th Euroseminar on Microscopy Applied to Building Materials (EMABM), 60(7): 680-685.

Hayashi, R., Murray, S. J., Marioni, M., Allen, S. M., and O'Handley, R. C. (2000). Magnetic and mechanical properties of FeNiCoTi magnetic shape memory alloy. Sensors and Actuators, 81: 219-223.

Hearn, N. and Morley, C. T. (1997). Self-healing property of concrete - experimental evidence. Material Structure, 30: 404-11.

Hu, D. (2012). Efficient finite element modeling of reinforced concrete columns confined with fiber reinforced polymers. A Master's Thesis Submitted to Louisiana State University.

Hu, J. F, Chen, H. Q. and Zhang, Z. B. (2009). Mechanical properties of melamine formaldehyde microcapsules for self-healing materials. Materials Chemistry and Physics, 118: 63-70.

Huang, H. and Ye, G. (2011). Application of sodium silicate solution as self-healing agent in cementitious materials. In Proceedings of International Conference on Advances in Construction Materials through Science and Engineering, Hong Kong, China, 530-536.

Hyde, G. W. and Smith, W. J. (1889). Results of experiments made to determine the permeability of cements and cement mortars. Journal of the Franklin Institute of Philadelphia, 199-207.

Jacobsen, S., Marchand, J., and Hornain, H. (1995). SEM observations of the microstructure of frost deteriorated and self-healed concretes. Cement and Concrete Research, 25(8): 1781-1790.

Jones, A. S., Rule, J. D., Moore, J. S., White, S. R., and Sottos, N. R. (2006). Catalyst morphology and dissolution kinetics of self-healing polymers. Chemistry of Materials, 18: 1312-1317.

Jonkers, H. M., Thijssen, A., Muyzer, G., Copuroglu, O., and Schlangen, E. (2008). Application of bacteria as self-healing agent for the development of sustainable concrete. The 1st international conference on biogeocivil engineering, Delft, The Netherlands; June 23-25.

Jonkers, H. M., Thijssen, A., Muyzer, G., Copuroglu, O., and Schlangen, E. (2010). Application of bacteria as self-healing agent for the development of sustainable concrete. Ecological Engineering, 36(2): 230-235.

Joseph, C., Jefferson, A. D., and Cantoni, M. B. (2007). Issues relating to the autonomic healing of cementitious materials. In: Proceedings of first international conference on self-healing materials, Noordwijk aan Zee, Netherlands. Paper 61.

Joseph, C., Jefferson, A. D., Isaacs, B., Lark, R., and Gardner, D. (2010). Experimental investigation of adhesive-based self-healing of cementitious materials. Magazine of Concrete Research, 62(11): 831-43.

Kainuma, R., Wang, J. J., Omori, T., Sutou, Y., and Ishida, K. (2002). Invar-type effect induced by cold-rolling deformation in shape memory alloys. Applied Physics Letters, 80(23): 4348-4350.

Kaltzakorta, I. and Erkizia, E. (2011). Silica microcapsules encapsulating epoxy compounds for self-healing cementitious materials. In Proceedings of 3rd International Conference on Self-Healing Materials, Bath, UK, 27-29 June.

Katsuhata, T., Ohama, Y., and Demura, K. (2001). Investigation of microcracks self-repair function of polymer-modified mortars using epoxy resins without hardeners. In Proceedings of 10th International Congress on Polymers in Concrete, Honolulu, HI, USA, 23-25 May.

Keller, M. W. and Sottos, N. R. (2006). Mechanical properties of microcapsules used in a self-healing polymer. Experimental Mechanics, 46: 725-33.

Kessler, M. R., Sottos, N. R., and White, S. R. (2002). Self-healing structural composite materials. Composites Part A, 34: 743-753.

Kessler, M. R., Sottos, N. R., and White, S. R. (2003). Self-healing structural composite materials. Composites Part A, 34: 743-753.

Kessler, M. R. and White, S. R. (2001). Self-activated healing of delamination damage in woven composites. Composites Part A, 32: 683-699.

Kirkby, E. L., Michaud, J., Manson, A. E., Sottos, N. R., and White, S. R. (2009). Performance of self-healing epoxy with microencapsulated healing agent and shape memory alloy wires. Polymer, 50: 5533-5538.

Kjellsen, K. O. and Jennings, H. M. (1996). Observation of microcracks in cement paste upon drying and rewetting by environmental scanning electron microscopy. Advanced Cement Based Materials, 3: 14-19.

Kuang, Y. and Ou, J. P. (2008). Self-repairing performance of concrete beams strengthened using superelastic SMA wires in combination with adhesives released from hollow fibers. Smart Materials and Structures, 17(2): 025020.

Kurinnyi, T. G. (1955). Determination of the strength of concrete on the same specimens. Byull. Stroit. Tekh., No.12.

Laboratory virtual instrument engineering workbench (LabVIEW) user's manual. (2003). National Instrument, Austin, TX.

Lam, L. and Teng, J. G. (2004). Ultimate condition of fiber reinforced polymer-confined concrete. Journal of Composites for Construction, ASCE,8(6): 539-548.

Lauer, K. K. and Slate, F. (1956). Autogenous healing of cement paste. JACY, 27, No.10.

Lee, C. Bonacci, J. F., Thomas, M. D. A., Maalej, M., Khajehpour, S., Hearn, N., Pantazopoulou, S., and Sheikh, S. (2000). Canadian Journal of Civil Engineering, 27: 941-948.

Li, G., Feng, Y., Gao, P., and Li, X. (2008). Preparation of mono-dispersed polyuria-urea formaldehyde double layered mirocapsules, Polym. Bull., 60: 725-731.

Li, V. C., Lim, Y. M., and Chan, Y. (1998). Feasibility study of a passive smart self-healing cementitious composite. Composites Part B, 29B(6): 819-827.

Li, W., Jiang, Z., Yang, Z., Zhao, N., and Yuan, W. (2013). Self-Healing efficiency of cementitious materials containing microcapsules filled with healing adhesive: mechanical restoration and healing process monitored by water absorption. PLoS ONE, 8(11): e81616. doi:10.1371/journal.pone.0081616.

Liu, X., Lee, J. K., Yoon, S. H., and Kessler, M. R. (2006). Characterization of diene monomers as healing agents for autonomic damage repair. Journal of Applied Polymer Science, 101: 1266-1272.

Liu, X., Sheng, X., Lee, J. K., and Kessler, M. R. (2009). Synthesis and characterization of melamine-urea-formaldehyde microcapsules containing ENB-based self-healing agents. Macromolecular Materials and Engineering, 294: 389-395.

Marusin, S. L. (1995). Sample preparation - the key to SEM studies of failed concrete. Cement and Concrete Composites, 17: 311-318.

Masoud, S. and Soudki, K. (2006). Evaluation of corrosion activity in FRP repaired RC beams. Cement and Concrete Composites, 28: 969-977.

Mertz, D. R., Chajes, M. J., Gillespie, J. W., Kukich, D. S., Sabol, S. A., Hawkins, N. M., Aquino, W., and Deen, T. B. (2003). Application of fiber reinforced polymer composites to the highway infrastructure. NCHRP Report 503, Transportation Research Board: Washington, D.C., USA.

Micelli, F. and Modarelli, R. (2013). Experimental and analytical study on properties affecting the behavior of FRP-confined concrete. Composites, Part B, 45: 1420-1431.

Mihashi, H., Kaneko, Y., Nishiwaki, T. and Otsuka, K. (2000). Fundamental study on development of intelligent concrete characterized by self-healing capability for strength. Translated from Japan Concrete Institute, 22(2): 441-50.

Monti, G. (2003). Seismic upgrade of reinforced concrete columns with FRP. Seminar on: Seismic Retrofitting of the South Tower, Tehran, Iran.

Motavalli, M. and Czaderski, C. (2007). FRP composites for retrofitting of existing civil structures in Europe: state-of-the art review. Composites and Polycon, American Composites Manufactures Association, Tampa, FL, USA.

Murphy, E. B. and Wudl, F. (2010). The world of smart materials. Progress in Polymer Science, 35: 223-251.

Nanni, A. and Bradford, N. M. (1995). FRP jacked concrete under uniaxial compression. Construction and Building Materials, 9(2): 115-124.

Nemati, K. M. (1997). Fracture analysis of concrete using scanning electron microscopy. Scanning, 19(6): 426-430.

Neville, A. M. (2012). Properties of concrete (5th Edition). Publisher: Prentice Hall.

Nonat, A. (2004). Structure and Stoichiometry of C-S-H. Cement and Concrete Research, 34(9): 1521-1528.

Okamoto, T., Sato, T., Kanbayashi, T., and Kato, C. (1989). Preparation of fine grain ice and dry clathrate water for manufacture of concrete and mortar, and manufacture of concrete and mortar. EP patent 338739. Mitsui Construction Co., Ltd., Shiiai Kemutekku K. K., Osaka Yuki Kagaku Kogyo Co., Ltd.

Ölander, A. (1932). An electrochemical investigation of solid cadmium-gold alloys. Journal of the American Chemical Society, 54(10): 3819-3833.

Omori, T., Koeda, N., Sutou, Y., Kainuma, Y., and Ishida, K. (2007). Superplasticity of Cu-Al-Mn-Ni shape memory alloy. Materials Transactions, 48(11): 2914-2918.

Palmquist, S. M., Kintzel, E., and Andrew, K. (2011). Scanning electron microscopy to examine concrete with carbon nanofibers. 5th Pan American Conference for NDT, 2-6 October, Cancun, Mexico.

Pan, X. M., York, D., Preece, J. A., and Zhang, Z. B. (2012). Size and strength distributions of melamine-formaldehyde microcapsules prepared by membrane emulsification. Powder Technology, 227: 43-50.

Pang, J. W. C. and Bond, I. P. (2005). A hollow fibre reinforced polymer composite encompassing self-healing and enhanced damage visibility. Composites Science and Technology, 65: 1791-1799.

Pantazopoulou, S. J., Bonacci, J. F., Sheikh, S., Thomas, M. D. A., and Hearn, N. (2001). Repair of corrosion-damaged columns with FRP wraps. Journal of Composites for Construction, February: 4-11.

Pantazopoulou, S. J. and Mills, R. H. (1995). Microstructural aspects of the mechanical response of plain concrete. ACI Materials Journal, 92(6): 605-616.

Pantelides, C. P., Gergely, J., Reaveley, L. D., and Volnyy, V. A. (2000). Seismic strengthening of reinforced concrete bridge pier with FRP composites. Proceedings, 12th World Conference on Earthquake Engineering, Auckland, New Zealand.

Parthy, K. (2003). Use of microencapsulated water for increasing fire resistance of construction materials. DE patent 10221939. Germany.

Pelletier, M. M., Brown, R., Shukla, A., and Bose, A. (2011). Self-Healing concrete with a microencapsulated healing agent, Cement and Concrete Research.

Pelletier, M., Brown, R., Shukla, A., and Bose, A. Self-healing concrete with a microencapsulated healing agent. Available online: http://energetics.chm.uri.edu/system/files/Self%20healing%20concrete%20-7-11.pdf (accessed on Nov 20th 2013).

Princic, T., Stukovnik, P., Pejovnik, S., Schutter, G. D., and Bosiljkov, V. B. (2013). Observation on dedolomitization of carbonate concrete aggregates, implications for ACR and expansion. Cement and Concrete Research, 54: 151-160.

Rahul, R. and Urmil, D. (2013). Behavior of GFRP wrapped RC columns of different shapes. Procedia Engineering, 51: 240-249.

Ramachandran, S. K., Ramakrishnan, V., and Bang, S. S. (2001). Remediation of concrete using micro-organisms. ACI Materials Journal, 98: 3-9.

Ramakrishnan, V. (2007). Performance characteristics of bacterial concrete - a smart biomaterial. The First International Conference on Recent Advances in Concrete Technology, Washington, DC, 67-78.

Reed, S. J. B. (2005). Electron microprobe analysis and scanning electron microscopy in geology. Cambridge University Press. New York City, New York.

Reinhardt, H. W., and Jooss, M. (2003). Permeability and self-healing of cracked concrete as a function of temperature and crack width. Cement and Concrete Research, 33:981-985.

Rule, J. D., Sottos, N. R., and White, S. R. (2007). Effect of microcapsule size on the performance of self-healing polymers. Polymer, 48: 3520-3529.

Sakai, Y., Kitagawa, Y., Fukuta, T., and Iiba, M. (2003). Experimental study on enhancement of self-restoration of concrete beams using SMA wire. Proceeding of SPIE, 50(57): 178-186.

Sampath, V. (2005). Studies on the effect of grain refinement and thermal processing on shape memory characteristics of Cu–Al–Ni alloys. Smart Materials and Structures, 14: S253-S260.

Sampath, V. (2006). Improvement of shape-memory characteristics and mechanical properties of copper-zinc-aluminum shape-memory alloy with low aluminum content by grain refinement. Materials and Manufacturing Processes, 21: 789-795.

Sawaguchi, T., Kikuchi, T., Ogawa, K., Kajiwara, S., Ikeo, Y., Kojima, M., and Ogawa, T. (2006). Development of prestressed concrete using Fe-Mn-Si-based shape memory alloys containing NbC. Materials Transactions, 47(3): 580-583.

Seible, F., Priestley, M., Hegemier, G., and Innamorato, D. (1997). Seismic retrofit of RC columns with continuous carbon fiber jackets. Journal of Composites for Construction, 1(2): 52-62.

Shao, Y., Zhu, Z., and Mirmiran, A. (2006). Cyclic modeling of FRP-confined concrete with improved ductility. Cement and Concrete Composites, 28(10): 959-968.

Sharp, S. R. and Clemena, G. G. (2004). State-of-the-art survey of advanced materials and their potential application in highway infrastructure. Final Report, Report No. FHWA/VTRC 05-R9, Virginia Transportation Research Council, Charlottesville, VA.

Song, G., Ma, N., and Li, H. N. (2006). Applications of shape memory alloys in civil structures. Engineering Structures, 28: 1266-1274.

Song, G. and Mo, Y. L. (2003). Increasing concrete structural survivability using smart materials. A proposal submitted to Grants to Enhance and Advance Research (GEAR), University of Houston.

Song, G., Mo, Y. L., Otero, K., and Gu, H. (2006). Health monitoring and rehabilitation of a concrete structure using intelligent materials. Smart Materials and Structures, 15(2): 309-314.

Spainhour, L. K. and Wootton, I. A. (2008). Corrosion process and abatement in reinforced concrete wrapped by fiber reinforced polymer. Cement and Concrete Composites, 30: 535-543.

Spoelstra, M. R. and Monti, G. (1999). FRP-confined concrete model. Journal of Composites for Construction, 3(3): 143-150.

Stutzman, P. (1991). Cement clinker characterization by scanning electron microscopy. Cement Concrete and Aggregates, 13: 109-14.

Stutzman, P. (2004). Scanning electron microscopy imaging of hydraulic cement microstructure. Cement and Concrete Composites, 26: 957-966.

Su, J. F., Huang, Z., and Ren, L. (2007). High compact melamine-formaldehyde microPCMS containing n-octadecane fabricated by a two-step coacervation method. Colloid Polymer Science, 285: 1581-1591.

Su, J. F., Schlangen, E., and Qiu, J. (2013). Design and construction of microcapsules containing rejuvenator for asphalt. Power Technology, 235: 563-571.

Su, J. F., Wang, L. X., and Ren, L. (2006). Fabrication and thermal properties of MicroPCMs: used melamine-formaldehyde resin as shell material. Journal of Applied Polymer Science, 101: 1522-1528.

Suh, K., Mullins, G., Sen, R., and Winters, D. (2007). Effectiveness of fiber-reinforced polymer in reducing corrosion in marine environment. ACI Structural Journal, 104: 76-83.

Sukhotskaya, S. S., Mazhorova, V. P., and Terekhin, Y. N. (1983). Effect of autogenous healing of concrete subjected to freeze-thaw cycles. Gidrotekhnicheskoe Stroitel'stvo, 6: 14-15.

Sun, L., Yu, W., and Ge, Q. (2011). Experimental research on the self-healing performance of micro-cracks in concrete bridge. Advanced Materials Research, 250-253, 28-32.

Sun, Z. and Xu, Q. (2009). Microscopic, physical and mechanical analysis of polypropylene fiber reinforced concrete. Materials Science and Engineering A, 527: 198-204.

Szabó, T., Molnár-Nagy, L., Bognár, J., Nyikos, L., and Telegdi, J. (2011). Self-healing microcapsules and slow release microspheres in paints. Progress in Organic Coatings, 72: 52-57.

Thao, T. D. P., Johnson, T. J. S., Tong, Q. S., and Dai, P. S. (2009). Implementation of self-healing in concrete - proof of concept. The IES J Part A: Civil and Structural Engineering, 2(2): 116-125.

Tittelboom, K. V., Belie, N. D., Muynck, W. D., and Verstraete, W. (2010). Use of bacteria to repair cracks in concrete. Cement and Concrete Research, 40: 157-166.

Tittelboom, K. V. and Belie, N. D. (2013). Self-healing in cementitious materials - a review. Materials, 6: 2182-2217.

Toohey, K. S., Sottos, N. R., Lewis, J. A., Moore, J. S., and White, S. R. (2007). Self-healing materials with microvascular networks. Nature Materials, 6: 581-585.

Trask, R. S. and Bond, I. P. (2006). Biomimetic self-healing of advanced composite structures using hollow glass fibres. Smart Materials and Structures, 15: 704-710.

Vincent, T. and Ozbakkaloglu, T. (2013). Influence of fiber orientation and specimen end condition on axial compressive behavior of FRP-confined concrete. Construction and Building Materials, 47: 814-826.

Voutou, B., Stefanaki, E. C., Giannakopoulos, K. (2008). Electron microscopy: the basics. Physics of Advanced Materials Winter School 2008.

Wang, H. P., Yuan, Y. C., Rong, M. Z., and Zhang, M. Q. (2007). Microencapsulation of styrene with melamine-formaldehyde resin. Colloid Polymer Science, 287: 1089-1097.

Wang, J. Y., Tittelboom, K. V., Belire, N. D., and Verstraete, W. (2012). Use of silica gel or polyurethane immobilized bacteria for self-healing concrete. Construction and Building Materials, 26: 532-540.

Wang, L. M. and Wu, Y. F. (2008). Effect of corner radius on the performance of CFRP-confined square concrete columns: Test. Engineering Structures, 30: 493-505.

Wang, S., Baxter, L., and Fonseca, F. (2008). Biomass fly ash in concrete: SEM, EDX and ESEM analysis. Fuel, 87: 372-379.

Wang, X. F., Xing, F., Zhang, M., Han, N. X., and Qian, Z. W. (2013). Experimental study on cementitious composites embedded with organic microcapsules. Materials, 6: 4064-4081.

White, S. R., Sottos, N. R., Geubelle, P. H., Moore, J. S., Kessler, M. R., Sriram, S. R., Brown, E. N., and Viswanathan, S. (2001). Autonomic healing of polymer composites. Nature, 409: 794-797.

Wiktor, V. and Jonkers, H. M. (2011). Quantification of crack-healing in novel bacteria-based self-healing concrete. Cement and Concrete Research, 33: 763-770.

Wilson, G. O., Caruso, M. M., Reimer, N. T., White, S. R., Sottos, N. R., and Moore, J. S. (2008). Evaluation of ruthenium catalysts for ring-opening metathesis polymerization-based self-healing applications. Chemistry of Materials, 20: 3288-3297.

Wootton, I. A, Spainhour, L. K., and Yazdani, N. (2003). Corrosion of steel reinforcement in carbon fiber-reinforced polymer wrapped concrete cylinders. Journal of Composites for Construction, ASCE, 7: 339-347.

Wu, D. Y., Meure, S., and Solomon, D. (2008). Self-healing polymeric materials: a review of recent developments. Progress of Polymer Science, 33: 479-522.

Wu, M., Johannesson, B., and Geiker, M. (2012). A review: self-healing in cementitious materials and engineered cementitious composite as a self-healing material. Construction and Building Materials, 28: 571-583.

Wu, Y. F. and Jiang J. F. (2013). Effective strain of FRP for confined circular concrete columns. Composite Structures, 95: 479-491.

Wu, Y. F. and Wei, Y. Y. (2010). Effect of cross-sectional aspect ratio on the strength of CFRP-confined rectangular concrete columns. Engineering Structures, 32: 32-45.

Yang, Y., Lepech, M. D., Yang, E. H., and Li, V. C. (2009). Autogenous healing of engineered cementitious composites under wet-dry cycles. Cement and Concrete Research, 39: 382-390.

Yang, Z., Hollar, J., He, X., and Shi, X. (2011). A self-healing cementitious composite using oil core/silica gel shell microcapsules. Cement and Concrete Composites, 33: 506-512.

Yin, T., Rong, M. Z., Zhang, M. Q., and Yang, G. C. (2007). Self-healing epoxy composites-preparation and effect of the healant consisting of microencapsulated epoxy and latent curing agent. Composite Science and Technology, 67: 201-12.

Yuan, L., Liang, G. Z., and Xie, J. Q. (2007). Synthesis and characterization of microencapsulated dicyclopentadiene with melamine-formaldehyde resins. Colloid Polymer Science, 285: 781-791.

Yuan, Y. C., Rong, M. Z., Zhang, M. Q., Chen, J., Yang, G. C., and Li, X. M. (2008). Self-healing polymeric materials using epoxy/mercaptan as the healant. Macro-molecules, 41: 5197-5202.

Zhang, X. X., Fan, Y. F., Tao, X. M., and Yick, K. L. (2004). Fabrication and properties of microcapsules and nanocapsules containing n-octadecane. Materials Chemistry and Physics, 88: 300-307.

Zhao, Y., Zhang, W., Liao, L. P., Wang, S. J., and Li, W. J. (2011). Self-healing coatings containing microcapsule. Applied Surface Science, 258: 1915-1918.

7 APPENDIX: SODIUM SILICATE MICROENCAPSULATION PROCEDURE

This microencapsulation of sodium silicate was accomplished by using in-situ polymerization in an oil-in-water emulsion. The main steps of this procedure can be summarized as follows:

1. Place 200 ml of DI water in a 1000 ml beaker;
2. Dissolve 50 ml of 2.5 wt.% EMA copolymer using a magnetic stirrer and ultra sound water bath to develop an aqueous solution;
3. Agitate using a IKA RW 20 digital mixer, with a driving 55 mm low shear three-bladed mixing propeller placed just above the bottom of the beaker;
4. Under agitation, add 5.00 g urea, 0.50 g resorcinol and 0.50 g ammonium chloride;
5. Set the pH by using sodium hydroxide (NaOH) and hydrochloric acid (HCl) drop-wise with a disposable pipet;
6. Add two to three drops of 1-octanol to reduce surface bubbles;
7. Allow the solution to stabilize for approximately 6 - 8 minutes at the appropriate pH and rpm agitation rate;
8. Mix 170 ml of DI water with 60 ml of an aqueous sodium silicate and add to the solution;
9. Agitate the solution for approximately 5 min. While under agitation, HCL was slowly added to the solution to form a gel/aqueous solution;
10. Add 100 ml of the gel/aqueous solution to the emulsion while maintaining a pH of 3.0 - 3.5;
11. Allow the solution to stabilize for 13 - 15 minutes before 12.7 g of 37 wt% aqueous solution of formaldehyde was added to the emulsion;
12. Wrap and cover the solution with aluminum foil, and slowly heat to the set temperature;
13. Turn off the hot plate after 4 hours of continuous agitation;

14. Once cooled to ambient temperature, the suspension of microcapsules was separated under vacuum filtration;
15. Rinse microcapsules with DI water three times with 500 ml of DI water, and then allow to air dry for 48 - 72 h.

8 VITA

Yueqiang Sui was born in 1988 in Qiqihaer, Heilongjiang, P.R.China. He graduated from Shouguang First High in Shouguang, Shandong, China in June, 2007 and began his undergraduate studies at Xiamen University at Xiamen, Fujian, China in the fall of the same year. He received his Bachelor of Engineering degree in Civil Engineering from Xiamen University in June of 2011. After graduating, he began his graduate studies as a master's student at Louisiana State University in August 2011. He is expected to receive his Master of Science degree in Civil Engineering in May of 2014.